UNIVERSITÀ DEGLI STUDI DI CAMERINO

School of Advanced Studies

Doctoral course in

Life and Health Sciences – Molecular Biology and cellular Biotechnology

XXXIII Cycle

NEUROPROTECTIVE EFFECT OF GUT MICROBIOTA MODULATION IN ALZHEIMER'S DISEASE: A PRECLINICAL STUDY

Doctoral Candidate
Dr. Olee Gogoi

Supervisor
Prof. Anna Maria Eleuteri

Coordinator of the PhD curriculum
Prof. Anna Maria Eleuteri

Acknowledgements

Sincere thanks to my supervisor Prof. Anna Maria Eleuteri for her continuous guidance and scientific support. I express my gratitude and warm appreciation for giving me the opportunity to learn from her knowledge and experience during the past three years of Ph.D. duration. Special thanks to my collaborators Dr. Valentina Cecarini and Dr. Laura Bonfili for their valuable insights, scientific recommendations and encouragement. I am grateful to Dr. Nazzareno Cannella for his precious help and support. Thanks to Prof. Mauro Angeletti and Dr. Massimiliano Cuccioloni for their endless help and generous advice.

I dedicate this work in loving memory of my mother for her unconditional love and support. I would like to thank my father and my brother for their love and support in all my decisions concerning my future.

Special thanks to my husband, Dr. Nityanand Bolshette, for being an amazing partner, who supports me with carrier advice, scientific discussions, friendship, love and care.

Nevertheless, I am ever grateful to these people who had made the entire Ph.D. duration a wonderful journey of my life:

Vania Karami, Rahul Parmar, Surender Nakka and Manideep Thummala.

Contents

List of tables:

List of Figures:

ABSTRACT

Abstract

Alzheimer's disease (AD) is the most common neurodegenerative disorder and the main cause of dementia in the elderly with intricate pathobiology. It is a complex multifactorial disease involving neuroinflammation, oxidative stress, impaired metabolic and proteolytic pathways and cognitive dysfunctions. Recently, the role of gut-brain axis in the onset and progression of the disorder has been elucidated. In this study, we used different approaches to demonstrate how a proper gut microbiota modulation can positively influence the progression of AD. In addition, considering that AD is characterized by extensive protein aggregation and that autophagy deeply regulates protein homeostasis, we also explored the mechanistic insight into regulation of this proteolytic pathway under the condition of Golgi fragmentation due to impaired tethering complex.

In details, 3xTg-AD mice were used as a model of AD and the effects of the probiotic formulation SLAB51, of p62-engineered Lactobacilli and of pasteurized beer on gut microbiota and brain, functions were evaluated. Upon wild-type and transgenic animals treatment with SLAB51, markers of glucose metabolism including brain expression levels of key glucose transporters, insulin-like growth factor receptor β, and glycated hemoglobin plasma levels were evaluated. For the p62-LAB study, neuronal proteolysis, oxidative stress, neuroinflammation and load of Aβ deposition in AD brain were monitored. Gut microbiota composition and gut-brain axis components were also studied.

Regarding the pasteurized beer treatment, upon mice sacrifice, amyloid-beta (Aβ) load and neuro-inflammatory markers were evaluated in the brain and plasma of treated animals. Finally, gut hormones as well as a possible shift in gut bacterial and fungal compositions were evaluated.

Cog3 knockout cell line was used to evaluate the effect of Golgi fragmentation in autophagy. To identify cellular trafficking or sorting defects, subcellular fractionation was performed in sucrose density

gradient. Then, colocalization of autophagy proteins with autophagosomal markers and their trafficking sites were studied under basal and starvation conditions.

Our results demonstrated that SLAB51 treatment, through gut microbiota modulation, positively influenced metabolic homeostasis in the brain, contributing to a reduction in neuroinflammation. The treatment restored the major neuronal glucose transporters GLUT3 and GLUT1 and significantly decreased p-Tau levels in AD brain. The oral administration of p62-enginereed LAB improved neuronal proteolysis reduced the load of Aβ deposition in AD brain and the amount of inflammatory and oxidative markers. However, the treatment did not have a pronounced effect on the gut microbiota composition or on hormones of the gut-brain axis. Beer-enriched with brewing yeasts ameliorate the cognitive functions of transgenic mice by reducing neuro-inflammatory markers and the levels of the Aβ(1–42) peptide, in the PFC and hippocampus of AD mice. In addition, treatments with beer and beer-yeast also increase the richness in gut bacterial population of AD mice.

Finally, the analysis of the autophagic process in Cog3 knockout cell line demonstrated that the cargo receptor p62 colocalized with the autophagosomal fraction without any glycosylation defect and observed functional for selective autophagy under basal condition.

Our studies deeply dissected the role of gut-brain axis in AD, evaluating the effect of different strategies for gut microbiota modulation. The tested strategies positively regulated neuronal processes in AD mice, restoring proteolysis and glucose metabolism, counteracting inflammation and oxidation and decreasing the load of amyloid aggregates. These results therefore suggest new approaches and opportunities for the development of therapies against neurological disorders.

Introduction

Chapter1: Introduction

1.1: Alzheimer's Disease

1.1.1: Overview on AD progression

Alzheimer's disease (AD) is the most common neurodegenerative disorder and the main cause of dementia in the elderly with complex pathobiology. It is characterized by loss of neurons in the hippocampus and cerebral cortex, shrinkage of the cortex, enlargement of ventricles, finally resulting in the progressive decline of cognitive functions. AD is associated with significant and progressive disability and death is an inevitable outcome generally occurring at 5–12 years after symptoms onset [1] Apathy and depression are often witnessed as early symptoms followed by other typical clinical conditions [2] characterized by early impairment in learning and memory, followed by alterations in complex attention, executive and visuospatial function, language, praxis, gnosis, behavior and/or social comportment [1, 3]. Progression of AD from unnoticeable brain changes to physical disability has been divided into three broad phases: preclinical AD, mild cognitive impairment (MCI) due to AD and dementia due to AD (figure 1). Based on the degree of severity of symptoms, dementia phase is further sub-divided into mild, moderate and severe stages of AD.

Preclinical AD:

This phase hardly shows any noticeable symptoms but positron emission tomography (PET) scans and in analysis of cerebrospinal fluid (CSF) show abnormal levels of Aβ and decreased metabolism of glucose in brain. At this phase brain can compensate for the damage and thus the individual can continue to function normally.

MCI due to AD:

In this phase, the individual develops mild problems with memory and thinking in addition to abnormal levels of Aβ in the brain. Mild cognitive disabilities would be noticeable to family and friends but they would not interfere with person's everyday activities. These mild changes in cognition occur when the brain can no longer compensate for the damage and death of nerve cells caused by AD.

Dementia due to AD:

This phase is characterized by evident cognitive impairment with person's inability to perform daily life activities. Degree of damage to nerve cells in different parts of the brain reflects symptoms that change over time and differ in every individual. Based on the severity of the symptoms, dementia can be categorized as follows:

Mild dementia:

In the mild dementia stage, the person is able to perform daily activities but experiences loss of memory of recent events and thus assistance is needed to remain safe.

Moderate dementia:

This is the longest and pronounced stage of AD where the individuals find difficulties in communicating and performing routine tasks (such as bathing and dressing); become incontinent at times; and start having personality and behavioral changes, including being anxious, suspicious and agitated at times.

Severe dementia:

It is the period of AD when the person becomes bedridden and needs assistance for daily living [4]. Severe damage to different areas of the brain are manifested and favor problems in locomotion,

swallowing that then leads to malnutrition and significantly increases the risk of serious acute conditions that can cause death [2, 5].

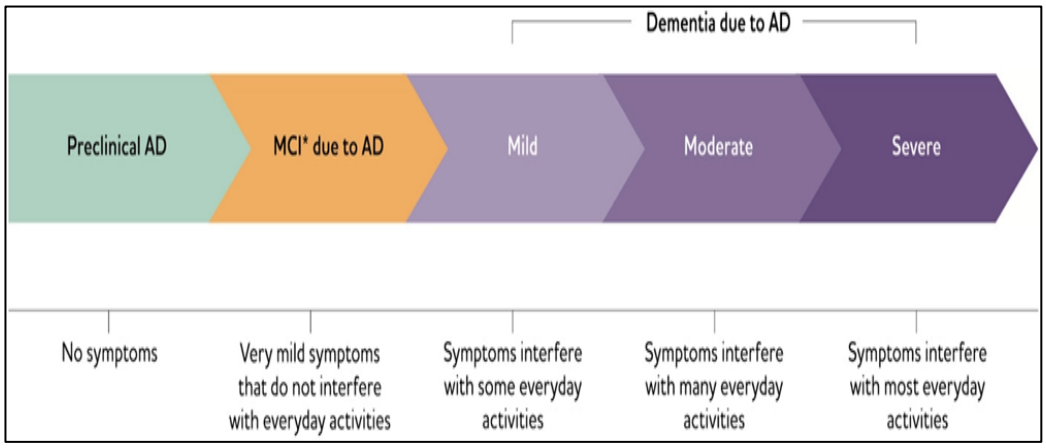

***Figure 1**: AD spectrum. *MCI is the acronym for mild cognitive impairment[4]*

1.1.2: Genetics of AD

The majority of AD cases are late onset forms of AD (LOAD) that occur after the age 65 and are also known as sporadic AD, while only 5% of cases constitute early onset of AD (EOAD), occurring earlier than age 65. Approximately 1 - 2% of cases are inherited in an autosomal dominant fashion which occurs at very early stage of life with rapid progression and it is designated as familial AD (FAD)[1] . FAD is typically due to mutations in genes encoding for the amyloid precursor protein (APP) or Presenilin, *PSEN1* and *PSEN2 [6, 7]*, or due to APP duplication indicating that increased wild-type APP can also confer increased risk of AD. In addition to these mutations several genetic factors have been discovered in recent years that largely contribute to AD progression [8]. Apolipoprotein E variant 4 (APOE4) is one of the established factor which is reported to have 2-3 fold increased risk of AD in heterozygous status and the risk is even higher than 10 folds when both alleles carry the predisposing variant [9]. Individuals carrying APOE4 have blood brain barrier (BBB) leakage in the hippocampus and parahippocampal gyrus, the regions of the brain responsible for memory and cognition, also at a very early stages of their life [10-12]. Until now, more than 20 genes have been identified that contribute to the increased risk of AD, namely: clusterin (CLU), sortilin-related receptor-1 (SORL1), ATP-binding

cassette subfamily A member 7 (ABCA7), bridging integrator 1 (BIN1), phosphatidylinositol binding clathrin assembly protein (PICALM), CD2 associated protein (CD2AP), complement component (3b/4b) receptor 1 (CR1), CD33, triggering receptor expressed on myeloid cells 2 (TREM2), and phospholipase D3 (PLD3) [4, 8, 13]. In addition to genetic factors, also environmental factors influence the risk of AD, primarily contributing to sporadic AD forms. These environmental factors, such as dietary changes, antibiotic exposure and infections, modify the gut homeostasis thus having potential influence on the central nervous system [14]. For this reason, the growing excitement towards the recent understanding of the gut microbiota brain axis (GMB) may represents an important platform to be exploited to positively influence different neurodegenerative disorders.

1.1.3: Major Hallmarks of AD

1.1.3.1: Protein aggregates in AD

Accumulation of protein aggregates is a distinct hallmark of AD. Aggregates destroy neurons and their connections in the hippocampus and cerebral cortex, resulting in the progressive decline in cognitive function. AD is distinctly defined by the presence of amyloid-beta (Aβ) plaques and intracellular neurofibrillary tangles (NFT). Plaques are extracellular deposits of amyloid peptides deriving from the cleavage of the APP and NFT are aggregates of the hyperphosphorylated tau protein. APP is a type I membrane protein that undergoes non-amyloidogenic cleavage process mediated by α-secretase and γ-secretase that generates a soluble APP fragment (sAPPα) and a membrane-bound C-terminal fragment of APP (αCTF) [15]. Alternatively, APP can be cleaved by β-secretase or BACE1 (β-site APP cleaving enzyme-1) and γ-secretase releasing two major fragments, sAPPβ and a C-terminal fragment located in the membrane (βCTF) (Figure 2). Further cleavage of βCTF results in the production of Aβ peptides ranging from 37 to 43 amino acid in length, with Aβ(1-40) and Aβ(1-42) being the most dominant and neurotoxic [16, 17]. Aβ(1-42) and tau are the renowned core cerebrospinal biomarkers, however recent research is moving towards the earlier phases of the disease, where Aβ oligomers and

synaptic markers are the most promising candidates [18]. Aβ monomers form small soluble Aβ oligomers that are considered more neurotoxic than insoluble fibers or amyloid plaques [19]. Although APP is ubiquitously expressed, it shows very high levels in the brain and, together with BACE1 levels, this explains why AD is a brain disease [16].

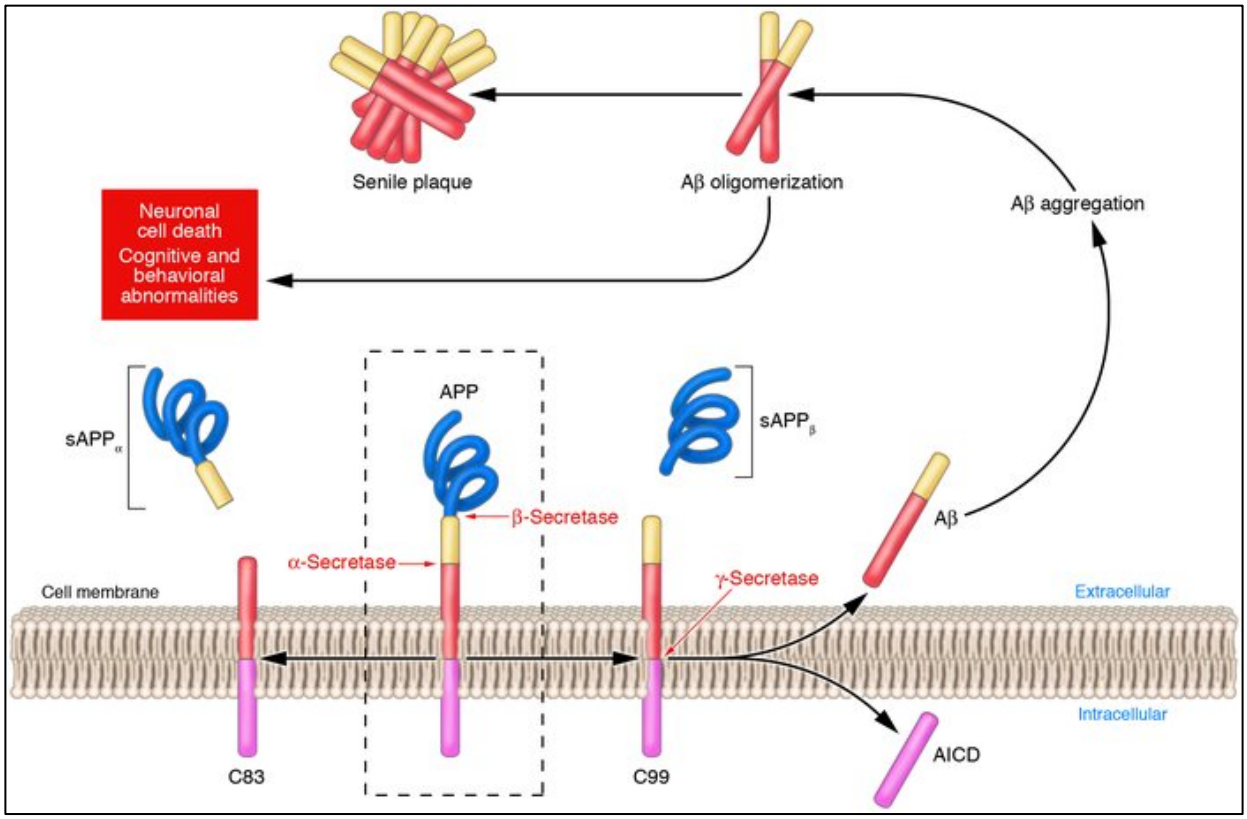

***Figure 2**: APP amyloidogenic and non-amyloidogenic cleavage process [20]*

As for the tau protein, it normally interacts with tubulin to promote its assembly into microtubules and helps to maintain their structure [21]. Tau is a phosphoprotein and its phosphorylation negatively regulates its ability to stimulate microtubule assembly. And in AD, abnormal hyperphosphorylation of tau at multiple serine/threonine sites leads to disassembly [20] and disruption of microtubules. Aggregated tau and phospho-tau take oligomeric forms known as neuropil threads localized inside neurons which later forms the intracellular NFT typical of AD brain [22].

Phosphorylation of tau introduces negative charges and acquires the ability of tau molecules to bind normal tau (Figure 3). Conversely, dephosphorylation of AD phospho-tau can inhibit the self-assembly of tau, suggesting that hyperphosphorylation was required for filament formation [23]. Hyperphosphorylated tau sequesters normal tau (N-tau), microtubule-associated protein (MAP) 1, and MAP2, and self-assembles to form paired helical filaments and disassembles microtubules [24]

In AD, hyperphosphorylated tau is several folds increased prior to the appearance of neurofibrillary tangles.

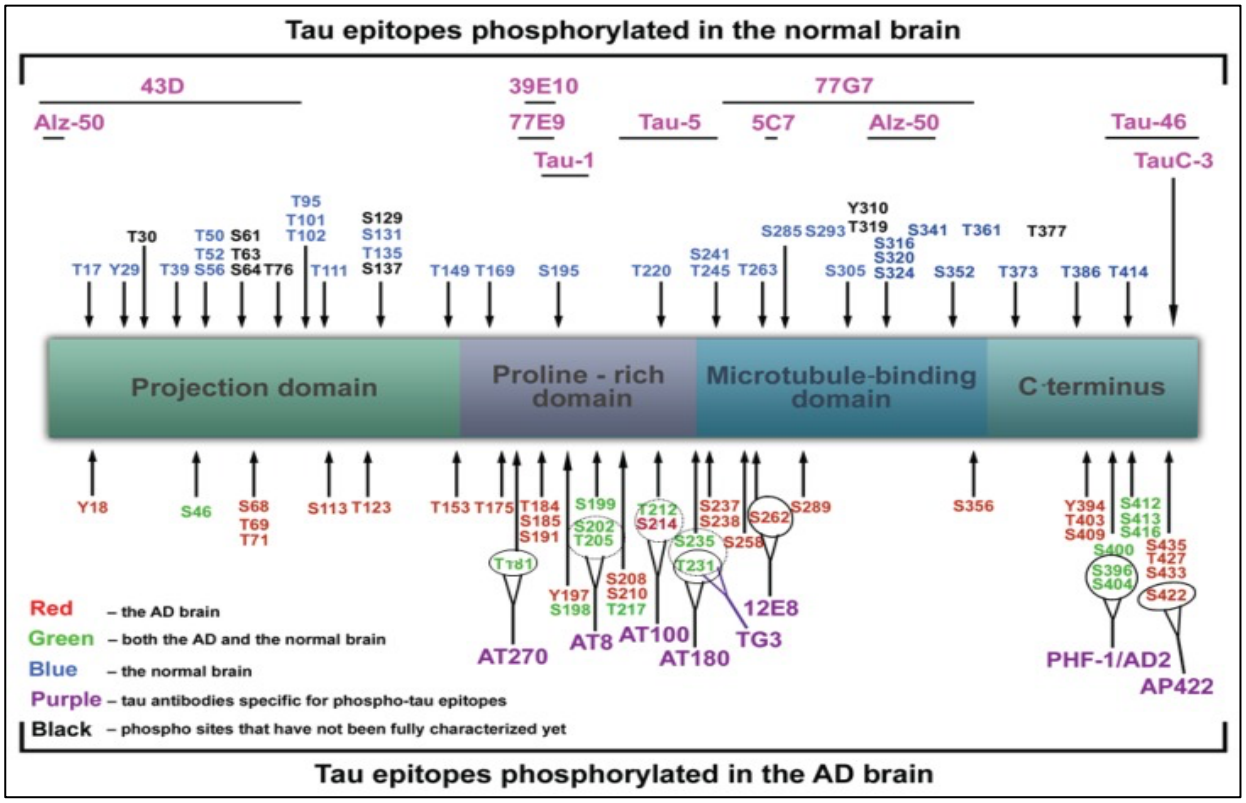

Figure 3: *Putative phosphorylation sites on tau protein and epitopes specific for major tau antibodies. Red color denotes amino acids phosphorylated in AD brain, green in both AD and normal brain, blue in normal brain, while black color means that those phosphorylation sites have not been fully characterized yet. Tau antibodies specific for phospho-tau epitopes are given in purple, while pink color denotes antibodies specific for non-phosphorylated tau epitopes: Alz-50 (aa 2–10, aa 312−342), 43D (aa 1–100), 77E9 (aa 185–195), 39E10 (aa 189–195), Tau-5 (aa 210–230), 5C7 (aa 267–278), Tau-1 (aa 195, 198, 199 and 202), 77G7 (aa 270–375), Tau-46 (aa 404–441), TauC-3 (tau cleaved on aa 421). Red—in the AD brain; Green—in both the AD and the normal brain; Blue—in the normal brain; Black—phosphorylation sites that have not been fully characterized yet; Purple—tau antibodies specific for phospho-tau epitopes; Pink—tau antibodies specific for unphosphorylated tau epitopes [24].*

1.1.4: Metabolic Impairment and Neuroinflammation

The human brain consumes ~60% of the blood glucose and CNS cells, being extremely metabolically active, depend solely on glucose as their fuel molecule [25]. An adequate supply of glucose from the blood stream depends on glucose transporters (GLUTs) [26, 27]. The major glucose transporters GLUT1 and GLUT3 [26] are found to be significantly reduced in AD brain which is supposed to be one of the leading factor to the progression and manifestation of the disease and its associated clinical pathologies. These reduced levels contribute to the significant impairment of glucose uptake in the cerebral cortex, leading to cerebral hyperphosphorylation of tau protein [27, 28].

Glucose uptake by the cell is regulated by critical metabolic sensors such as adenosine monophosphate-activated protein kinase (AMPK) and protein kinase B (Akt). AMPK can directly phosphorylate tau and Akt activity is also found to be upregulated in AD [29, 30]. AMPK and Akt are the central regulators of energy homeostasis and their functional abnormalities are marked at the preclinical stage of AD progression. Phosphorylated Akt causes aberrant phosphorylation of tau and increased Aβ deposition [31, 32]. Akt induces signaling of insulin-like growth factor I (IGF-I) and other trophic factors. Insulin and insulin-like growth factor-I (IGF-I) reduce Aβ deposition by decreasing APP phosphorylation and thus reduced level of insulin and IGF-I results in increased Aβ deposition [33, 34]. Significantly decreased levels of both IGF-I and its receptor were observed in the hippocampus and somatosensory cortex of aged mice and were shown to have age-related abnormalities [35]. Abnormal insulin level in the brain is often due to insulin resistance (IR) and is associated with tau hyperphosphorylation [36]. An increasing number of studies correlate glucose intolerance and impairment of insulin metabolism with a higher risk of developing AD.

Glycated hemoglobin (HbA1c) is a naturally occurring, non-enzymatic product from the exposure of hemoglobin to glucose. HbA1c turnover depends on the erythrocyte lifespan and therefore correlates with the glucose blood levels over the last 90-120 days. Elevated levels of HbA1c have been

associated with cognitive impairment. In addition, advanced glycation end products (AGEs) that derive from the Maillard reaction between proteins or lipids and aldose sugars, are increased in hippocampal neurons of AD subjects. The formation of AGEs is determined by the rate of turnover of proteins for glycoxidation and the extent of oxidant stress [37]. Furthermore, AGEs contribute to the Aβ aggregation and accumulation, and thereby favor AD progression [38].

Contribution of neuroinflammation to AD is more disastrous then accumulating senile plaque and neurofibrillary tangles. Microglia are the resident phagocytes of the CNS that defend against invasion, maintain synaptic remodeling and synaptic plasticity [39]. Once activated, microglia recognize and phagocyte Aβ by receptor-mediated endocytosis that activates signaling pathways and cytokine production in a ligand-dependent manner [40]. In AD, microglia are activated and polarized to the pro-inflammatory (M1) phenotype. M1 microglia produce cytokines and chemokines (IL-1β, IL-6, IL-12, TNF-α, CCL2) and express NADPH oxidase generating reactive oxygen and nitrogen species [14]. The M2 state instead is characterized by secretion of the anti-inflammatory cytokines IL-4, IL-10, IL-13 and transforming growth factor-beta (TGF-β), and elevated phagocytic capacity without production of toxic NO [39].

Glial cells, such as astrocytes and microglia, release cytokines upon every inflammatory challenge in their defense [41, 42] However, released cytokines, such as IL-1β and IL-12, have been known to elicit the progression of AD pathology, a schematic representation of neuroinflammation cycle in AD is shown in figure 4 [43, 44]. Elevated levels of IL-1β were identified in serum of individuals with mild cognitive impairment, a putative prodromal phase of dementia [45]. A growing body of literature reported associations between IL-1β polymorphisms and the onset of AD pathology [44]. IL-1β polymorphisms along with apolipoprotein E (APOE)-ε4 are linked with higher levels of IL-1β in the blood and sleep disturbances in AD individuals [46]. IL-12 is involved in the regulation of the adaptive

and innate immune system [47]. Vom Berg *et al.* suggested that IL-12/IL-23 pathway inhibition may attenuate AD pathology and cognitive deficits due to a decrease in the IL-12p40 subunit and its receptor activity [48]. Another major pro-inflammatory cytokine is TNF-α. Elevated levels of TNF-α are often reported in AD individuals. It is known to enhance the production of Aβ, decrease Aβ clearance, increase neuronal degeneration, and thus it is implicated in cognitive decline in AD [49].

On the other hand, anti-inflammatory cytokines, deletion of IL-10 attenuated AD-related deficits, such as altered synaptic integrity and behavioral deficits in APP/PS1 mice [50].

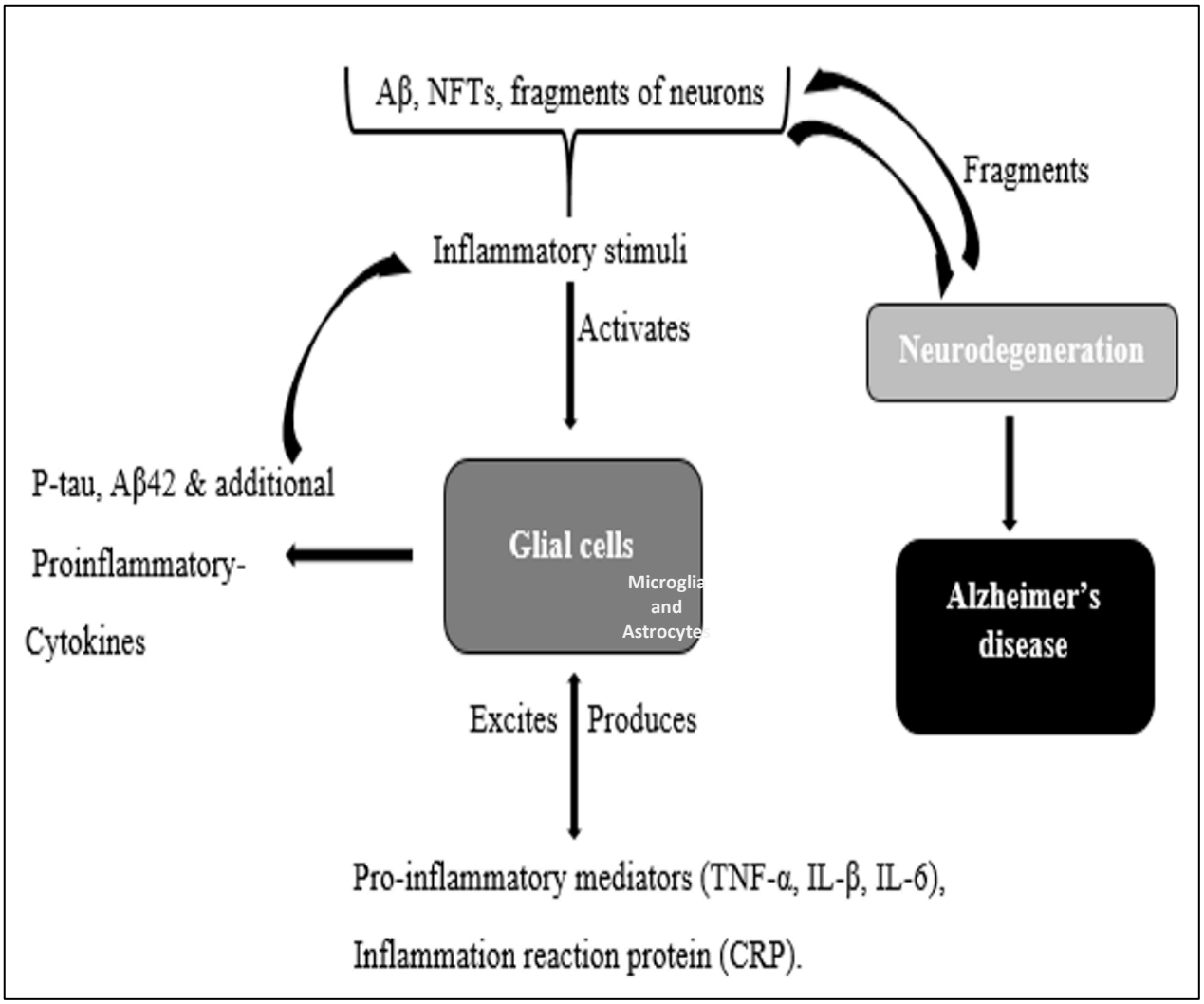

***Figure 4**: Schematic representation of neuro-inflammation in AD. Inflammatory stimuli (such as Aβ, NFTs, and fragments of neurons) activate glial cells which in turn produce pro-inflammatory mediators and inflammatory reaction proteins. These products have the ability to excite glial cells which further stimulates the production of P-tau, Aβ42, and additional pro-inflammatory cytokines, and the cycle is maintained. The cycle promotes neurodegeneration and other AD pathologies [51].*

In AD, microglia are able to bind to soluble Aβ oligomers and Aβ fibrils via receptors including class A scavenger receptor A1, CD36, CD14, α6β1 integrin, CD47 and toll like receptors (TLR2, TLR4, TLR6 and TLR9) [52]. Chronic activation of microglia by Aβ is detrimental and induces protracted inflammation and disproportionate Aβ deposition, thus rushing neurodegeneration. The early pro-inflammatory process is characterized by neuronal and microglia-derived cytokines and chemokines as well as by mobilization of microglia toward Aβ-burdened neurons [53, 54]. In addition to Aβ, extracellular non-phosphorylated tau, rather than hyperphosphorylated tau (p-tau), activates the p38 mitogen-activated protein kinase (MAPK) pathway, eliciting a pro-inflammatory reaction [41].

1.2: Intracellular Proteolytic Pathways in neurodegeneration

1.2.1: Autophagy: selective and non-selective pathway

Autophagy, meaning "self-eating", is a ubiquitous process that occurs in all eukaryotic cells. It is a complex catabolic process in which double-membrane vesicles (known as autophagosomes) engulf large intracellular components, such as organelles or proteins, and then fuse with lysosomes to finally degrade its content by acidic lysosomal hydrolases [55]. Autophagy plays a major role in maintaining cellular homeostasis during nutrient deprivation and in eliminating damaged proteins and organelles that accumulate during stress[55]. Autophagy is involved in cell death and tumor suppression[56], neurodegeneration [57], ageing [58], inflammation [59], immunity [60] and genome stability [59]. Autophagy is induced by various factors, which includes starvation, hypoxia, metabolic, osmotic and oxidative stresses [61-64].

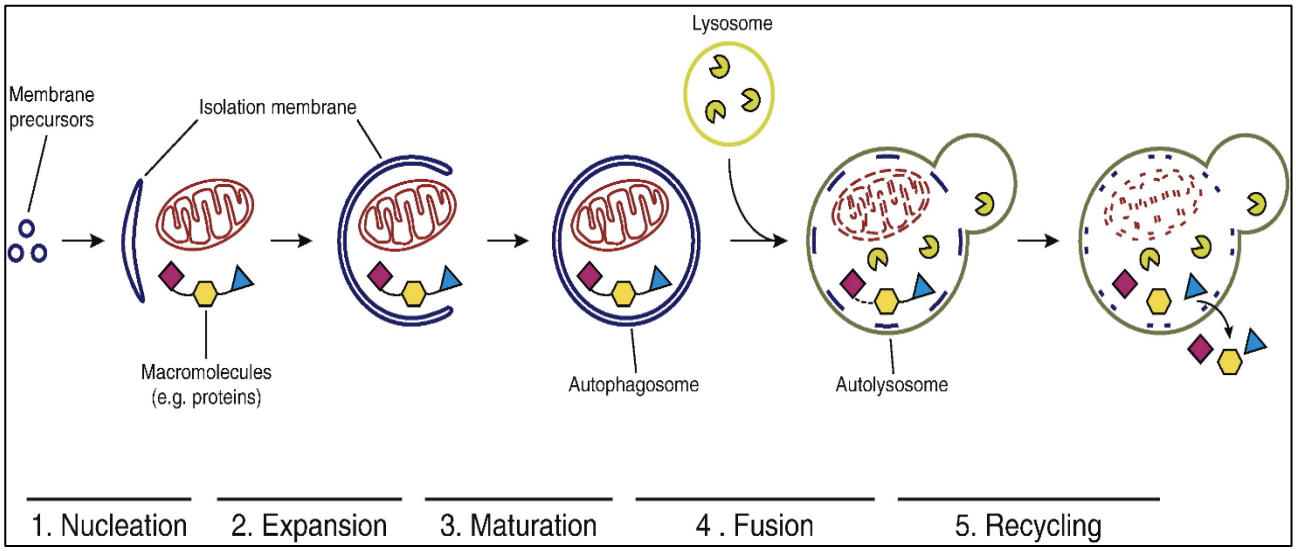

***Figure 5**: Stages of autophagy: Nucleation, Expansion, Maturation, Fusion and Recycling [65]).*

The autophagic process is highly dynamic and consists of consecutive steps and can be distinctly subdivided into: nucleation, expansion, maturation, fusion and recycling (figure 5). These steps are determined by the recruitment of specific Autophagy related (Atg) proteins or protein complexes. Autophagy starts with the establishment of a phagophore assembly site (PAS in yeast; omegasomes in

mammals) followed by membrane expansion to form a double-membrane phagophore that surrounds and engulfs cargo destined for autophagy. This structure is known as the autophagosome, which is then carried to and fuses with the lysosome for cargo degradation and recycling [61]. Depending on the selection of cargo destined for degradation, autophagy can be selective or non-selective autophagy.

1.2.2 Selective autophagy

Selective autophagy is involved in the degradation of intracellular protein aggregates, pathogens and damaged organelles. Selective autophagy can be activated in response to various external stimuli such as oxidative stress, osmotic or hypoxic condition [60, 62, 63]. Selective autophagic pathways are driven by selective autophagy receptors, which recognize their specific cargo for degradation and initiate the autophagic process. The receptors incorporates the cargo to the core autophagic machinery at the omegasome and activates a particular selective pathway to the exclusion of other selective and non-selective autophagic processes [65].

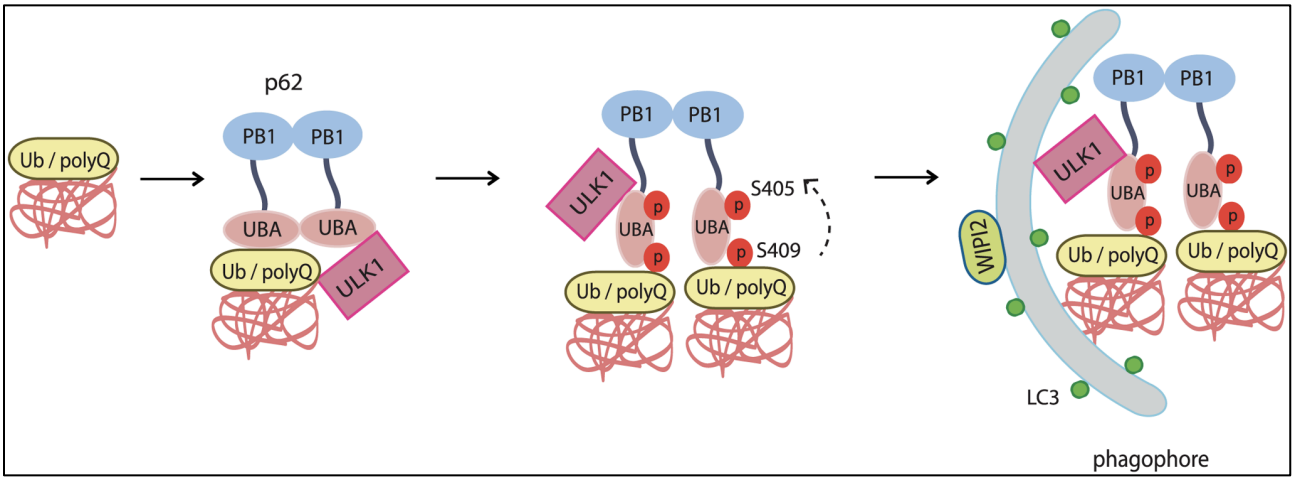

Figure 6: *p62 recruits ubiquitinated cargo to phagophore decorated with LC3 for fusion with lysosome [66].*

One of the major cargo receptor for selective autophagy is p62/SQSTM1/Sequestosome-1, herein p62 [67]. p62 is a multidomain adaptor protein that interacts with numerous proteins and exhibits diverse

roles in metabolic and catabolic processes of the cell. It selectively recruits cargos destined for lysosomal degradation through autophagy (Figure 6). p62 is a scaffold protein with six known interacting domains: N-terminal Phox-BEM1 domain (PB1), a ZZ-type zinc finger domain, a nuclear localization signal (NLS), a nuclear export signal (NES), LC3-interacting region (LIR), a Keap1-interacting region (KIR), and a C-terminal ubiquitin-associated domain (UBA). p62 interacts with ubiquitinated substrates by binding ubiquitin and connects to the membrane-bound light chain 3 (LC3), through its LIR domain (2). LC3 is a protein derived from post-translational modification of microtubule-associated protein-LC3 (MAP-LC3) and is specifically associated with autophagosomal membranes. Thus, p62 protein level is critical to maintain cellular homeostasis through the regulation of cellular protein degradation.

1.2.3: Non selective Autophagy

Non-selective autophagy is a non-selective catabolic process that mediates the recycling and the turnover of bulk cytoplasmic contents within the lysosome/vacuole. This process is activated under starvation conditions [68]. The process is driven by the core Atg proteins which can be divided into different functional subgroups:

(A) Atg1/ULK complex (Atg1, Atg11, Atg13, Atg17, Atg29 and Atg31) which is the initiation complex that regulates the induction of autophagosome formation;

(B) Atg9 and its cycling system (Atg2, Atg9 and Atg18) responsible for membrane delivery to the growing phagophore after the assembly of Atg1/ULK complex at the PAS/omegasome;

(C) PtdIns 3-kinase (PI3K) complex (Vps34, Vps15, Vps30/Atg6, and Atg14) is involved in vesicle nucleation, and recruits PI3P-binding proteins to the PAS/omegasome;

(D) Ubiquitin-like (Ubl) conjugation systems: the Atg12 (Atg5, Atg7, Atg10, Atg12 and Atg16) and Atg8 (Atg3, Atg4, Atg7 and Atg8) conjugation systems contributes to vesicle expansion [69-72].

The mammalian Atg9 homolog ATG9A localizes to the *trans*-Golgi network and late endosomes in nutrient-rich conditions. ATG9 appears to have a conserved role in coordinating membrane transport from donor sources to the phagophore and displays a cycling pattern [68]. Atg9 is the only transmembrane protein part of the Atg machinery. Recent discoveries demonstrated a lipid scramblase activity for Atg9 that provides a better picture for the understanding of lipid translocation to the growing phagophore [73]. However, the exact mechanism remains elusive.

1.2.4 Ubiquitin Proteasome System (UPS)

The ubiquitin-proteasome system (UPS) is one of the crucial protein degradation system in eukaryotes [74]. An extensive body of work associates UPS dysfunctions with AD pathogenesis and progression. The catalytic core of the UPS is the 20S proteasome that associates with the 19S cap forming the so-called 26S proteasome, responsible for the ATP- and Ub-dependent degradation of substrates. The 20S core is a barrel-shaped structure made of four heptameric rings stacked in a αββα fashion that forms three continuous chambers inside. The outer α-rings predominantly play a structural role, creating a gate that controls the substrate entry into the central proteolytic chamber made of β-rings (Figure 7) [75]. The two inner β-rings harbor the active sites, which are responsible for different proteolytic activities: β1 subunits express the peptidylglutamyl-peptide hydrolyzing (PGPH, cleaving after acidic residues) activity, β2 subunits express the trypsin-like activity and β5 subunits harbor the chymotrypsin-like activity. Proteasomes also possess two additional distinct activities, one cleaving preferentially after branched-chain amino acids (BrAAP activity) and the other cleaving after small neutral amino acids (SNAAP activity) [76]. Treatment with inflammatory cytokines induces the transcription of three additional active subunits, known as β1i, β2i, and β5i, that replace constitutive homologues during

proteasome assembly [77]. Proteasome proteolytic activities depend on the hydroxyl group of the N-terminal threonine (Thr-1) residue, responsible for cleaving peptides through a nucleophilic attack [78].

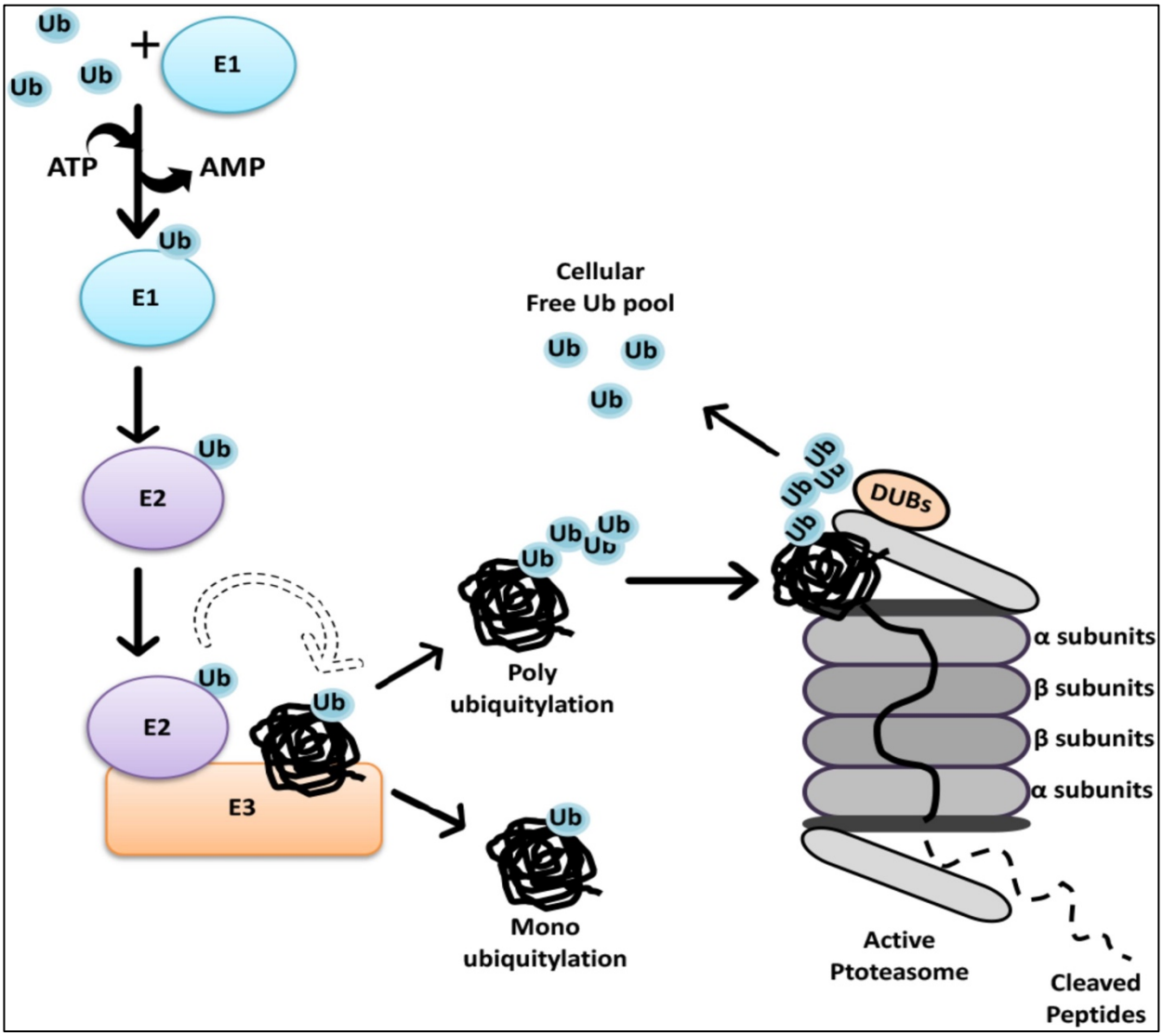

Figure 7: *Polyubiquitinated cargo destined for proteasomal degradation enters the proteolytic chamber at center of β-ring [79].*

Substrates, in order to be degraded by the UPS, need to be tagged by a ubiquitin chain through a process known as ubiquitination. Ubiquitin is a small protein made of 76 amino acids that can be covalently linked to lysine residues of proteasome substrates. At the beginning of this process, ubiquitin is activated through the ATP-dependent formation of a high energy thioester bond between the active site cysteine of the ubiquitin activating enzyme (E1) and the carboxyl terminus of ubiquitin. Ubiquitin

is then transferred to a ubiquitin-conjugating enzyme (E2), and is finally conjugated to lysine residues within the substrate or to the N-terminal amino group, by an ubiquitin (E3) ligase, which recognizes specific motifs in the targeted protein [80]. The substrate can be modified by either a single ubiquitin molecule (monoubiquitination), which regulates endocytosis of receptors and repair of DNA damage, or multiple amino groups (multi-monoubiquitination), or a chain of ubiquitin molecules (polyubiquitination), which is found in proteins targeted for intracellular proteolysis. The process is reversible because specific deubiquitinating enzymes can partially cut the polyubiquitin chains or completely strip all the ubiquitin molecules from the substrate [81].

1.2.5: p62 in the crosstalk between UPS and autophagy and its role in AD

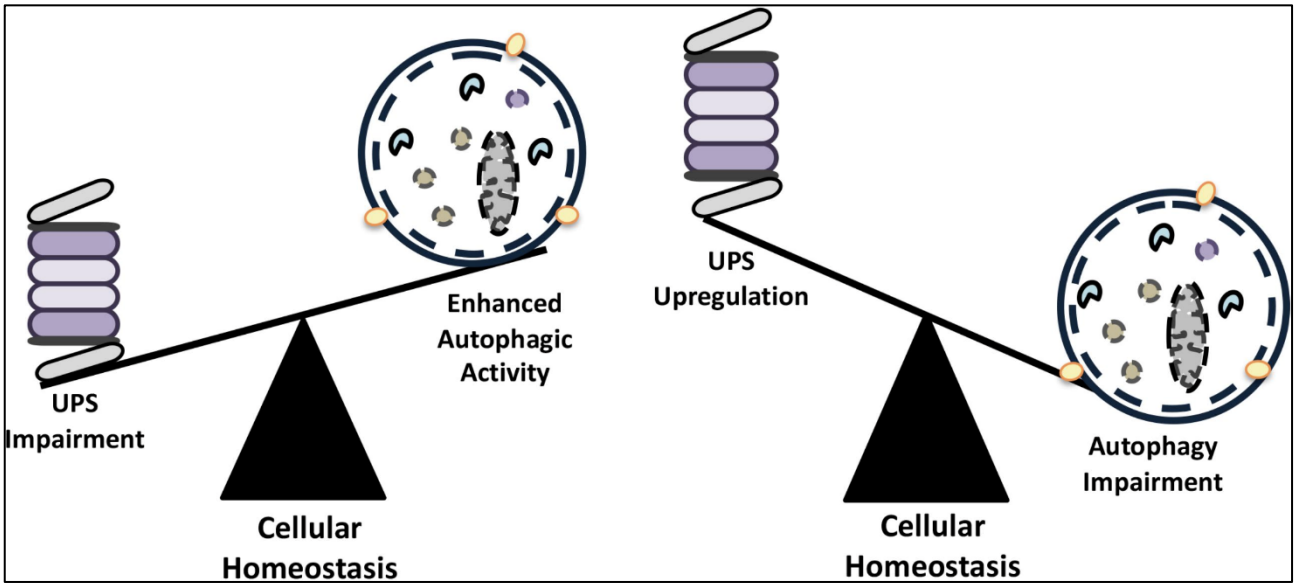

Figure 8: *The activities of autophagy and the UPS requires compensatory balance in order to maintain cellular homeostasis. Impairment in either of the system is compensated by upregulation of the other system. [79]*

Aging is characterized by excessive oxidative stress, DNA damage, defective DNA repair mechanisms together with impaired cellular antioxidant machinery. Increased oxidative stress and impaired protein degradation pathways result in the accumulation of misfolded protein aggregates that further impair proteolysis severely damaging cellular homeostasis (Figure 8) and favoring the onset of neurodegenerative diseases frequently reported in the elderly such as Alzheimer's Disease, Parkinson's Disease, Huntington's Disease etc. Considering AD condition, the increased deposition of Aβ highlights the inefficient removal of misfolded protein. p62/SQSTM1 plays a key role in the selective removal of misfolded proteins. Increased oxidative stress observed in AD has been linked to a decreased expression of p62 in the brain, mostly due to oxidative damage to the p62 promoter [82]. Evidences suggest that increasing the level of p62 before the diseased condition becomes exacerbated could serve as a potent therapeutic tool to counteract the manifestation of the disease.

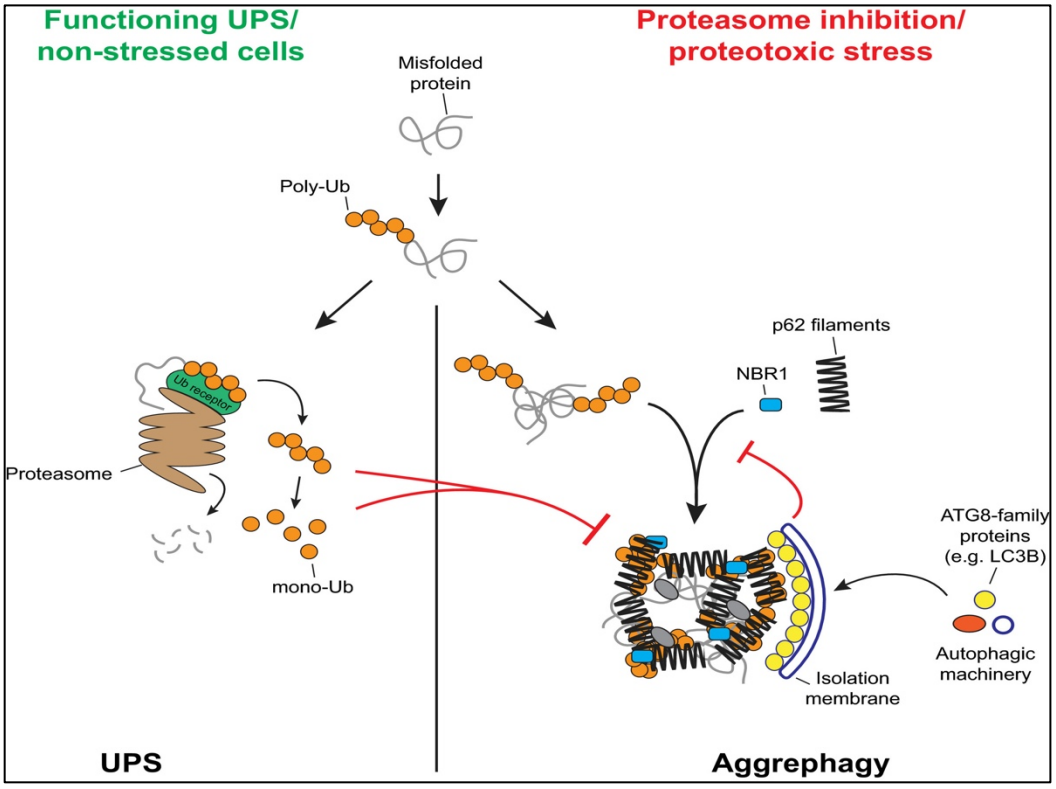

***Figure 9**: p62 sequesters ubiquitinated cargo towards autophagy degradation when UPS is overloaded under stressed condition [83]*

The two major protein degradation processes, the UPS and autophagy, were considered for a long time as two completely independent processes. Conversely, numerous data now indicate that they are strictly correlated and together participate in the maintenance of cellular homeostasis. Interestingly, the signaling molecule ubiquitin marks the protein cargo to be delivered towards one system or the other. In fact, K48-linked polyubiquitin chains target substrates degraded by UPS whereas K63-linked chains or monoubiquitinated substrates are destined to autophagy [84]. The autophagy adaptor protein p62 directs the specifically tagged ubiquitin cargo to be degraded by UPS or the autophagy machinery (figure 9). Its UBA domain binds to the polyubiquitin chain of the target protein and drives the cargo towards its destined degradation machinery. Therefore, p62 becomes a potent target for directing the desired cargo to the specific degradation pathway. Studies have shown that under stress or pathological condition, when the degradation machineries are overloaded or malfunctional, p62 sequesters aggregated cargo to the autophagic machinery for its efficient or bulk degradation [85].

1.3: Gut Microbiota Brain (GMB) axis

Microorganisms that reside in our body include bacteria, virus, fungi and archaea and they are 10 times more abundant than total eukaryotic cells in the body. Their collective genome is estimated as 150 times larger than the human genome [86]. Microbiota inhabits unique niche even inside our body and grows as a community of commensal, symbiotic and pathogenic associations [38]. They colonize different parts of the body that include skin, respiratory tract, urogenital tract and gastrointestinal (GI) tract, with the most dominant (>95%) niche of microbiota residing in the GI tract. These microbes influence and react to neuronal, humoral, metabolic, or immune signaling that together constitute the so-called gut microbiota brain (GMB) axis (figure 10) [87]. Interestingly, a human fetus is without any evident microorganism and has a sterile gut. Microbes colonize and diversify as the child grows and the diversity of the colonizing microbiota is influenced by the gestational age, mode of delivery, diet, environmental factors, level of sanitation and antibiotics exposure [88-91]. The recent advancements in genomic and metagenomic analyses, along with sophisticated microbiota profiling techniques, brought into light the functional interaction between microbiota and host. There is growing body of evidences on the profound interdependency between the microbiome and the central nervous system (CNS) and on their bidirectional communication [92].

The gut microbiota brain axis have challenged the traditional concept of nervous system. The gut-brain axis represents a biochemical signaling system connected to the functions of the sympathetic nervous system, endocrine glands, and specific regions of the brain, such as the hypothalamus and the frontal cortex [38]. It can influence CNS development and behavioral performances in normal as well as in pathological conditions.

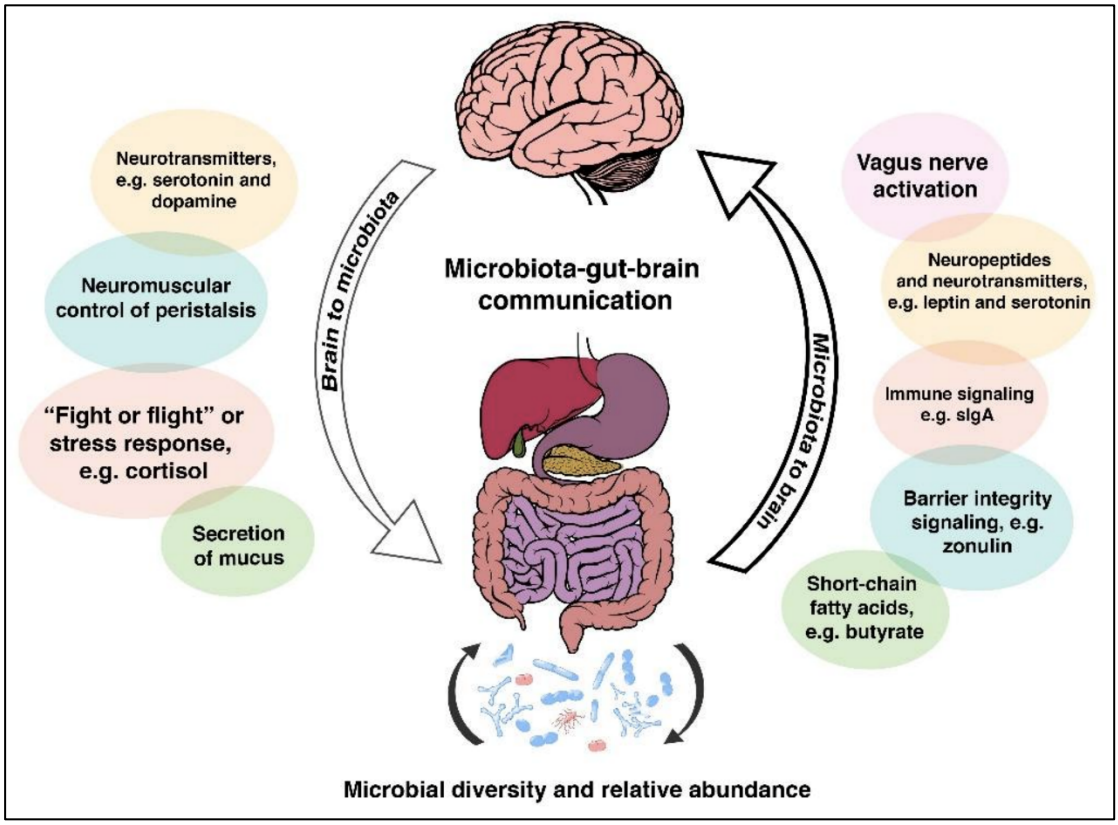

***Figure 10**: An illustration of the bidirectional communication pathways between the gut microbiota and the brain. Range of molecules originating in the gut that are involved in the upstream part of the communication system [93].*

A diverse group of microorganisms was deemed to play multiple roles in the human body that include fermentation of indigestible carbohydrates to produce short chain fatty acid (SFCA), conjugated linoleic acid, gamma-aminobutyric acid (GABA), metabolism of complex proteins and essential substances (bile acids, sterols and drugs), synthesis of Vitamin B and K, and protection against invading pathogens [90, 91] Apart from this communication via sympathetic and parasympathetic nervous system, CNS communicates via both afferent and efferent autonomic pathways (ANS) with muscle and gut mucosal layer. Thus, the brain regulates gut motility, immunity, permeability and secretion of mucus whereas the gut communicates with the hypothalamic–pituitary–adrenal axis (HPA axis)[91] This bidirectional communication plays a critical role in the onset and progression of different neurodegenerative disorders, including AD (figure 11), as described in the following paragraphs.

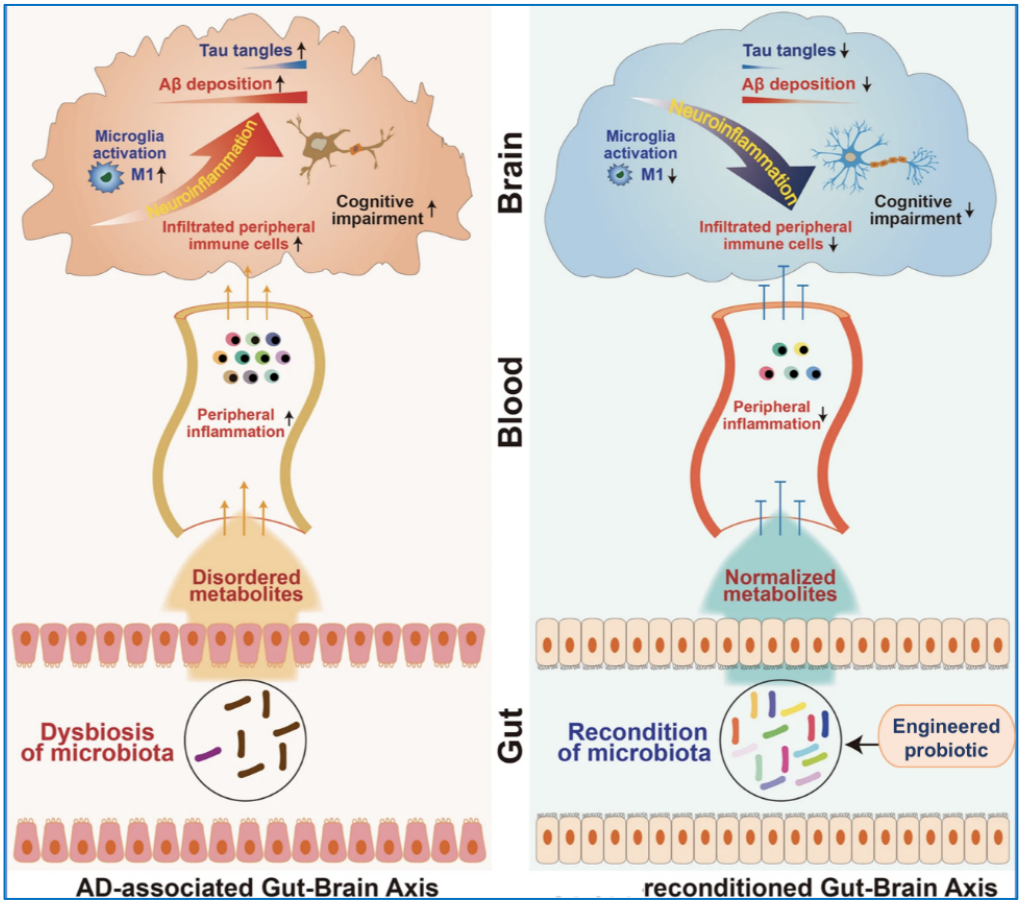

***Figure 11**: Therapeutical remodeling of gut microbiota lowers the progression of AD [fig is modified from [94]]*

1.3.1: Microbiota

The dense and diverse ecosystem of gut microbiota is dominated by bacteria extensively studied in recent years. Accumulating data suggest the involvement of microbiota in host health and pathology. 90% of gut microbiota is represented by two phyla, Firmicutes and Bacteroidetes, along with Actinobacteria, Proteobacteria, Fusobacteria, and Verrucomicrobia, accounting for the dominant microbiota phyla in healthy gut [95]. Firmicutes phylum is composed of more than 200 different genera, with *Lactobacillus*, *Bacillus*, *Clostridium*, *Enterococcus,* and *Ruminicoccus* as the most dominant genera. 95% of the phylum is represented by *Clostridium*. Bacteroidetes consist of predominant genera such as *Bacteroides* and *Prevotella*. The Actinobacteria phylum is proportionally less abundant and mainly represented by the *Bifidobacterium* genus. Firmicutes bacteria are Gram-positive and play a key role in

the nutrition and metabolism of the host through SCFAs synthesis [95]. A relative increase in Gram-negative bacteria is however considered as a major detrimental factor associated with age-related decline in health [96]. A growing body of literature also highlights their crucial role in regulating development, homeostasis, and function of innate and adaptive immune cells of the host body [97].

1.3.2: Mycobiota

The 16s rRNA sequencing revealed about 10^{11} bacterial cells compared to 10^{6}-10^{7} fungal cells present per gram of faecal matter [98]. Despite their lower number, these eukaryotic fungal cells are 10-fold longer and 100 fold larger than the prokaryotic bacterial population. Similar to gut microbiota, gut mycobiota is also strongly influenced by environmental factors like diet, drug exposure, lifestyle and geographical location [99]. Fungal diversity along the GI tract is poorly studied so far, however, it is estimated that the fungal population is relatively stable in the gut while the bacterial concentration increases from stomach to the colon [99-101].

The most common phyla reported in a healthy gut are the *Ascomycota and the Basidiomycota* (representing 70% and 30%, respectively), and the *Zygomycetes[102]*. *Candida* (particularly *Candida albicans*), *Saccharomyces* (particularly *Saccharomyces cerevisiae*), *Penicillium, Aspergillus, Cryptococcus, Malassezia* (particularly *Malassezia restricta*), *Cladosporium, Galactomyces, Debaryomyces* and *Trichosporon* show a lower abundance [99]. These cells remotely influence the host immune system. In early life, intestinal fungi contribute to the maturation of secondary lymphoid organs, it stimulates CD45+CD103+RALDH+ dendritic cells to migrate to the peripheral lymph nodes [103].

1.3.4: Gut microbiota and metabolism

The preservation of a normal and healthy gut microbiota plays a critical role in maintaining a good health. The rational manipulation of intestinal microbiota through appropriate administration of probiotic mixture may attenuate the age-related deficit in long-term potentiation and impact on several regulatory genes as observed in rodent brains [104]. Gut microbiota modulation inevitably impacts key metabolic functions such as glucose homeostasis and bile acid metabolism. Changes in diet can have rapid alteration of gut microbiome composition and affect the insulin sensitivity and glycemic control [105]. SCFA, regulation gut hormone secretion, synthesis of amino acids and systemic levels circulating amino acid are strictly regulated by the gut microbiome community (figure 12) [105].

Accumulating evidences report on impaired gut microbiome community or dysbiosis in individuals with mild to advanced AD [105]. The measure of the *Bacteroidetes/Firmicutes* ratio is a rough method to characterize one's microbiota proportion [106].

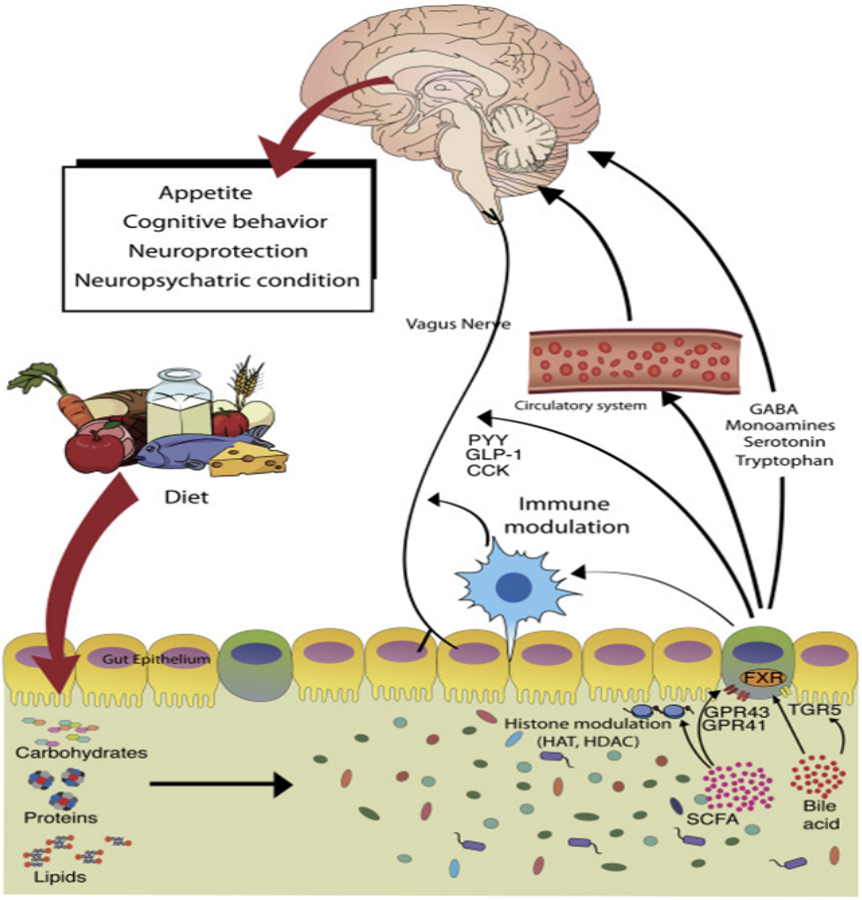

***Figure 12**: Schematic illustration of dietary intake influencing the production of microbial metabolites that communicates to the CNS through systemic circulation [107].*

SCFAs are produced from bacterial fermentation of indigestible carbohydrates in the colon and are the main bidirectional signaling molecules between gut and host metabolic system [108]. In addition, 17–38% of SCFAs are also produced during amino acid catabolism by gut bacteria [90]. SCFAs are able to stimulate endocrine cells of the gastrointestinal tract to synthetize neuroactive compounds like histamine, serotonin, γ-aminobutyric acid, β-alanine, peptide YY, ghrelin and leptin [109-111]. Gut peptide hormones are another major signal modulator between the midgut and other peripheral organs/tissues [112]. Ghrelin and leptin are neurotrophic hormones [60, 113]. Ghrelin affects both glucose and lipid metabolism and also influences mitochondrial respiration and exerts neuroprotective effects. It is involved in the aetiopathogenesis of neurodegenerative disorders, representing a link between metabolism and neurodegeneration [114]. Plasma leptin concentration is inversely correlated with Aβ levels due to its direct regulatory effect on γ-secretase [115] Also, the treatment with leptin reduced both Aβ and p-tau levels in AD animal models [116, 117]. Reduced cerebral insulin growth factor I (IGF-I) level is associated with compromised Aβ clearance [33] and reduced proteolysis of oxidized proteins by the proteasome [118].

The regulation of secretion of several gut hormones, including GLP-1 and the anorectic hormone peptide YY (PYY), is influenced by SCFAs [119]. They are known to regulate energy homeostasis and glucose metabolism upon food intake and also modulate various nervous functions such as learning and memory [60, 120, 121]. The dominant gut commensal microbiota (*Lactobacillus plantarum* and *Acetobacter pomorum*) is considered as a major regulator of the systemic insulin signaling [112]. A novel formulation of lactic acid bacteria and bifidobacteria (namely SLAB51) was observed to defend cognitive decline, reduce Aβ aggregates and brain damages through influencing key systemic metabolic functions in 3xTg-AD mice model of AD [122]. Oral administration of SLAB51

improved energy metabolism through enhancement of glycolysis and gluconeogenesis. Mice plasma had increased concentrations of glucagon-like peptide-1 (GLP-1) and glucose-dependent insulinotropic polypeptide (GIP) [122, 123].

Gut peptide hormones, also known as incretin hormones, such as GLP-1 and GIP, are able to stimulate insulin secretion and control the blood glucose level [106]. 4-weeks supplementation with *Lactobacillus reuteri* improved GLP-1, insulin, and C-peptide levels in response to an oral glucose load, but did not alter insulin sensitivity in glucose-tolerant adults [124].

1.3.5: Gut microbiota and neuroprotection

Neuroinflammation plays a central role in the pathogenesis of AD. A cascade of molecular events involves the activation of microglia, CNS-resident macrophages and primary immune cells of CNS. Dysbiosis and intestinal infection can trigger systemic immune response and cerebral inflammatory processes in AD (figure 13) [93]

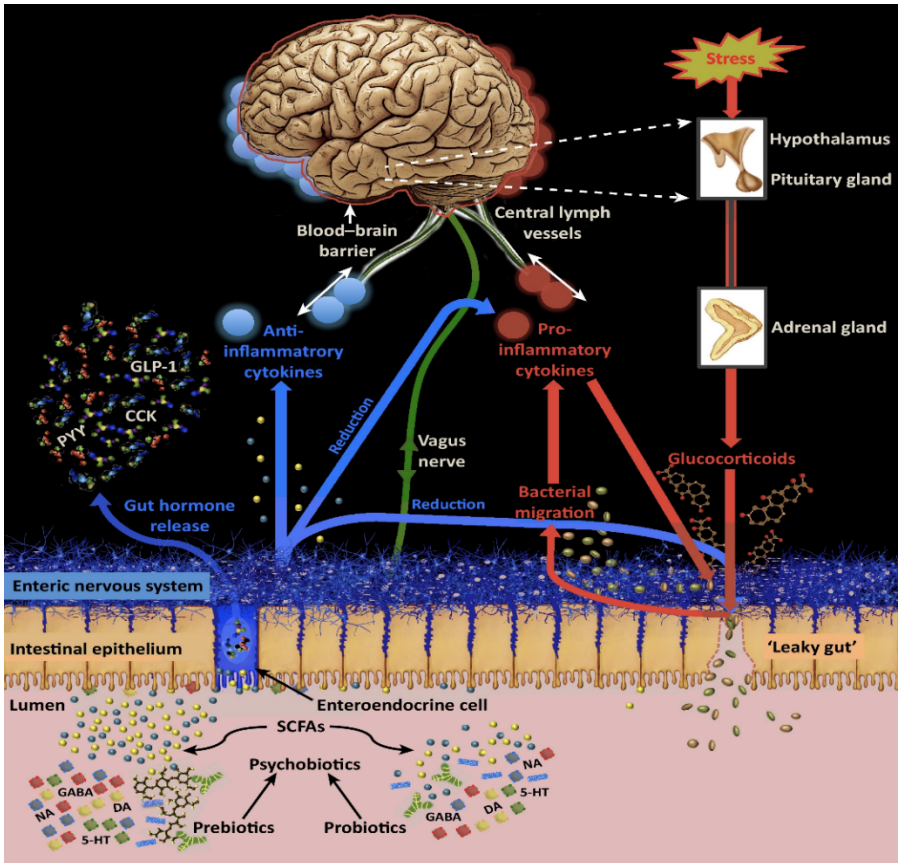

Figure 13: *Overview of psychobiotic (probiotics and prebiotics that confer mental health benefits) action. Neuroprotective and anti-inflammatory signals from enteric system to the CNS are indicated with blue arrows. Bacterial infiltration and elicitation of neuroinflammation in response to stress are indicated by red arrows [90].*

Under physiological conditions, microglia monitor brain microenvironment to ensure neuronal health. Upon exogenous stimuli or endogenous dangers, microglia get rapidly activated and phagocytize pathogens, including toxic Aβ and damaged neurons. With the elimination of harmful stimuli, neuroinflammation is resolved and microglia return to its resting state [125]. However, the chronic inflammation present in AD implies a constant release of proinflammatory cytokines. IL-1β, TNFα and IL-6 are pronouncedly up-regulated in AD tissues and prominently associated with AD lesions.

Interestingly, SCFAs are identified as key mediators of gut microbiota-microglia interaction. These anti-inflammatory bioactive bacterial metabolites can translocate from colonic mucosa and can affect CNS function [125]. They can directly regulate the expression of the gene coding for tryptophan hydroxylase, the key enzyme in the serotonin biosynthesis pathway [126]. SCFAs interfere with the activity of DNA repair enzymes by decreasing the functionality of chromosome histone deacetylases (HDACs); for example, the HDAC inhibitor 4-phenylbutyrate was investigated for its ability to restore dendritic spine density in the hippocampus of Tg2576 mice, coupled with decreased Aβ load and tau phosphorylation, producing positive effects on cellular protein homeostasis [127].

A growing body of studies has highlighted changes in relative abundance of taxa in cognitively impaired individuals. Elderly population showed increased abundance of the pro-inflammatory bacteria *Escherichia/Shigella*, whereas individuals with evidence of amyloid deposition on PET imaging exhibited decreased abundance of the anti-inflammatory bacteria *Eubacterium rectale* [128].

Our lab has recently reported on the beneficial properties of SLAB51, a formulation of lactic acid bacteria and bifidobacteria able to modulate microbiota in 3xTg-AD mice increasing the relative abundance of *Bifidobacterium* spp. and decreasing *Campylobacterales*, bacterial groups differently

involved in the regulation of inflammatory pathways. These changes in microflora composition, together with enriched gut concentration of SCFAs and increased plasma levels of neuroprotective gut peptide hormones, contributed to counteract cognitive decline through a reduction in Aβ aggregates and brain damages, and a partial restoration of impaired neuronal proteolytic pathways [122]. SLAB51-mediated microbiota modulation also mitigated oxidative stress by activating SIRT1-dependent mechanisms and restored glucose homeostasis in 3xTg-AD mouse brain [38, 129].

ProBiotic-4, another formulation containing *B. lactis, L. casei, B. bifidum* and *L. acidophilus*, significantly improved cognitive functions and attenuated intestinal and BBB injury in aged SAMP8 mice through inhibition of both TLR4 and RIG-I-mediated NF-κB signaling pathways and inflammatory responses [130]. Short-term administration of *Bifidobacterium breve* strain A1 prevented cognitive decline in AD mice, with a reduction in the immune response and neuronal inflammation. However, the authors did not detect a marked effect on intestinal microbiota composition, indicating the involvement of other mechanisms in the overall probiotic effect, such as the gut–brain communication via stimulation of the vagus nerve [131]

1.4: Mechanistic insight of autophagy regulation in neurodegeneration

1.4.1: Cog Complex (Conserved Oligomeric Golgi) and neurodegeneration

Eukaryotic cells have strict mechanism for docking and fusion of intracellular transport carriers tightly regulated by multi-subunit tethering complexes (MTC) that sequentially and/or simultaneously interact with other components of vesicle docking and fusion machinery [132, 133]. The main MTC functioning at the Golgi is the Conserved Oligomeric Golgi (COG) complex, a key player in intra-Golgi retrograde trafficking [134, 135]. The COG complex is conserved throughout evolution. The complex comprises 8 proteins, termed COG1 - COG8, which form two lobes: lobe A (COG1-4) and lobe B (COG5-8). The lobes are interconnected by interactions between COG1 and COG8 (figure 14) [136].

As a tethering complex, the COG complex interacts with multiple Soluble NSF Attachment protein Receptors (SNARE), both in the intra-Golgi and trans-Golgi, thereby assisting retrograde transport of vesicles [137]. The essential function of the COG complex is dependent upon interactions with other components of the trafficking machinery, such as Rab-GTPases and SNAREs. COG-interacting Rabs and SNAREs have been implicated in neurodegenerative diseases, like Alzheimer's disease and Parkinson's disease [138]. Defects in Golgi maintenance disrupt trafficking and processing of essential proteins, frequently associated with compromised neuronal function and human diseases. Recent studies have shown that impairments in COG complex interrupt the autophagic pathway and that its mutations are associated with severe disruptions of the autophagic machinery, although the exact contribution is yet to be fully understood. Autophagy-related (ATG) proteins regulate and control different steps of autophagy. The localization of Atg8/LC3 (a marker of autophagosomes) and Atg9A (which is essential for double-membrane vesicle formation) to the site of autophagosome formation was disrupted in COG mutants under autophagy-inducing conditions [139]. The endoplasmic reticulum-

Golgi intermediate compartment (ERGIC) and the reticular trans-Golgi network (rTGN) integrity are essential to provide a template for LC3 lipidation and further ubiquitination[140].

.

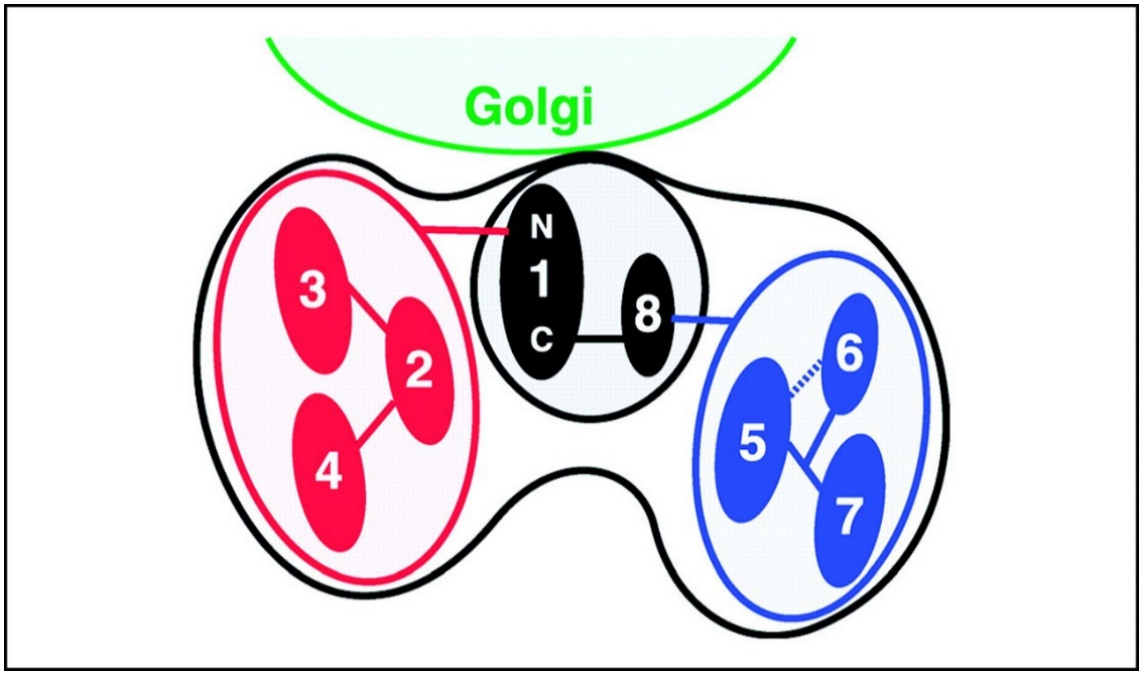

***Figure 14**: Proposed model of COG architecture. Lobe A consists of COG1-4, lobe B consists of COG5-8, both lobes are connected through COG1 and COG8 [136].*

There is a growing number of reports on the involvement of the COG complex in the autophagosome formation and on its role in the correct sorting of various ATG proteins and autophagy receptors to the omegasome or to the growing autophagosome [139].

1.4.2: Impact of COG complex on Atg9 trafficking and spatial translocation of Atg9A sorting from TGN to ERGIC

ATG9A is the only multi-spanning membrane protein in the autophagic pathway and it has been shown to deliver membranes from the TGN to the phagophore [141]. Supporting this hypothesis, it was revealed that in yeast, inefficient transport of ATG9A from the Golgi, due to defects in the COG complex, leads to a compromised autophagic pathway [139]. Golgi regulates the transport of Atg9A that serves as a membrane source for the growing phagophore [141]. A study from Schekman's lab revealed that there is an additional pathway from the endoplasmic reticulum exit site (ERES) to the ERGIC for autophagosome biogenesis (figure 15). In details, starvation induced phosphatidylinositol 3-kinase (PI3K) that drives the COPII machinery from ERES to ERGIC to form autophagic COPII vesicles. These structures will provide precursor membrane templates for LC3 lipidation and phagophore initiation [142, 143].

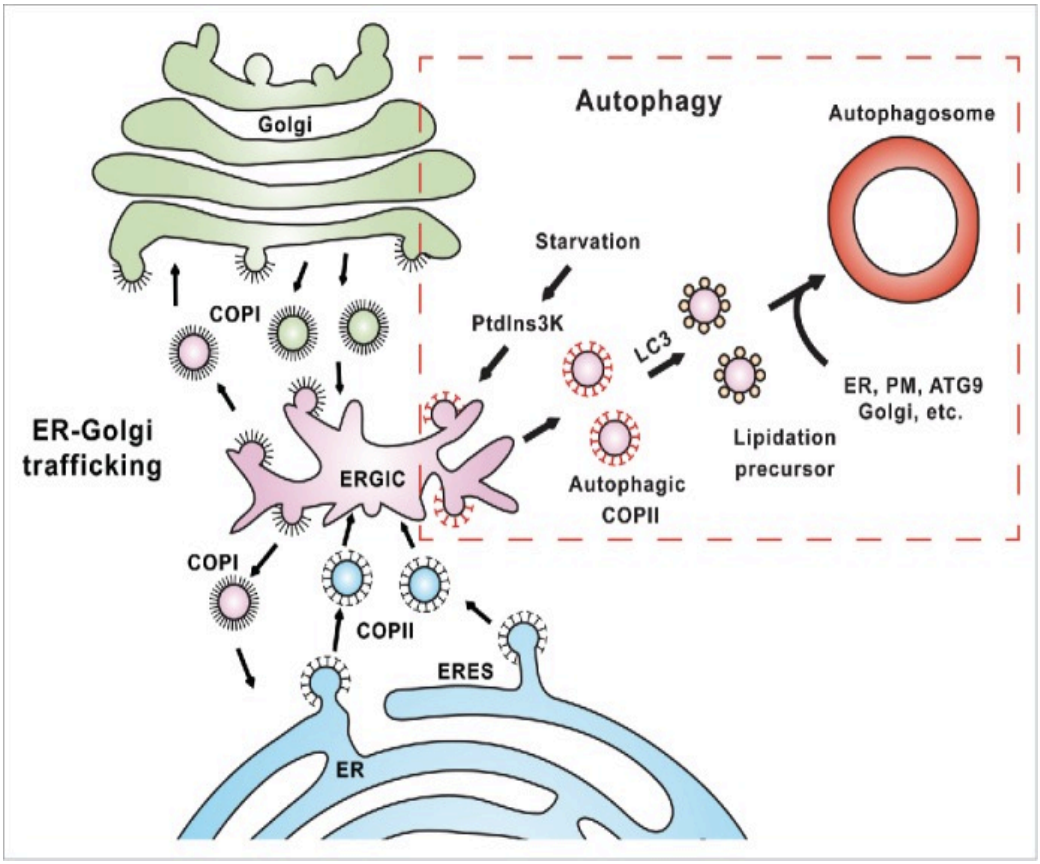

***Figure 15**: A suggested model for the diversion of COPII machinery from ER-Golgi trafficking to autophagosome biogenesis [142].*

ER and Golgi are sites for glycosylation, a highly dynamic process that approximately requires the 2% of the human genome to encode enzymes and trafficking components for the proper maturation of newly formed glycan chains [144]. COG deficiency can cause a redistribution of COG-dependent Golgi resident proteins, including glycosylation enzymes [138]. In addition, COG regulates the recycling of vesicles containing glycosylation enzymes and other resident Golgi proteins in a *trans*-to-*cis* (retrograde) direction [138, 145]. A recent report from Guardia *et al.*, that used high-resolution cryoelectron microscopy, revealed the structure of Atg9A consisting of a homotrimer with a complex network of internal cavities [146]. Mutations in this structure lead to smaller autophagosomes [147].

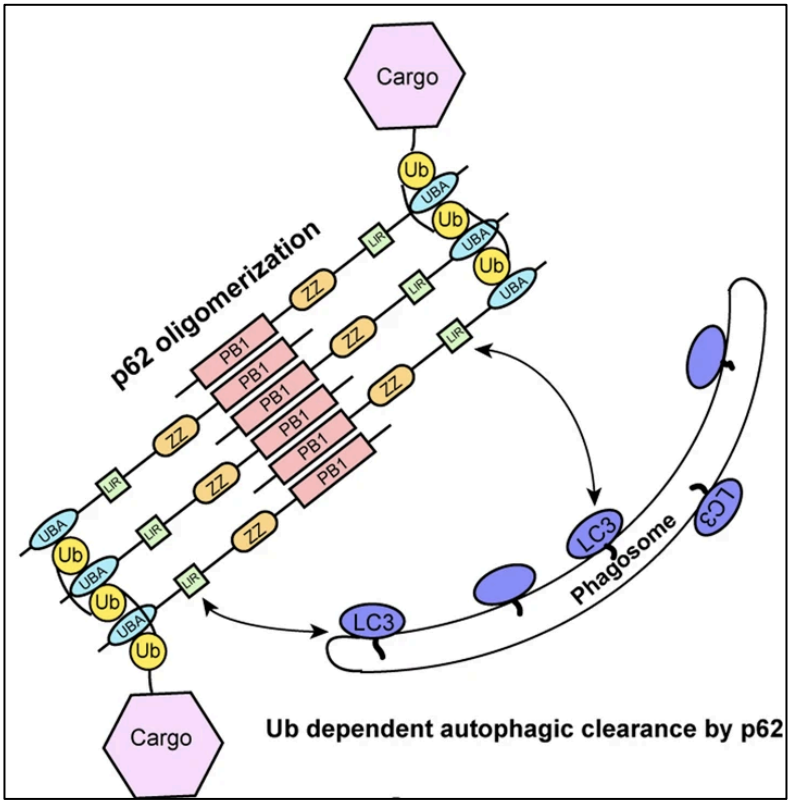

***Figure 16**: p62 oligomerizes through its N-terminal PB1 domain and delivers ubiquitinated cargo to the growing phagophore for autophagic degradation [148].*

p62, on the other hand, which is a scaffold protein that binds with ubiquitin and LC3 via its C-terminal UBA and LIR domain, respectively, oligomerizes through its N-terminal PB1 domain and delivers ubiquitinated cargo to the growing phagophore for autophagic degradation (figure 16) [83]. Starvation increases p62 molecular weight, which can be reversed by serum supplementation suggesting structural remodeling of p62 [149]. Therefore, we wanted to verify if COG3 knockout (KO), which is known to be involved in ER-Golgi transport, could have any influence on Atg9A and, if yes, how Atg9A are recruited. In addition, we checked if it can also impact LC3 lipidation and induce structural modification in p62.

Neurodegenerative disorders characterized by misfolded protein aggregation are hard to address and to cure the pathological consequences. Here, we have shown different strategies through which AD markers can be counteracted exploiting the bidirectional communication between the gut and the brain, the so-called gut-brain axis. We have explored the role of the probiotic formulation SLAB51, of an engineered Lactobacillus strain expressing p62 and of moderate consumption of beer in mitigating the pathological conditions of progressing AD in 3xTg-AD mice. The different strategies explored in this study can successfully ameliorate the impaired cerebral glucose metabolism and neuronal proteolytic processes through enhanced autophagy, favoring the reduction of abnormal tau hyperphosphorylation and removal of Aβ load. Further, we have also explored the effect of moderate beer consumption to protect against neurodegenerative conditions through microbiota modulation. Additionally, the

mechanism of autophagy regulation is also dissected under severe conditions of Golgi fragmentation, prevalent in many neurodegenerative diseases.

RESULTS

Chapter 2: Role of gut microbiota manipulation in glucose homeostasis

2.1: Materials and methods

2.1.1: Reagents and chemicals

SLAB51 probiotic formulation has been provided by Ormendes SA (Jouxtens-Mézery, Switzerland, https://agimixx.net). SLAB51 contains 8 different live bacterial strains: *Streptococcus thermophilus* DSM 32245, *Bifidobacterium lactis* DSM 32246, *B. lactis* DSM 32247, *Lactobacillus acidophilus* DSM 32241, *Lactobacillus helveticus* DSM 32242, *Lactobacillus paracasei* DSM 32243, *Lactobacillus plantarum* DSM 32244, and *Lactobacillus brevis* DSM 27961. Membranes and reagents for western blotting analyses were purchased from Merck KGaA (Darmstadt, Germany). ELISA kit for HbA1c measurement was from MyBioSource (San Diego, CA, USA).

2.1.2: Animal model

AD triple-transgenic mice, B6;129-Psen1^{tm1Mpm} Tg (amyloid precursor protein [APP]Swe, tauP301L)1Lfa/J (named 3xTg-AD) and the wt B6129SF2 mice (separate line), were purchased from the Jackson Laboratory (Bar Harbor, ME, USA). 3xTg-AD mice contain 3 mutations associated with frontotemporal dementia or familial AD (APPSwe, tau MAPT P301L, and presenilin-1 M146V). This reliable model of human AD displays both plaque and tangle pathology, with Ab intracellular immunoreactivity detectable at 3 months of age and hyperphosphorylation of tau protein occurring by 12-15 months of age [150]. Experiments were in accordance with the guidelines laid down by the European Communities Council (86/609/ECC) for the care and use of laboratory animals and with a protocol approved by the Italian Ministry of Health (518/2018-PR). Mice were housed in plastic cages (Makrolon, Covestro A.G., Filago, Italy) (4 animals per cage) in a temperature- controlled room (21 5 C) and 60% humidity on 12-hour light/ dark reversed cycle (light was switched on at 8:00 p.m.) and

maintained on laboratory diet (Mucedola, Italy) and water ad libitum. Appropriate measures minimized pain and discomfort in experimental animals.

2.1.3: Experimental design

Eight-week-old AD male mice (n= 48) were divided in 2 groups: one administered SLAB51 dissolved in water (n = 24), and the control group administered water (n = 24). Simultaneously, 48 age-matched wt mice were organized into wt control (n = 24) and wt treated (n = 24) groups. The dosage of SLAB51 (200 billion bacteria/kg/d) was determined by application of the body surface area principle. The body weight was monitored during the treatment to ensure single-housed animals received the proper intake of the probiotic. Preliminary studies were performed to evaluate both viability and stability of the probiotic formulation on solubilization in water at 21 $\pm$ 5°C. The percentage of vital bacteria was determined, for the entire time course of the experiment, by fluorescence microscopy, which revealed that 88% of the strains survived after 30 hours under the aforementioned conditions. Thus, probiotic drinking solution was freshly prepared every day. Eight mice per group were euthanized by CO_2 overdose at 8, 24, and 56 weeks of age, and the tissues were properly collected for both biochemical and immunohistochemical analyses. In detail, murine brains were quickly removed and placed on an ice-cold glass plate. Coronal sections were sagittally bisected: one portion was immediately frozen in liquid nitrogen and stored at -80°C for biochemical analysis, and the other was fixed in 10% formalin for 8-10 hours, properly washed in PBS, dehydrated, and embedded in paraffin for sectioning.

2.1.4: Preparation of brain extracts

On sacrifice, brain was homogenized (1:5 weight/volume of buffer) in 50 mM Tris buffer, 150 mM KCl, 2 mM EDTA, pH 7.5. Homogenates were immediately centrifuged at 13,000 g for 20 minutes at 4°C and the supernatants were used. Protein concentration was measured with the Bradford protein assay [151].

2.1.5: Western blotting analyses

Brain homogenates were analyzed through western blotting assays to measure the levels of GLUT3(Abcam), GLUT1(Abcam), IGF-IRβ(Santa Cruz Biotechnology), AMPK(Cell Signaling Technology Europe BV), p- AMPK(Cell Signaling Technology Europe BV), Akt(Cell Signaling Technology Europe BV), p-Akt, tau(Santa Cruz Biotechnology), p-tau(Abcam), and AGE(Abcam). In detail, for each time point, brain homogenates (30-mg total protein) were separated through SDS-PAGE on 10% or 12% gels, and electroblotted onto poly- vinylidene fluoride membranes. Successively, on incubation with specific antibodies, the immunoblot detections were carried out with an enhanced chemiluminescence (ECL) western blotting analysis system. Molecular weight markers (6.5-205kDa) were included in each gel. Glyceraldehyde-3-phosphate dehydrogenase (GAPDH) was used to check equal protein loading. The densitometric analysis has been conducted as previously described (34). Briefly, each western blot was scanned (16-bit gray scale) and the obtained digital data were processed through Image J (NIH) to calculate the background mean value and its standard deviation. The background-free image was then obtained subtracting the background intensity mean value from the original digital data. The integrated densitometric value associated with each band was then calculated as the sum of the density values over all the pixels belonging to the considered band having a density value higher than the background standard deviation. The band densitometric value was then normalized to the relative GAPDH signal intensity. The ratios of band intensities were calculated within the same western blot. All the calculations were carried out using the MATLAB environment (The MathWorks Inc, Natick, MA, USA). For AGE, both bands have been included in the analysis.

2.1.6: Immunohistochemical analysis

The effects of SLAB51 on glucose transporters GLUT3 and GLUT1 in specific brain regions were investigated immunohistochemically (IHC). Three 3 mm-thick brain sections from each animal (n=8 per sub-group), at ~0.84, 1.20, and 1.56 mm lateral from the midline, were prepared.

Selected sections were deparaffinized and rehydrated according to standard protocols and used for GLUT1, GLUT3, and p-tau immunohistochemical detection. For each time point, brain sections from treated and untreated wt and AD mice (n = 8 per subgroup) were fixed in a 50:50 mixture of methanol and acetone for 5 minutes and incubated with the specific antibody. For GLUT1 detection, brain sections were incubated overnight with anti-glucose transporter GLUT1, diluted 1:100, cross-reacting with mouse, rat, and human. For GLUT3 detection, brain sections were incubated overnight with anti-glucose transporter GLUT3, diluted 1:150, cross-reacting with mouse, rat, and human. Nonspecific binding was blocked by incubation for 10 minutes with a protein-blocking agent (Dako, Carpinteria, CA, USA) before overnight incubation with the primary antibody in a moist chamber. The immunoreaction with streptavidine-immunoperoxidase (Abcam, Cambridge, UK) was visualized with 3,3'-diaminobenzidine substrate (Vector Laboratories, Burlingame, CA, USA). Tissues were counterstained with Mayer's hematoxylin. For negative immunohistochemical controls, the primary antibodies were omitted.

In addition, fibrillar deposits of highly phosphorylated tau in brain samples were visualized immunohistochemically using the rabbit monoclonal antibody [EPR2605] to p-tau (phosphor-S404) diluted 1:150. The binding of the antibody was detected with the Elite kit (Vector Laboratories), and the immunoreaction was developed using 3,3'-diaminobenzidine substrate (Vector Laboratories). Positive cells were quantified in different brain areas from 10 appropriate fields and arithmetic means were calculated for each brain region. Results are expressed as IHC-positive cells per 62,500 mm^2. For all parameters, cells on the margins of the tissue sections were not considered for evaluation to avoid inflation of positive cell numbers. Positive cells were quantified using an image-analysis system consisting of a light microscope (Carl Zeiss, Jena, Germany), attached to a Javelin JE3462 high-resolution camera and a personal computer equipped with a Coreco-Oculus OC- TCX frame grabber and high-resolution monitor. Computerized color-image analysis was performed by using Image-Pro Plus software (Media Cybernetics, Rockville, MD, USA). The entire cerebral cortex and hippocampus were

separately sampled with the counting frame size 250 mm 250 mm for cortex and 100 mm 100 mm for hippocampus. The area of each section in all brain cross- sections in each mouse was recorded, as was the total number of neurons determined by immunostaining as previously described. For each mouse, the total brain area was calculated as the sum of the areas of all fields in all brain cross-sections on one slide. For GLUT1 and GLUT3, positive cells were counted per section, and stained cell densities were expressed as the number of cells per square millimeter of analyzed section area [152]. The area of interest in the hippocampus was CA1. p-tau immunoreactive area was measured in the threshold segmented cortical and hippocampal regions of interest and normalized to the total region of interest area. The pathologist performing quantification of amyloid burden was blind to age, treatment type, and genotype of mice.

2.1.7: ELISA assay for HbA1c levels determination

Glycated hemoglobin concentration was measured in plasma samples promptly supplemented with protease inhibitors (Pefabloc and TPCK) using a Mouse Glycated hemoglobin A1c ELISA Kit (MyBioSource) according to the manufacturer's instructions. of SLAB51 treatment, statistical significance of treated mice compared with age-matched untreated mice of the same genotype is indicated with hashtags (#$p < 0.05$).

2.1.8: Statistical analysis

Biochemical and IHC data are expressed as mean values standard error (S.E.). Statistical analysis was performed with one-way ANOVA, followed by the Bonferroni test using Sigma-Stat 3.1 software (SPSS, Chicago, IL, USA). Statistical significance of treated mice compared with untreated 8-week-old mice of the same genotype is indicated with asterisks (*$p < 0.05$). To describe the effect of SLAB51 treatment, statistical significance of treated mice compared with age-matched untreated mice of the same genotype is indicated with hashtags (#$p < 0.05$).

2.2: Results

2.2.1: SLAB51 oral administration influences glucose uptake in AD mice

GLUT3 and GLUT1 are the major neuronal glucose transporters. IHC analysis showed a decrease of both proteins of AD untreated mice at 56 weeks compared with 8 weeks of age, particularly in the hippocampal CA1 region (Fig. 17A), in the subgranular zone and the molecular layer of the dentate gyrus for GLUT3, and in the blood capillaries of the dentate gyrus for GLUT1 consistently with previous reports [153]. Positive cells significantly increased in treated animals at 56 weeks of age relative to age-matched untreated animals. Western blotting analyses confirmed that expression levels of both GLUTs significantly decreased in untreated 56-week-old AD mice, in agreement with the impaired functionality of brain cells [154], and were restored with SLAB51 treatment (Fig. 17B), suggesting a positive effect of probiotic oral consumption on glucose uptake. No significant variations have been observed in the wt group.

Several key regulators can influence the expression level of GLUTs. Interestingly, the AMPK activity plays a central role in cellular glucose uptake, with increased activity interfering with the expression of GLUTs. In fact, AMPK has been characterized as a critical regulator of cellular function in response to energy stress within cells. Accordingly, increased levels of total AMPK were detected in aged AD mice with respect to 8-week-old mice (Fig. 18A). The phosphorylated form of AMPK, corresponding to the activated form, increased in untreated AD mice at 24 and 56 weeks of age compared with 8 weeks of age, and diminished with SLAB51 treatment in the 24- and 56-week-old mice relative to the age- matched untreated mice. No significant variations were observed in wt animals. Akt is another kinase implicated in regulating the translocation and the biosynthesis of insulin- sensitive glucose transporters in most cell types. AD mice showed an increase of the phosphorylated/activated form of Akt that was only significantly mitigated with SLAB51 treatment at 56 weeks of age. Again, no significant variations were observed in wt animals (Fig. 18B). Functional abnormalities of these critical

metabolic sensors (both AMPK and Akt) cause energy metabolism impairment and correlate with tau hyperphosphorylation, which is one of the main features of AD.

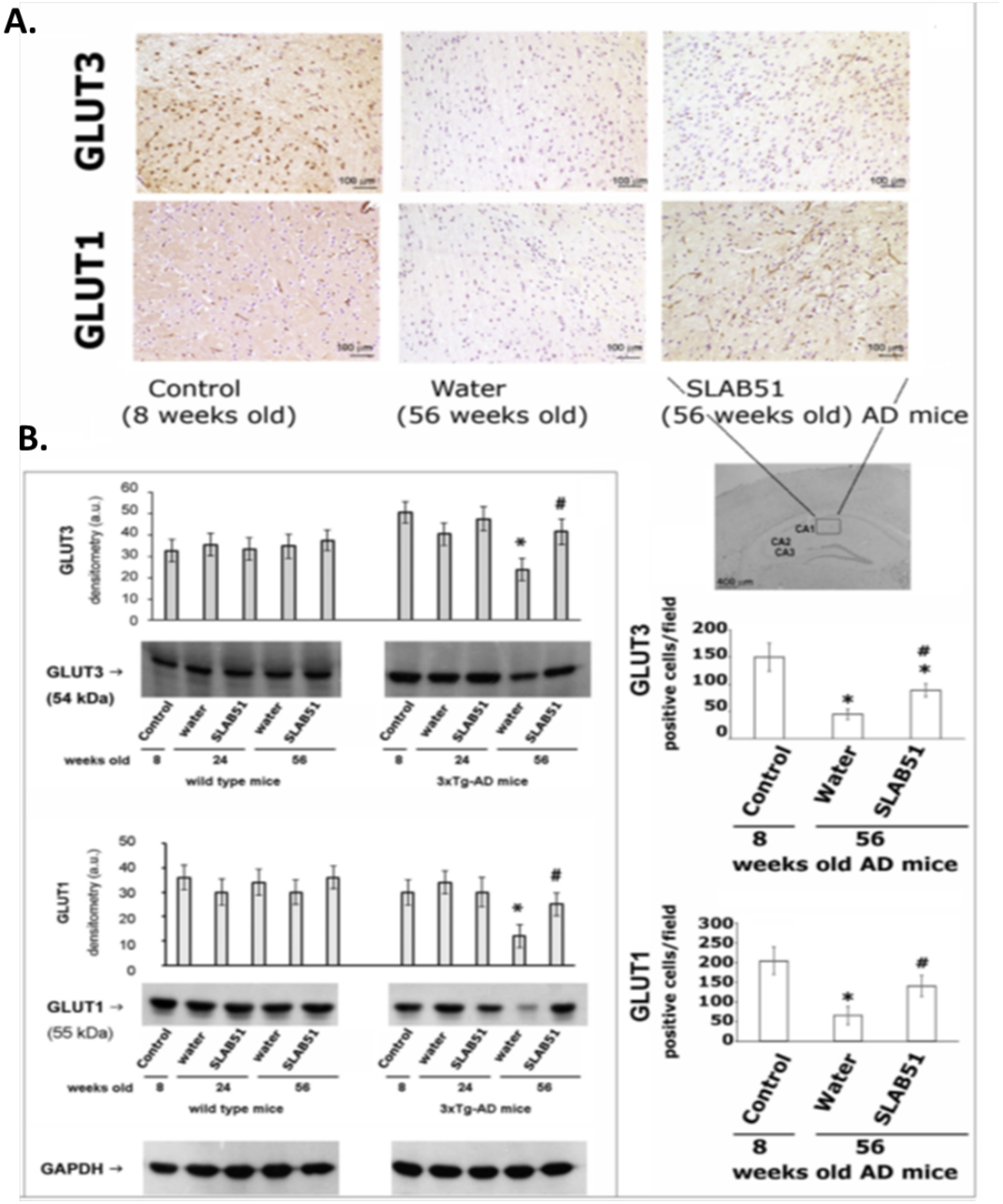

Figure 17: *Glucose transporters in the brain of wt and AD mice orally administered with SLAB51 for 16 and 48 weeks. (A): GLUTs IHC staining. Immunodetection of GLUT3 and GLUT1 proteins in brain sections of 8- and 56-week-old AD mice. Representative images of immunohistochemical staining of hippocampal area CA1 are shown (the hippocampal region of interest is indicated in the 5image). The histograms show the GLUT3- and GLUT1-positive cells/field, respectively. (B): GLUT3 and GLUT1 brain expression levels. Representative immunoblots obtained from ECL western blotting analysis system and corresponding densitometric analyses derived from 6*

*separate blots are shown. Equal protein loading was verified by using an anti-GAPDH antibody. In A and B, data points marked with an asterisk are statistically significant compared with 8-week-old untreated control mice of the same genotype (*p < 0.05). Data points marked with a hashtag are statistically significant compared with age-matched untreated mice (#p < 0.05).*

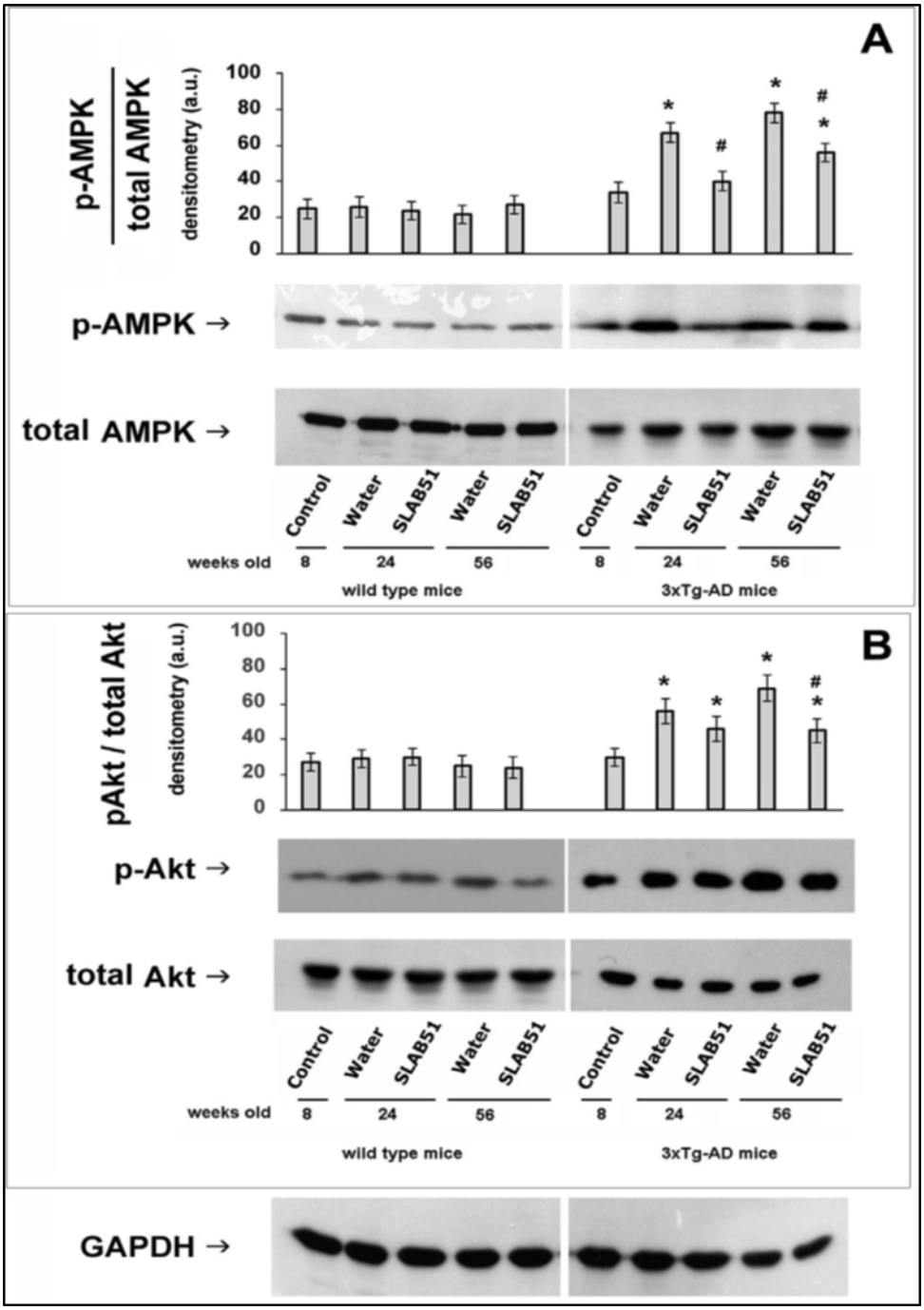

Figure 18 *:Phosphorylation levels of AMPK (A) and Akt (B) in wt and AD mice orally administered with SLAB51 for 16 and 48 weeks. Representative immunoblots and the ratio of intensity of the bands for p-AMPK/total AMPK and p-Akt/total Akt are reported. Equal protein loading was verified by using an anti-GAPDH antibody. The detection was performed using an ECL western blotting analysis system. Data points marked with an asterisk are statistically significant compared to 8-week-old untreated control mice (*p< 0.05). Data points marked with a hashtag are statistically significant compared to age-matched untreated mice (#p < 0.05).*

2.2.2: Phosphorylated tau levels in SLAB51-treated mice

The extent of tau phosphorylation was evaluated using a p-tau (Ser404) antibody by western blotting and IHC. As expected, p-tau increased in untreated 24- and 56-week-old AD mice (Fig. 19). Western blotting analysis revealed a significant decrease of p-Tau levels in the brains of mice treated with SLAB51 (Fig. 19A). IHC staining of brain sections showed progressive accumulation of p- tau in the hippocampus of untreated AD mice between 8 and 56 weeks of age. The process culminated in the formation of differently sized aggregates especially in the hippocampus of 56- week-old untreated AD mice in association with some morphological evidence of hippocampal atrophy. Hyperphosphorylated tau aggregates decreased in number and size in treated animals at both 24 and 56 weeks of age (Fig. 19B).

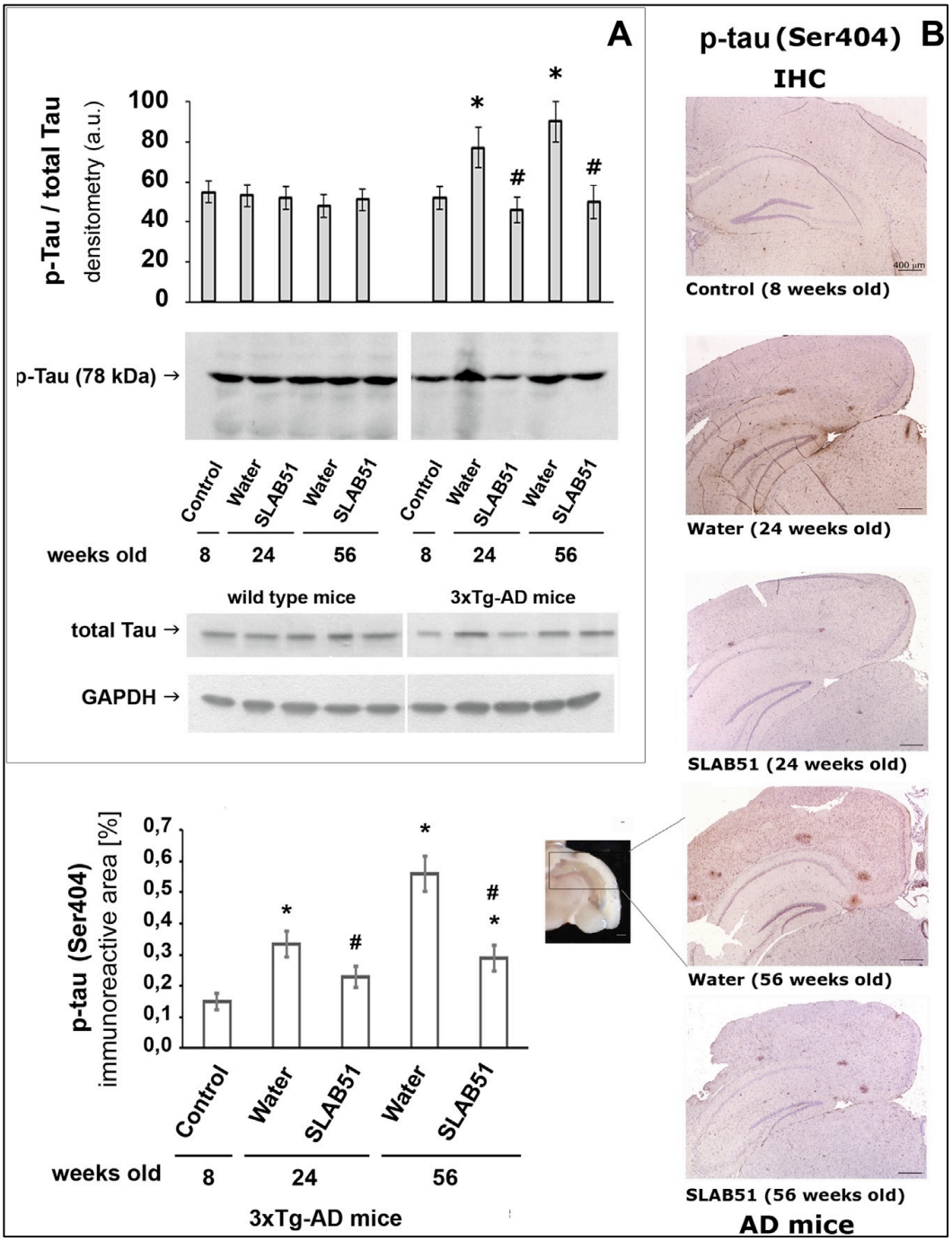

Figure 19: *Phosphorylated tau levels in wt and AD mice treated with SLAB51 for 16 and 48 weeks. (A): Representative immunoblots and the ratio of intensities of the bands p-tau/total tau are shown. Equal protein loading was verified by using an anti-GAPDH antibody. The detection was executed by an ECL western blotting analysis system. (B): p-tau (Ser404) IHC staining. Representative images of p-tau IHC staining are shown. Magnification 5x, Bars = 400 mm. The histogram shows p-tau immunoreactive area [%]. Data represent 5 sections for each brain (n = 8). In A and B, data points marked with an asterisk are statistically significant compared with 8-week-old mice (*p < 0.05). Data points marked with a hashtag are statistically significant compared to age-matched untreated mice (#p < 0.05)*

2.2.3: Glycated hemoglobin plasma levels

Elevated fasting serum glucose and insulin resistance have been linked to decreased memory and AD. Considering that glycated hemoglobin is currently considered an excellent indicator of insulin resistance and a reliable retrospective index of average blood glucose level [155], plasma concentrations of HbA1c were measured in control and treated groups of mice. Fig. 20 shows an age-dependent increase of HbA1c in untreated AD mice. SLAB51 attenuated the increase in HbA1c plasma concentrations, proving that this probiotic mixture positively in- fluences glucose metabolism in AD mice.

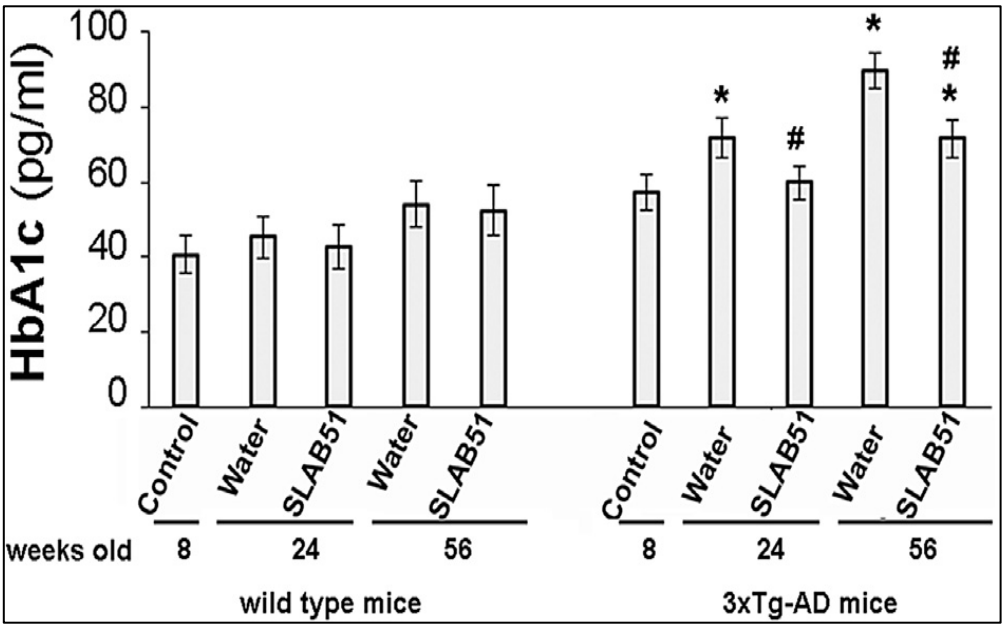

***Figure 20** : Glycated hemoglobin plasma concentrations. HbA1c plasma concentration of both wt and AD mice are expressed as picograms per milliliter. Data points marked with an asterisk are statistically significant compared to 8-week-old untreated control mice (*p < 0.05). Data points marked with a hashtag are significantly different compared to age-matched untreated mice (#p < 0.05).*

2.2.4: Insulin-like growth factor-I receptor brain expression

It has been largely described that the dysregulation of blood glucose homeostasis due to increased glucose production, impaired insulin production, and insulin resistance represents a risk factor for AD. Considering that IGF-I has a role in the proteasome- mediated removal of oxidized proteins in the brain

acting as a promising therapeutic target in AD, the expression levels of IGF-IRβ have been measured in the brain of both wt and AD mice treated or not with SLAB51. Decreased amounts of IGF-IRβ were detected in 56-week-old 3xTg-AD mice, in agreement with previously published data [156]; whereas no changes were observed in wt animals. Interestingly, the receptor concentration significantly increased in the brain of AD mice administered with SLAB51 (Fig. 21).

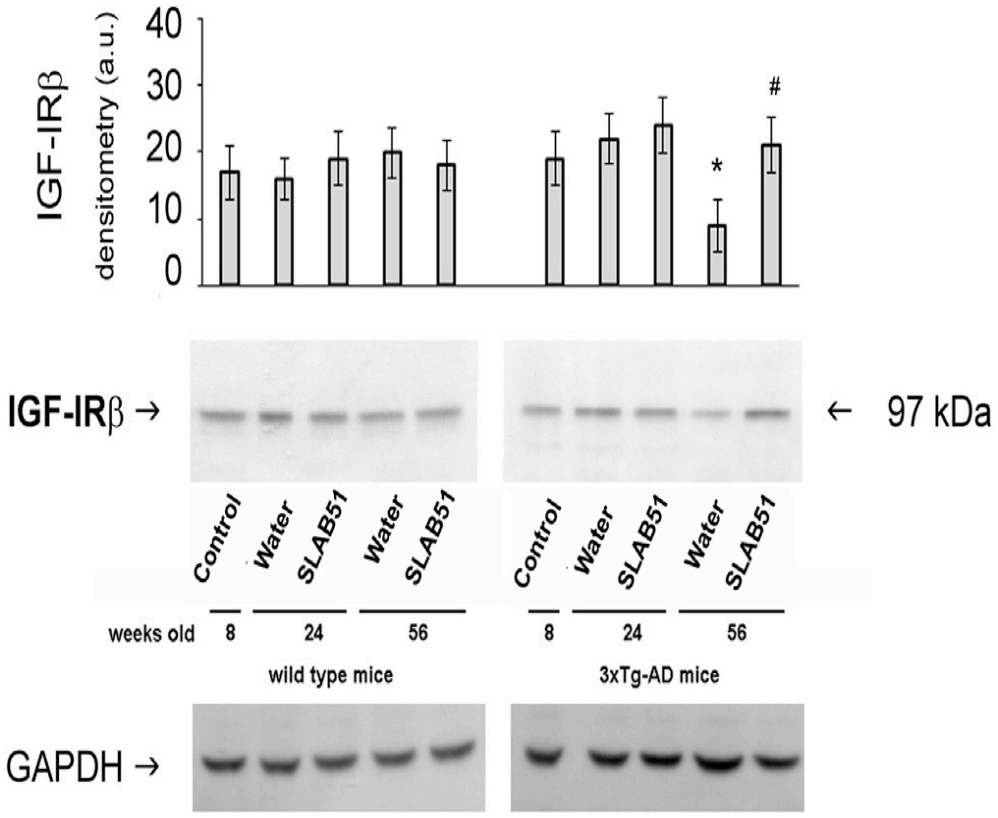

Figure 21*: IGF-IRβ levels in the brain of wt and AD mice treated with SLAB51 for 16 and 48 weeks. Representative immunoblots and corresponding densitometric analyses (expressed as arbitrary units, a. u.) obtained from 6 separate blots are shown. Anti-GAPDH antibody was used to verify equal protein loading. The detection was by an ECL western blotting analysis system. Data points marked with an asterisk are statistically significant compared with 8-week-old untreated control mice (*p < 0.05). Data points marked with a hashtag are significantly different compared to age-matched untreated mice (#p < 0.05).*

2.2.5: Advanced glycation end products in AD mice

Insulin resistance and high glucose concentration together with increased oxidative stress in AD brain contribute to the accumulation of AGEs, harmful products that have been associated with many chronic diseases. AGEs significantly increased in untreated AD mice and SLAB51 supplementation was effective in reducing their amount in both 24- and 56-week-old mice (Fig 22).

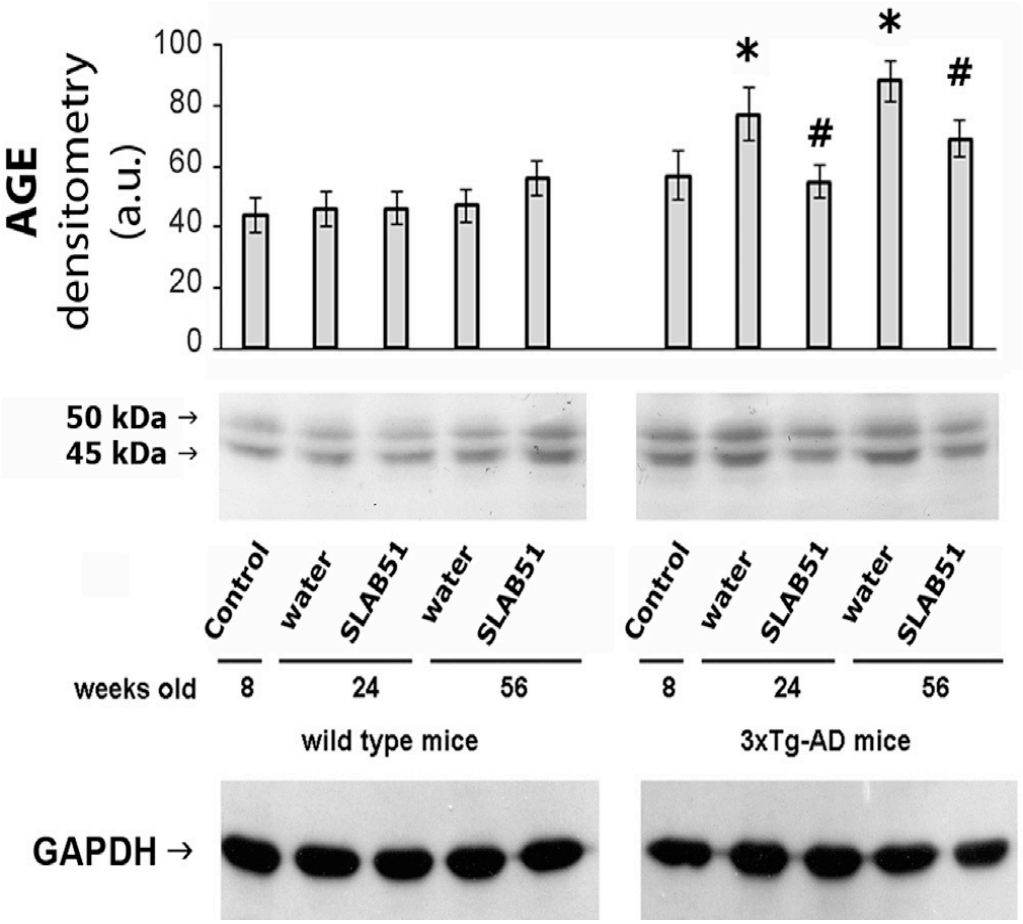

***Figure 22**: AGE levels in the brain of wt and AD mice treated with SLAB51 for 16 and 48 weeks. Representative immunoblot and corresponding densitometric analysis obtained from 6 separate blots are shown. Equal protein loading was verified by using an anti-GAPDH antibody. The detection was executed by an ECL western blotting analysis system. Data points marked with an asterisk are statistically significant compared with 8-week-old untreated control mice (*p < 0.05). Data points marked with a hashtag are significantly different compared with age-matched untreated mice (#p < 0.05).*

2.3: Discussion

Current established treatments for AD are only able to delay the symptoms but it can neither be prevented nor stopped. Recently with the increasing understanding on the gut-brain axis multiple neurochemical pathways [157, 158] and oral bacteriotherapy are being employed and exploited for the prevention and treatment of several disorders, including CNS-related diseases [104, 159-162]. Recently in Bonfili, L., et al., 2017, our lab have demonstrated that the oral administration of SLAB51 probiotic formulation modified gut microbiota in 3xTg- AD mice, where the treatment induced larger microbial shifts particularly increase in *Bifidobacterium spp.* and reduction in *Campylobacterales;* that favored several metabolic pathways associated with energy metabolism, amino acid metabolism, and nucleotide metabolism. *Bifidobacterium* strains possess anti-inflammatory properties while *Campylobacter jejuni* is known to increase the expression of pro-inflammatory cytokines and this was observed as reduced plasma concentrations of pro-inflammatory cytokines in SLAB51 treated AD mice. Improvement of cognitive performances observed in these mice was supported by increased plasma concentrations of neuroprotective gut hormones and correlated with decreased Aβ load and partial recovery of neuronal proteolytic pathways with consequent delay of AD progression [122, 129].

Considering that impaired cerebral glucose metabolism strongly contributes to AD onset and progression, we focused this work on the evaluation of the effects of SLAB51 oral administration on glucose uptake and metabolism using 3xTg-AD mice and the wt B6129SF2 mice. As expected, AD mice showed impaired glucose uptake compared with wt animals. In detail, levels of GLUTs decreased in the brain of aged AD animals together with the increase of phosphorylated AMPK and Akt. In fact, these kinases play a central role in glucose uptake, influencing GLUTs' expression.

Here, we demonstrate for the first time that probiotics are able to counteract insulin resistance by restoring the brain expression level of GLUTs and reducing the phosphorylation of key metabolic

regulators such as AMPK and Akt, consequently decreasing tau phosphorylation. Our results are consistent with previous in vivo and in vitro studies describing AMPK increased activity during glucose deprivation, metabolic stress, ischemia, and hypoxia in neurons [163]. The levels of p-AMPK and p-Akt decreased in SLAB51-treated AD mice by a similar amount, with the latter being implicated in regulating the translocation and biosynthesis of insulin-sensitive glucose transporters in most cell types.

Functional abnormalities of both AMPK and Akt cause energy metabolic impairment and correlate with tau hyper-phosphorylation, one of the main features of AD. It has been indicated that AMPK is a key player in the development of AD pathology because it can phosphorylate tau [164].

As expected, increased tau phosphorylation was observed in 24- and 56-week-old AD mice, particularly in the hippocampus. The percentage of phospho-tau-positive staining decreased in SLAB51-treated AD animals in accordance with the reduced levels of phosphorylated/activated AMPK and Akt [28, 164] and with the partial restoration of GLUTs expression levels. These data are in line with previous studies showing that defective glucose transport determines glucose metabolism impairment, together with abnormal tau phosphorylation [165]. Tau hyperphosphorylation in the hippocampus of untreated AD mice, together with the increase of pAMPK and pAkt and the decrease of GLUTs expression levels are in agreement with papers demonstrating the involvement of AMPK in AD-associated Aβ and tau pathology [158]. Moreover, several studies propose that defective glucose transport leads to reduced glucose metabolism, causing abnormal tau phosphorylation [166]. Reduced glucose availability in brain was shown to promote tau neuropathology and synaptic dysfunction[167]. Inhibition of energy metabolism causes post-transcriptional increase in BACE-1 levels, thereby elevating the levels of Aβ formation and deposition [168]. The increase of AMPK and Akt-mediated cerebral glucose metabolism is another mechanism through which SLAB51 counteracts AD progression. In fact, besides increasing tau phosphorylation, p-AMPK is also involved in the generation and accumulation of Aβ. In Bonfili, L., et al., 2017, our lab have demonstrated that SLAB51 treatment contributed to a consistent reduction in

the amount of cerebral Aβ, both in the forms of peptides and oligomers in brains of SLAB51- treated AD mice. The study have also shown that administration of the probiotic formulation counteracted the typical morphological alterations of AD, including the reduction in brain weight, the decline of cortical areas, and the general brain damage and shrinkage. [122] and herein we reinforce the idea that AMPK activation has "non-neuroprotective" properties [169]. Recently, tau has been linked to impaired insulin sensitivity and conversely insulin resistance can also trigger tau pathology resulting in a vicious cycle of these events [36]. Abnormal brain insulin signaling is correlated with hyperphosphorylated tau [170] and glucose intolerance and insulin resistance were described in AD mouse models [171].

Accordingly, we detected an increase in HbA1c plasma concentration in untreated 3xTgAD mice and decreased levels with SLAB51 administration. As a reliable retrospective indicator of long-term glycemic history, the increase of HbA1c in aging and neurodegenerations inevitably suggests an impaired memory function. And high HbA1c was found as key contributor to brain cognitive decline especially for verbal memory function [172]. The ability of SLAB51 to decrease HbA1c plasma levels demonstrates a positive effect on glucose homeostasis and is correlated with the increase in gut peptide hormones, such as GLP-1 and GIP, involved in glucose metabolism, and with the enriched gut content in metabolites that improve insulin sensitivity [122, 173].

Moreover, we observed decreased brain levels of IGF-IRβ, which regulates food intake, energy metabolism, reproduction, and cognitive functions [174]. The expression level of this receptor significantly increased on SLAB51 treatment with positive implications not only on glucose metabolism but in general on AD-like progression because IGF-I is involved in the proteasome-mediated proteolysis of oxidized proteins [118]. IRβ is also associated with significant elevations in GLUT3 expression thereby significantly mediating neuronal glucose metabolism [175]. The amelioration of glucose uptake and metabolism is also consistent with the decreased formation of AGEs in treated AD mice, indicating that, by controlling glucose metabolism and favoring the clearance of oxidized species, the formation of

harmful products such as AGEs can be counteracted. Furthermore, it would be interesting to see the effect of SLAB51 administration on other pathologies that are featured by insulin-resistance and altered glucose homeostasis. Collectively, these data are in perfect agreement with our previous publication demonstrating that probiotics consumption reduces oxidative stress in 3xTg-AD mice by activating SIRT1-dependent mechanisms [129]. Accordingly, another study shows that AGEs increase ROS production, stimulating downstream pathways related to APP processing, Aβ production, and SIRT1 [176]. AGEs cross-linked with Aβ forming AGE-Aβ decrease plaques clearance by microglia [177].

Concluding, SLAB51 oral administration in 3xTg-AD mice ameliorated impaired glucose metabolism confirming the efficacy of oral bacteriotherapy in the prevention and treatment of AD. Till date this formulation has been studied over a range of animal models and human cell lines, however no clinical studies on this field are currently available. Data presented here reinforce the idea that gut microbiota modulation can influence multiple signaling pathways in the host and further contribute to the explanation of the observed ameliorated cognitive functionality in these AD mice [122].

Chapter 3: Neuroprotective effects of p62 (SQSTM1)-engineered lactic acid bacteria in Alzheimer's disease

3.1: Materials and methods

3.1.1: Engineered bacterial cells growth and lyophilization

The Lactobacillus lactis subsp. cremoris MG1363 strain, both control (LAB) and p62-pExu transformed cells (p62-LAB), were obtained from the laboratory of Prof. Azevedo at the Federal University of Minas Gerias (Belo Horizonte, Brazil) [178]. These cells were maintained as stock cultures in glycerol at -80°C until use. Transformation of L. lactis, pExu plasmid construction and in vitro and in vivo functionality evaluation were described by Mancha-Agresti et al. [178]. The p62 ORF fragment was inserted into pExu MCS using the restriction enzymes, resulting in pExu:p62. The pExu:p62 plasmid was then established by transformation in L. lactis MG1363 strain [178] Two populations of L. lactis subsp. cremoris MG1363 were grown: LAB added with the pExu:empty plasmid (indicated as LAB), LAB added with the pExu vector encoding for human p62 (pExu:p62, indicated as p62- LAB). L. lactis subsp. cremoris MG1363 was grown in M17 medium (Sigma-Aldrich) containing 0.5% glucose (Sigma-Aldrich) and 125 μg/mL erythromycin (Sigma- Aldrich) at 30 °C without agitation. For bacteria lyophilization, culture medium containing 5×108 CFU/mL (corresponding to 1 O.D.) was centrifuged and the supernatant discarded. Pellet was suspended in pasteurized skimmed milk and aliquoted in 2 mL tubes each containing the daily dose of bacteria for 8 mice (8×109 cells) Tubes were frozen and then dried for 24 h. Cell viability and number were checked upon lyophilization. Lyophilized bacteria were stored at 4 °C.

3.1.2: Animals and treatment

Triple transgenic mice 3xTg-AD were purchased from Jackson Laboratory (Bar Harbor, Maine, USA). This is a widely used animal model for AD due to its three distinguished mutations corresponding to familial AD (APP Swedish, tau P301L, and PSEN1 M146V). Translation of the overexpressed transgenes are confined to the central nervous system, including the hippocampus and cerebral cortex. Aβ deposition is continuous, with first signs surfacing within 3 to 4 months of age in the frontal cortex and becoming more extensive by 12 months [150, 179]. 8-weeks-old male mice were divided into four groups as follows: untreated 8-weeks-old mice (T0, n=8); mice treated with lyophilized milk (C, n=8), mice treated with control lyophilized LAB (pExu:empty, n=8) and mice treated with lyophilized p62-LAB (LAB(pExu:p62), n=8). Bacteria were dissolved daily in mice drinking water and given to the animals. Mice received 109 bacteria every day. After a two-month treatment, mice were sacrificed. According to the guidelines of the European Communities Council (86/609/ECC) for the care and use of laboratory animals, mice were maintained in a temperature-controlled room (21±5 °C) under an inverted 12 h light/dark cycle (lights on at 8:00 pm) and provided with rodent standard food (Mucedula, Italy) and water ad libitum. All appropriate measures were taken to minimize pain and discomfort in these experimental animals. General observations regarding possible changes in skin and fur, mucous membranes, diarrhea, sleep, movements and posture were performed. Additionally, local injuries and mortality (if any) were recorded throughout the experimental period. The body weight was measured at the beginning of the treatment and then once a week to ensure adequate food intake.

3.1.3: Novel object recognition

Behavioral tests were performed during the animals' dark phase starting from 8:00 to 15:00. Animals were handled for 3 days before testing in order to accustom them to the experimenter. The investigators were blinded to the groups' allocation during the tests. The novel-object recognition test (NOR, based on the spontaneous tendency of rodents to spend more time exploring a novel object than

a familiar one) was used to evaluate recognition memory. The first step is the habituation, during which the animal is allowed to explore the empty arena for 5 min and then returns to the home cage. Following a training period dedicated to the exploration of two identical objects, the animal is removed from the arena for a delay period of 3 h, and it is then placed back within the arena, where one of the two identical objects is replaced by a new, dissimilar novel object (test phase). The time the rodent spends exploring each object in 10 min provides a measurement of the extent of memory integrity and attention. Results were expressed as discrimination scores (the ratio between the time spent with novel object and total time spent with both objects). A lower score indicates memory impairment in this task. Objects were different in shape, color and texture and maintained throughout the study to obtain reproducible data. Preliminary experiments were done to select novel and familiar object pairs, so that each object in the pairs elicited the same amount of spontaneous investigation.

3.1.4: Mice sacrifice and tissues preparation

After the treatment, mice were sacrificed, and feces frozen for microbiota determinations. Blood and organs were collected, brains weighed, dissected and photographed, and immediately frozen or fixed in 10% buffered formalin for morphological analyses and immunohistochemistry. A portion of the brains was homogenized (1:5 weight/volume of buffer) in 50 mM Tris buffer, 150 mM KCl, 2 mM EDTA, pH 7.5. Homogenates were immediately centrifuged at 13000×g for 20 min at 4 °C and supernatants collected for enzymatic assays and western blotting. An aliquot of the supernatants was supplemented with protease inhibitors (Pefabloc and TPCK) for ELISA determinations. The Bradford method was used to measure the protein concentration in homogenates, using bovine serum albumin (BSA) as a standard [180].

3.1.5: Oral administration of LAB (pExu:egfp) in 3xTg-AD mice

Administration of *L. lactis* MG1363 strain expressing the pExu:*egfp* vector. 8-weeks-old 3xTg-AD mice were administered with LAB containing the pExu:egfp plasmid by oral gavage (109 CFU

dissolved in 100 μL of PBS). Animals (n=8 each group) were sacrificed 6, 12, 24, 48, 72, 168 and 216 h after bacteria administration, tissues were immediately placed into 3 M ammonium sulfate in 1 M potassium citrate buffer, rinsed several times, blotted dry, and oriented in cryomolds with OCT embedding compound (Tissue- Tek Division, Miles Laboratories, Naperville, IL). Tissues were frozen by plunging the mold into nitrogen cooled isopentane. Frozen tissue blocks were stored at - 70 °C until use. Four micron frozen sections were cut in a cryostat (- 20 °C) and mounted at room temperature on acid-cleaned glass slides. Slides were immediately immersed for 5-10 mm in - 20° C acetone and then sections were washed in PBS and immediately mounted in PBS: glycerol (1:9), and allowed to dry at room temperature in a dark camera. The same sections were then used for direct immunofluorescence evaluation using a LEICA DM 2005 microscope and a Retiga 2000R digital camera (QImaging, Surrey, BC, Canada).

3.1.6: ELISA assay for Aβ levels

Brain homogenates (supernatant fraction) supplemented with protease inhibitors (Pefabloc and TPCK), were used to measure Aβ(1–40) and Aβ(1–42) levels using enzyme-linked immunosorbent assay NOVEX® ELISA kits (Thermo Fisher Scientific Inc., Waltham, MA USA). Based on preliminary tests, samples were diluted at 1:5 with diluent buffer provided with the kit. Plates were read at 450 nm on a visible plate reader (Biotrak, Amersham). Assays were performed according to the manufacturer's directions.

3.1.7: Immunohistochemistry

For immunohistochemistry, brains, intestines, mesenteric lymph-nodes, and spleens were collected, formalin fixed, paraffin embedded and 3μm sections were prepared. Murine and human p62 levels were measured using two distinct anti- p62/SQSTM1 antibodies from Cell Signaling Technology (Leiden, The Netherlands, dilution 1:100), the anti-rodent p62/SQSTM1 antibody, produced in rabbit against synthetic peptides corresponding to residues surrounding Gly-300 of mouse p62 protein, and the

anti-human p62/SQSTM1 protein antibody, produced against synthetic peptides corresponding to residues surrounding Pro-220 of human p62 protein. Aβ(1-42) deposition was evidenced and scored using the anti-Aβ(1-42) antibody from Merck Millipore (Merck KGaA, Darmstadt, Germany). The anti-Aβ (6E10) antibody was purchased from BioLegend (BioLegend Way San Diego, CA, USA). For double- labeling immunohistochemistry, slides were first incubated with the anti-Aβ(1-42) antibody and with the anti-murine p62/SQSTM1 antibody and then with the biotin-labeled goat anti-rabbit secondary antibody (1:200, Jackson ImmunoResearch, West Grove, PA). The binding of the antibody was detected with the Elite kit (Vector Laboratories) and the immunoreaction was developed using two different chromogens: violet (VIP, Vector, Burlingame UK) for mouse and human p62 protein stain and brown (DAB, Vector) for anti-Aβ(1- 42) antibody. Tissues were counterstained with Mayer's hematoxylin. For negative immunohistochemical controls, the primary antibodies were omitted. Lower- power digitized images were acquired with a BX-60 microscope (Olympus, Melville, NY) equipped with a DEI-470 digital camera (Optronics, Goleta, CA). The immunoreactivity in the tested areas was quantified at the indicated magnification and analyzed using ImageJ/Fiji 1.52p software (NIH, USA) [17] defining a region of interest (ROI) for the colors to be measured. The absence of primary antibody did not result in immunoreactivity. The pathologist was blinded to the group allocation.

3.1.8: Western blot analysis

Western blot analysis was performed as explained earlier (chapter 2.1, sub-section 2.1.5). The anti-rodent p62/SQSTM1 antibody and the anti-human p62/SQSTM1 protein antibody were purchased from Cell Signaling Technology (Leiden, The Netherlands). The two antibodies, especially the anti-murine p62, recognize regions of the proteins with a low degree of conservation. In details, the SQSTM1/p62 (D6M5X) Rabbit mAb (Rodent Specific, product #23214) is produced by immunizing animals with a synthetic peptide corresponding to residues surrounding Gly-300 of mouse SQSTM1/p62 protein. The SQSTM1/p62 (D5L7G) Mouse mAb (product #88588) is produced by immunizing animals

with a synthetic peptide corresponding to residues surrounding Pro-220 of human SQSTM1 protein. The anti-Aβ(1-42) antibody was from Merck Millipore (Merck KGaA, Darmstadt, Germany). Recombinant human p62/SQSTM1 protein was obtained from Abcam plc (Cambridge, UK). The anti-LC3 antibody was from Thermo Fisher Scientific (MA, USA). The intracellular levels of beclin-1, p27, p53, ubiquitin-conjugates, 3-nitrotyrosine (3-NT), 4-hydroxy-2-nonenal (4-HNE), 8- oxo-7,8-dihydro-2′-deoxyguanosine (8-oxodG) and 8-oxoguanine DNA glycosylase-1 (OGG1) were determined using primary antibodies from Santa Cruz Biotechnology, in accordance to their related protocol/information sheet. Primary antibodies used to detect pro- and anti-inflammatory cytokines were from Abcam plc (Cambridge, UK). Molecular weight markers (6.5 to 205kDa) were included in each gel. Glyceraldehydes-3-phosphate dehydrogenase (GAPDH) was used as a control to check equal protein loading [181]. Immunoblot images were quantified using ImageJ 1.52p software (NIH, USA).

3.1.9: Oxyblot analysis

Carbonyl groups in proteins were measured with the Oxyblot kit (Appligene-Oncor, Strasbourg, France). Briefly, brain homogenates (15 μg of total proteins) were incubated at room temperature with 2,4- dinitrophenylhydrazine (DNPH) in order to form 2,4- dinitrophenylhydrazone (DNP-hydrazone), according to the manufacturer data sheet. Then, the obtained products were separated by SDS-PAGE and electroblotted onto PVDF membranes. The detection step and data analysis were performed as described in the Western Blot Analysis section [182]

3.1.10: Proteasome activity assays

Proteasome peptidase activities in brain homogenates (supernatant fraction) were determined using the synthetic fluorogenic peptides Suc-Leu-Leu-Val-Tyr-AMC for ChT-L activity, Z-Leu-Ser-Thr-Arg-AMC for T-L activity, Z-Leu-Leu-Glu-AMC for PGPH activity, and Z-Gly-Pro-Ala-Phe-Gly-pAB for BrAAP activity [20]. The mixture contained the brain homogenate (15 μg total proteins), the appropriate substrate (5 μM final concentration) and 50mM Tris–HCl pH 8.0, up to a final volume of

100 μL, and was incubated at 37 °C for 60 min. The 26S proteasome ChT-L activity was tested including 10 mM MgCl2, 1 mM dithiothreitol, and 2 mM ATP in the reaction mix. The fluorescence of the hydrolyzed 7-amino-4-methyl-coumarin (AMC) and 4-aminobenzoic acid (pAB) (AMC, λexc = 365 nm, λem = 449 nm; pAB, λexc = 304 nm, λem = 664 nm) was detected on a SpectraMax Gemini XPS microplate reader.

3.1.11: Cathepsin B and L activities

Cathepsin B and L proteolytic activities were measured using the fluorogenic peptides Z-Arg-Arg-AMC and Z- Phe-Arg-AFC, respectively, at a final concentration of 5 μM [40]. The mixture for cathepsin B, containing 7 μg of brain homogenate, was pre-incubated in 100 mM phosphate buffer pH 6.0, 1 mM EDTA and 2 mM dithiothreitolfor5 minat30°C. Upon the addition of the substrate, the mixture was incubated for 15 min at 30 °C. The mixture for cathepsin L, containing 7 μg of proteins, was incubated in 100 mM sodium acetate buffer pH 5.5, 1 mM EDTA and 2 mM dithiothreitol for 5 min at 30 °C and, upon the addition of the substrate, the mixture was incubated for 15 min at 30 °C. The fluorescent signal released by the hydrolyzed 7-amino- 4-methyl-coumarin (AMC, λexc = 365 nm, λem = 449 nm) and 7-amino-4-trifluoromethylcoumarin (AFC, λexc = 397 nm, λem = 500 nm) was detected on a SpectraMax Gemini XPS microplate reader.

3.1.12: ELISA assay for ghrelin, leptin and GIP, GLP-1

Plasma hormone concentrations were measured through ELISA using plasma treated with protease inhibitors (Pefabloc and TPCK). The Rat/mouse Ghrelin Active ELISA kit (Invitrogen) is a sandwich ELISA based on the capture of ghrelin molecules (active form) in the plasma by anti-ghrelin IgG and the immobilization of the resulting complex to the wells of a microtiter plate coated by a pre-tittered amount of anchor antibodies. Leptin and glucose-dependent insulinotropic polypeptide (GIP) (Merck KGaA, Darmstadt, Germany) were determined using sandwich ELISA kit based on anti-leptin and anti-GIP monoclonal antibodies, respectively. Similarly, the quantitative determination of mouse

glucagon like peptide-1 (GLP-1) was performed using a sandwich ELISA kit (CUSABIO, Houston, Texas). Plates were read on a visible plate reader (Biotrak, Amersham). Assays were performed following manufacturer's indications.

3.1.13: 16S rRNA gene sequencing

Bacterial DNA extraction from fecal samples was performed using a commercially available kit according to the manufacturer's instructions and as described elsewhere [183] Bacterial tag-encoded FLX-titanium amplicon pyrosequencing (bTEFAP) based on the V1–V3 region (E. coli position 27–519) of the 16S rRNA gene was performed on fecal samples from mice (groups T0, C, LAB and p62-LAB) as described previously [184], with forward primer 515F (GTGCCAGCMGCCGCGGTAA) and reverse primer 806RB (GGACTACNVGGGTWTCTAAT). Sequence data were uploaded into the NCBI GenBank database under submission number SRP225114. Raw sequence data were screened, trimmed, deionized, filtered, and chimera depleted using a QIIME2 pipeline. Sequence were demultiplexed and the Operational taxonomic units (OTUs) table was created using DADA2 [185]. OTUs were defined as sequences with at least 97% similarity using Greengenes v.13.8 database [186]. The OTU table was rarefied at 23,365 sequences/ sample for even depth of analysis. Phylogeny-based UniFrac distance metric analysis was used as a measure of beta (β)-diversity to investigate differences in microbial communities. For this, the analysis of similarity (ANOSIM) function in Primer6 was used on the UniFrac distance matrixes, both weighted and unweighted. Alpha (α) diversity was assessed as a measure of species richness and evenness in all samples. The Chao1, Shannon index and Observed Species data and plots were generated. Univariate statistics were performed on alpha-diversity data and on OTU tables with Kruskal-Wallis, using Graphpad Prism 7. P-values were adjusted for multiple comparisons by the Benjamin and Hochberg FDR. Statistical significance was set at $p<0.05$. Post hoc Dunn's multiple comparison test was used to determine the group differences in bacterial taxa.

PICRUSt (Phylogenetic Investigation of Communities by Reconstruction of Unobserved States) was used to predict functional gene content based on 16S rRNA gene data present in the Greengenes database and the KEGG database [187] using QIIME2. Linear discriminant analysis effect size (LEfSe) was used to elucidate bacterial taxa and genes that were associated with each treatment. LEfSe was calculated using Calypso, a web-based software package that allows mining and visualizing of microbiome-host interactions [188].

3.1.14: Statistical analyses

Data are expressed as mean values ± S.D. Statistical analysis was performed with one way ANOVA, followed by the Bonferroni post hoc test using Sigma-stat 3.1 software (SPSS, Chicago, IL, USA) and $p<0.05$ was considered statistically significant.

3.2:Results

3.2.1: Evaluation of treatment-related toxicity

3xTg-AD mice received a daily oral administration of 109 CFU live p62-engineered LAB or corresponding controls for a period of two months. The treatment did not cause mortality or toxicity signs in any of the animals. No diarrhea, changes in general appearance or other treatment-related sickness were recorded and there was no weight loss or reduction in food intake (data not shown).

3.2.2: Effects of p62-LAB treatment on mice cognitive functions

Prior to sacrifice, the novel object recognition (NOR) test was performed on the four groups of mice to evaluate the effects of the treatment on hippocampal functions and recognition memory. No significant difference was observed comparing control, LAB and p62-LAB groups with the T0 group whereas a statistically significant difference ($p<0.05$) was observed in p62-LAB treated mice with respect to both control and LAB group, as shown in Fig 23. In detail, AD mice treated with p62-LAB showed a better "discrimination index" than control and LAB treated animals of the same age.

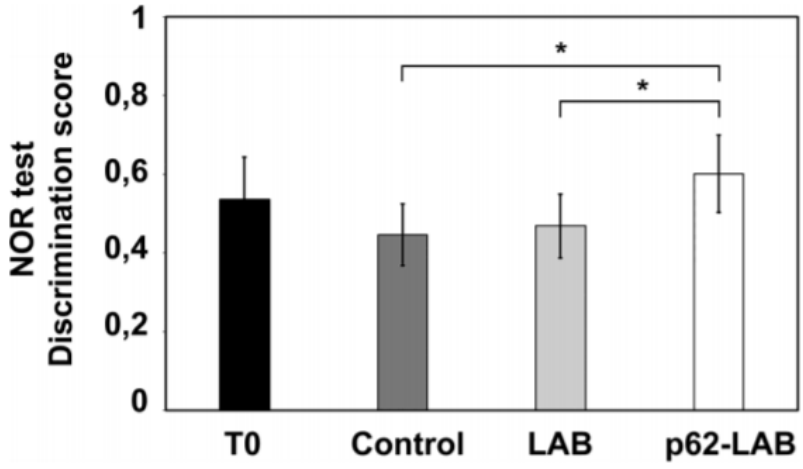

***Figure 23**: Novel Object Recognition (NOR) test. The effect of p62-LAB treatment on mice memory performance was assessed by the NOR test. The discrimination scores obtained for the four groups of mice are reported. The asterisk indicates statistical significance ($p<0.05$).*

3.2.3: Functionality of the LAB: pExu vector and distribution of the p62 protein in mice tissues

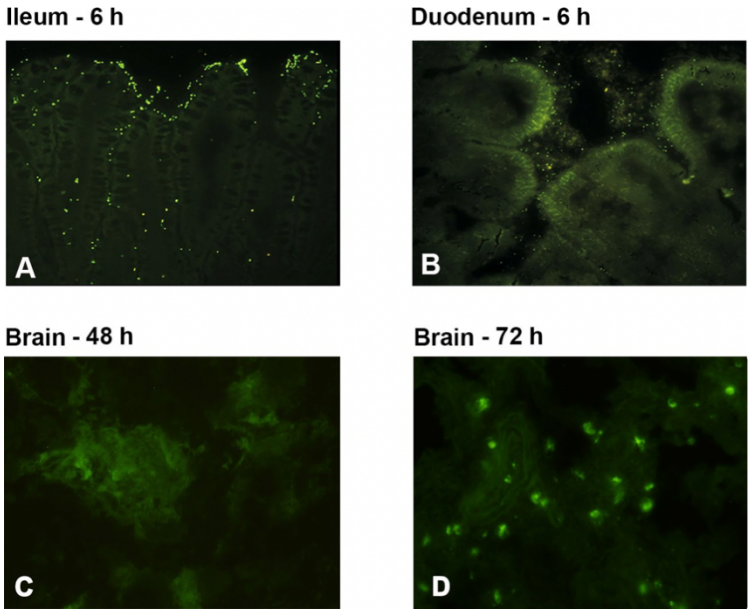

Figure 24. *eGFP expression in 3xTg-AD mice orally administered with LAB (pExu:egfp). Detection of eGFP in the intestine (ileum (A) and duodenum (B) portions) and brain (C, D) of 3xTg-AD mice. Fluorescence in intestinal cells was detected 6 h after the treatment and fluorescence in the brain was evidenced from 48 h to 72 h after gavage.*

The functionality of the LAB-pExu system was evaluated upon the oral administration of L. lactis MG1363 (pExu:egfp) to 3xTg-AD mice. Interestingly, the expression of the eGFP was detected in intestinal cells 6 h after the treatment and in brain cells from 48 h to 72 h after gavage (Figure 24) [185]

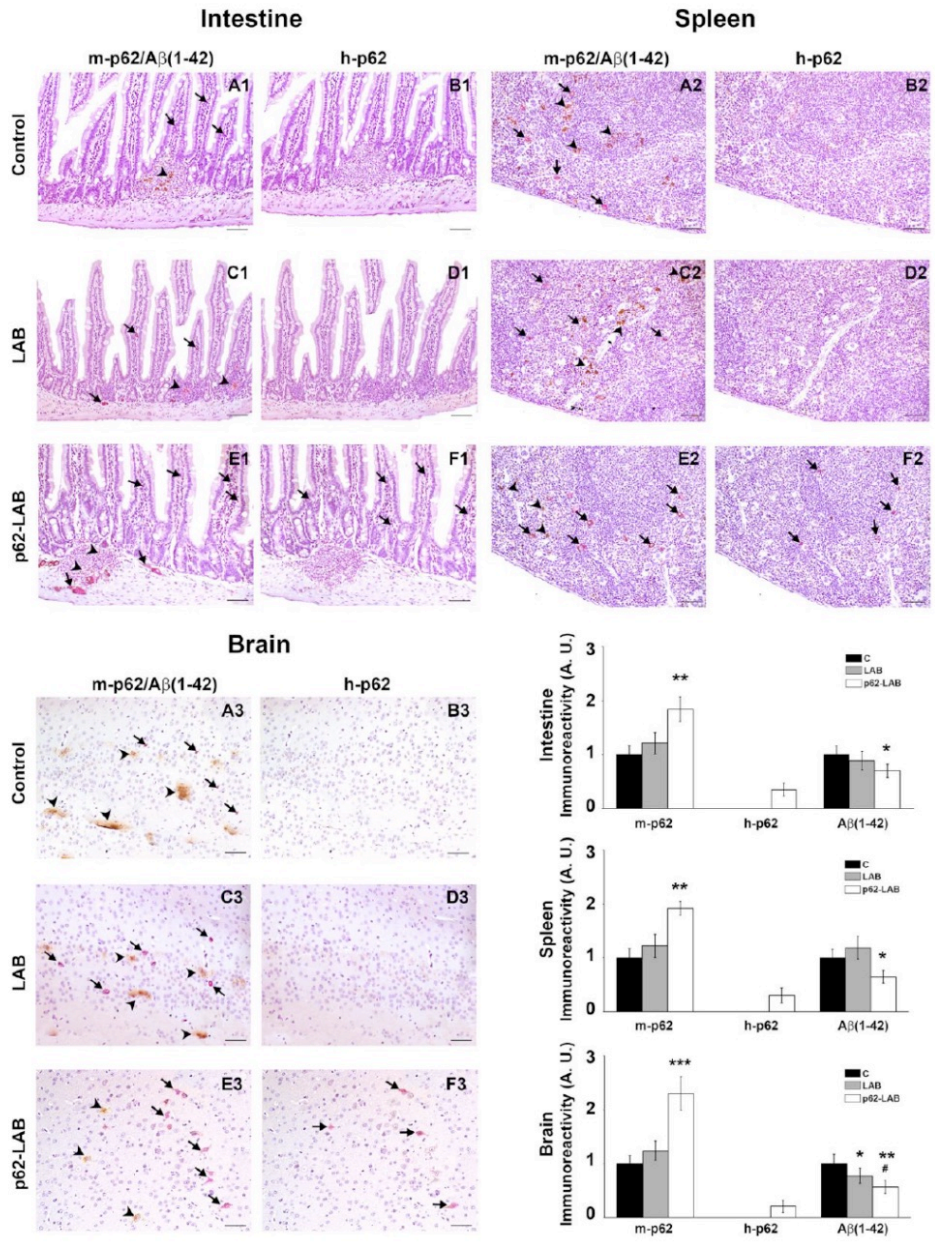

***Figure 25**: IHC analysis of intestine, spleen and brain from control, LAB and p62-LAB treated mice. Tissue sections from duodenal mucosa, spleen and brain, specifically the hippocampal region, were stained with an anti-rodent p62 antibody (purple), an anti-human p62 antibody (purple) and an anti-Aβ(1-42) antibody (brown). Panels A1-B1, C1-D1, and E1-F1 show consecutive intestinal sections, panels A2-B2, C2-D2, and E2-F2 show consecutive spleen sections and panels A3-B3, C3-D3, and E3-F3 show consecutive brain sections. Immunohistochemical double-staining for m-p62 (arrows) and Aβ(1-42) (arrowheads) is shown (IHC, intestine and spleen 20×, scale bar = 100 μm; brain 40×, scale bar = 200 μm, *p<0.05, **p<0.01 vs C and LAB, #p<0.05 vs LAB).*

The distribution of the p62 protein, both the endogenous (murine, m-p62) and the exogenous (human and plasmid-associated, h-p62) form, was determined by immunohistochemistry (IHC) of intestinal, lymphoid and nervous tissues from control, LAB and p62-LAB groups (Figure 25). In order to discriminate between the two p62 isoforms, the analysis was conducted on sequential slices using an anti-rodent and an anti-human p62 monoclonal antibody. In untreated and LAB treated mice, the immunohistochemical analysis of duodenal mucosa evidenced endogenous p62 in few scattered mononuclear cells along villi (Figure 2, panels A1 and C1). Interestingly, p62-LAB treatment induced an evident increase of m-p62 in neuronal ganglia and in some mononuclear and interstitial cells of villi (Figure 25, panel E1). A sporadic and weak expression of the exogenous p62 in interstitial cells of the villi was observed (Figure 25, panel F1). In the spleen, a modest positivity for endogenous p62 was measured in control and LAB treated mice (Figure 25, panel A2 and C2) whereas p62-LAB treatment induced a clear expression of the same protein in many mononuclear and megakaryocyte cells of the white pulp (Figure 25, panel E2). The analysis of consecutive spleen sections revealed a weak expression of the h-p62 (Figure 25, panel F2). Finally, in the hippocampal region of control and LAB brains, a poor expression of the endogenous form of p62 was observed (Figure 25, panels A3 and C3). Similar to intestine and spleen, brains of p62-LAB treated mice showed an evident up-regulation of endogenous p62 (Figure 25, panel E3) and a rare positivity for the human p62, with few weakly labeled neurons in the hippocampus, evident only at higher magnification of the neuronal region (Figure 25, panel F3). Concerning the brain of p62-LAB mice, neuronal cells showed a weak-to-strong cytoplasmic reactivity to p62 (the most significant signals are indicated by the arrows). No positivity was observed for h-p62 in tissue sections from control mice and LAB treated mice (Figure 25, panels B1, B2 and B3, D1, D2 and D3). An increased expression of the endogenous p62 protein upon p62-LAB treatment was also detected in mesenteric lymph nodes (Figure 26).

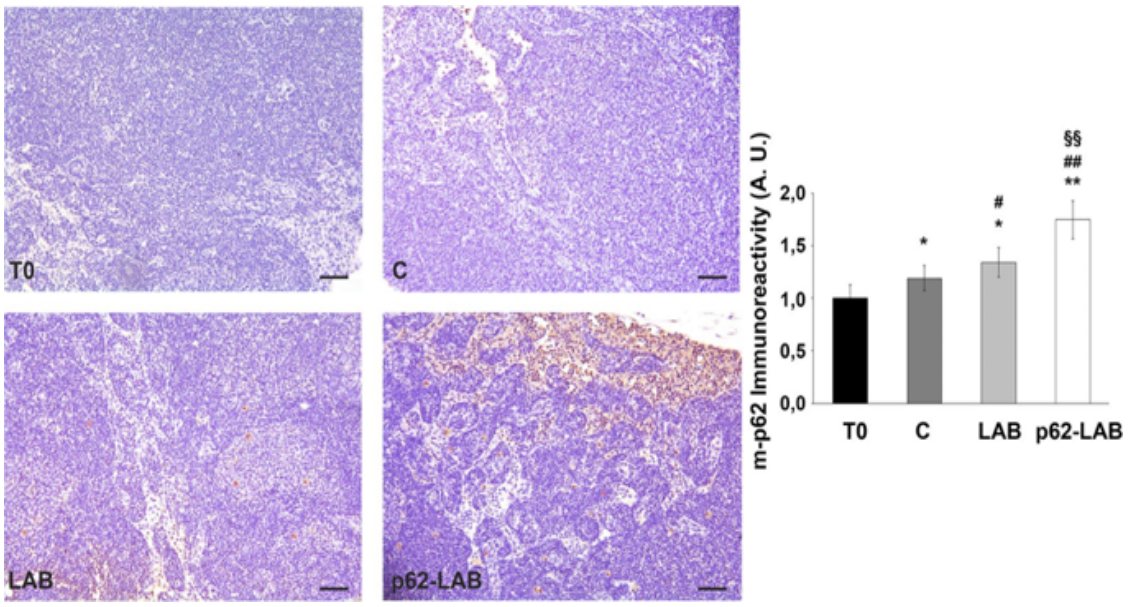

***Figure 26**. Immunodetection of the m-p62 protein in mesenteric lymph nodes of 3xTg-AD mice. Mesenteric lymph nodes of p62-LAB treated 3xTg-AD mice (panel D) show a strong positivity of large groups of cells (morphologically related to mature macrophages, with some mononuclear cells). An anti-murine p62 antibody was used in the immunoassay (10×, Bar= 250μm) (*p<0.05 and **p<0.01 vs T0, #p<0.05 and ##p<0.01 vs C, §§p<0.05 vs LAB).*

These in-situ morphological data on murine p62 up-regulation was then confirmed by western blot analysis performed on total brain homogenates (Figure 27, panel A). No signal was detected for the human p62 protein (Figure 27, panel B), likely due to the small percentage of neuronal cells expressing this protein.

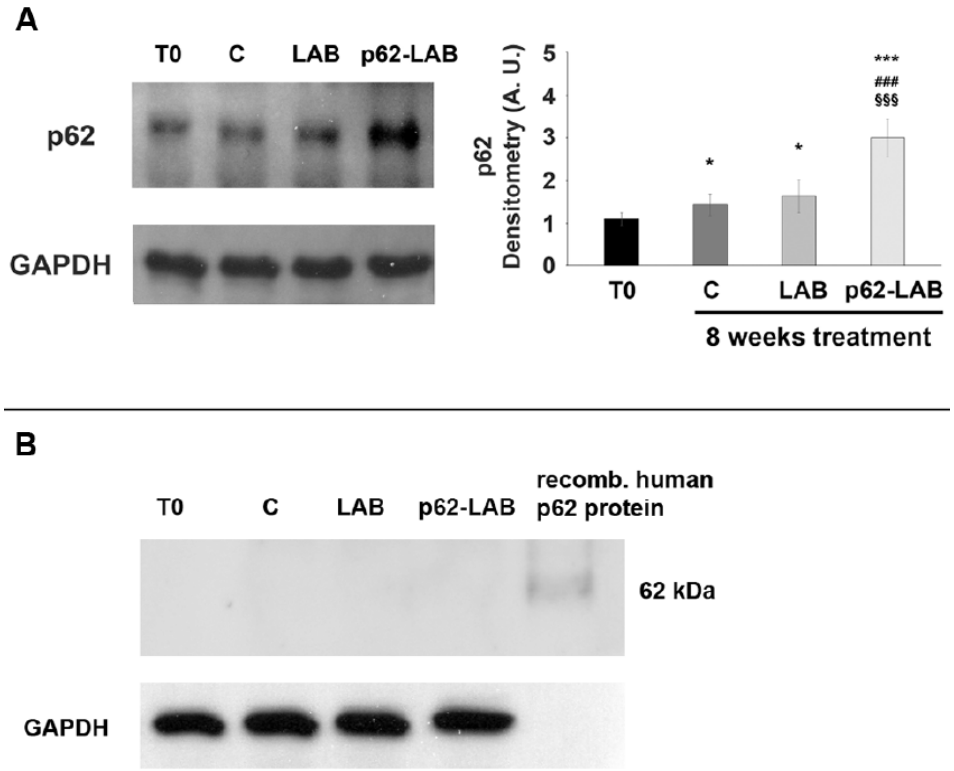

Figure 27*: Immunodetection of the p62 protein in brain homogenates of T0, control and treated 3xTg-AD mice. Panel A shows detection of the m-p62 using a monoclonal anti-murine p62 antibody. GAPDH was used as a control to check equal protein loading. Densitometry is shown on the right (*p<0.05 and ***p<0.001 vs T0, ###p<0.001 vs C, §§§p<0.001 vs LAB). Panel B shows detection of the h-p62 protein in brain homogenates of T0, control (C) and treated 3xTg-AD mice using a monoclonal anti-human p62 antibody. 3 µg of a recombinant human p62 protein were loaded as control. GAPDH was used as a control to check equal protein loading.*

3.2.4: Reduction of brain amyloid load after oral administration of p62-LAB

Increased production and release of amyloid peptides are major hallmarks of AD and responsible for neuronal degeneration. Herein, the effect of p62-LAB treatment on the amyloid load in the brain, spleen and intestine of 3xTg-AD mice was evaluated through IHC and ELISA. Furthermore, in order to establish a correlation between p62 expression and Aβ(1–42) peptide levels, a double staining analysis (purple and brown staining, respectively) was performed in the above mentioned tissues (Figure 25). In detail, aggregates of Aβ(1-42), shown in the sections as brown deposits, were observed in the duodenal mucosa of control and LAB treated animals (Figure 25, panels A1 and C1) and were significantly reduced in p62-LAB treated mice (Figure 25, panel E1). Similarly, the strong labeling of the amyloid peptide in the spleen of control and LAB mice (Figure 25, panels A2 and C2) resulted decreased upon treatment (Figure 25, panel E2). As for the brain, p62-LAB exposure (Figure 25, panel E3) markedly reduced the clear Aβ(1–42) deposition observed in untreated mice (Figure 25, panel A3). A less evident but significant decrease of this amyloid peptide was also detected upon LAB exposure (Figure 25, panel C3).

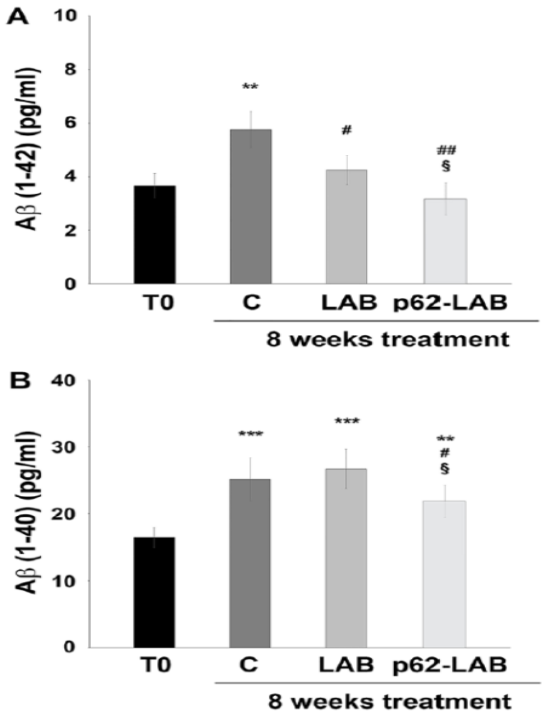

***Figure 28**: Amyloid peptides load in the brain of 3xTg-AD mice. Levels of Aβ(1-42) (panel A) and Aβ(1-40) (panel B) peptides measured by ELISA on brain homogenates of 3xTg-AD mice, T0, C, LAB and p62-LAB groups. Concentrations are expressed as pg/mL (**p<0.01 and ***p<0.001 vs T0, #p<0.05 and ##p<0.01 vs C, §p<0.05 vs LAB).*

Interestingly, the double staining analysis clearly indicated a correlation between the increased levels of endogenous p62 and the reduction in Aβ(1–42) peptide. These data on the diminished levels of the amyloid peptide were also confirmed by additional IHC analysis performed on brain sections stained with the 6E10 antibody that reported a reduction of amyloid amounts upon p62-LAB treatment (Figure 29).

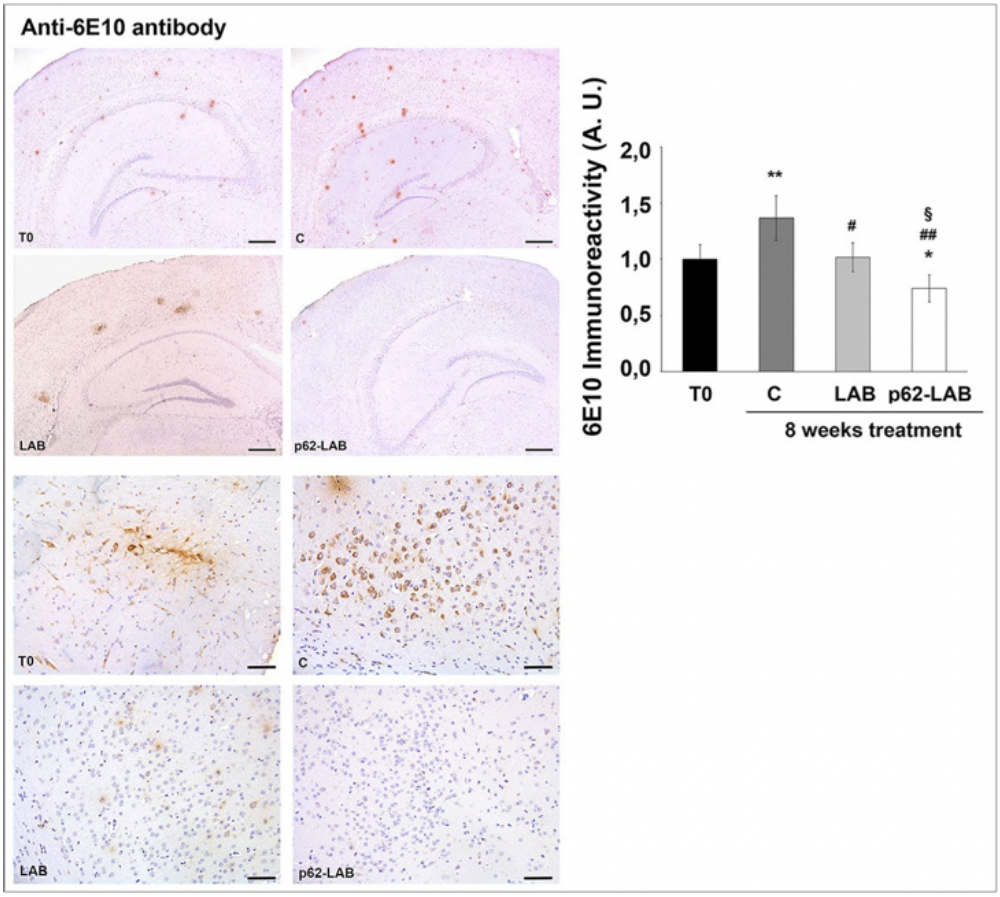

***Figure 29** Immunodetection of amyloid peptides in brain sections of 3xTg-AD mice using the anti-6E10 antibody. Immunohistochemical analysis of brain sections (magnifications 2× and 10×) from T0, C, LAB and p62-LAB groups stained with the 6E10 antibody, specific for Aβ(1–40) and Aβ(1–42) peptides and the amyloid precursor protein, and relative immunoreactivity (*p<0.05 and **p<0.01 vs T0, #p<0.05 and ##p<0.01 vs C, §p<0.05 vs LAB).*

Both Aβ(1–42) and Aβ(1–40) peptides were quantified in brain homogenates by ELISA and lower levels were observed upon treatment with p62-engineered Lactobacilli compared to C and LAB groups (Figure 28, panels A and B, respectively). In detail, the most evident effect was detected on the Aβ(1–42) peptide (42% decrease compared to controls) whose concentration was also partially reduced by the treatment with LAB (30% decrease compared to controls). As expected, 16-weeks-old untreated mice showed higher brain amounts of both peptides compared to T0 group: 1.5 7- and 1.52-fold increase for Aβ(1–42) and Aβ(1–40), respectively.

3.2.5: Effects of p62-LAB treatment on neuronal proteolysis

Concerning cellular proteolysis, the p62 protein drives substrates to the UPS or autophagy for degradation [28,29]. We explored whether the administration of p62-engineered LAB could modulate brain proteolysis, with a special emphasis on these two major proteolytic systems. As expected, an age-dependent decrease in proteasome activity was detected in brain homogenates of the control group when compared to T0 animals (Figure 30, panel A). Compared to control mice, only the T-L activity was significantly decreased in the LAB treated group, whereas an evident subunit-dependent inhibition of the complex was observed in p62-LAB treated mice, with the T-L and BrAAP activities as the most influenced by the treatment (70% and 50% inhibition, respectively). Only the PGPH subunit was not affected by the treatment (Figure 30, panel A). The inhibition of this enzymatic system in the brain of p62-LAB treated animals was also confirmed by the accumulation of the proteasomal substrates p27, p53 and ubiquitinated proteins (Figure 30, panel B).

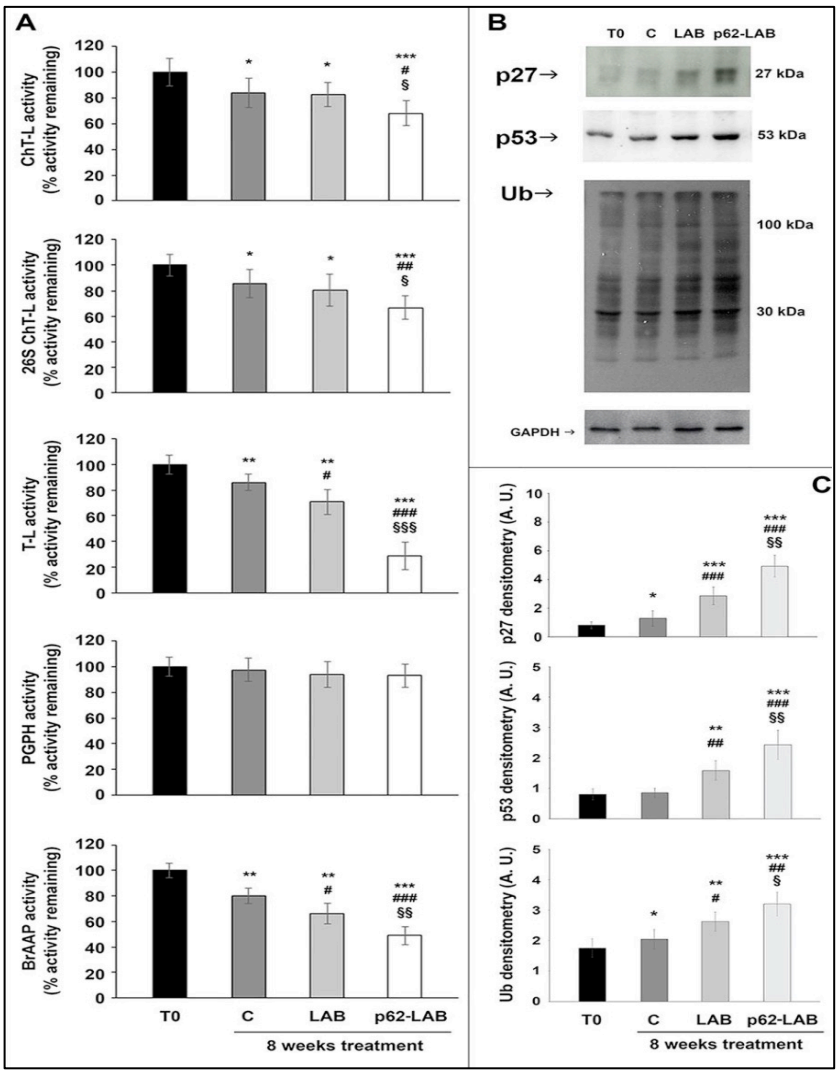

Figure 30: *Proteasome functionality in brain homogenates of 3xTg-AD mice. The ChT-L, T-L, PGPH and BrAAP components of the 20S proteasome and the ChT-L activity of the 26S proteasome were measured using fluorogenic peptides as reported in the Material and Method section (panel A) (*p<0.05, **p<0.01 and ***p<0.001 vs T0, # p<0.05, ## p<0.01 and ###p<0.001 vs C, §p<0.05, §§p<0.01 and §§§p<0.001 vs LAB). Immunodetection of the proteasome substrates p27, p53 and Ub-protein conjugates in brain homogenates of 3xTg-AD mice, T0, C, LAB and p62-LAB groups (panel B) and related densitometry (panel C). GAPDH was used as a control to check equal protein loading (*p<0.05, **p<0.01 and ***p<0.001 vs T0, #p<0.05, ## p<0.01 and ###p<0.001 vs C, §p<0.05 and §§p<0.01 vs LAB).*

To evaluate the effects on autophagy, we immunodetected the levels of the autophagy-related proteins beclin-1, involved in the recruitment of membranes to form autophagosomes, and LC3 II, the lipidated form of LC3, localized in autophagosomal membranes.

The expression of both proteins was significantly up-regulated by p62-LAB treatment and an increased conversion of LC3-I into LC3-II was detected (Figure 6, panel A). Then, to estimate lysosomal function, we measured the activity of two major lysosomal hydrolases, cathepsin B and cathepsin L (Figure 31, panel B) [189].

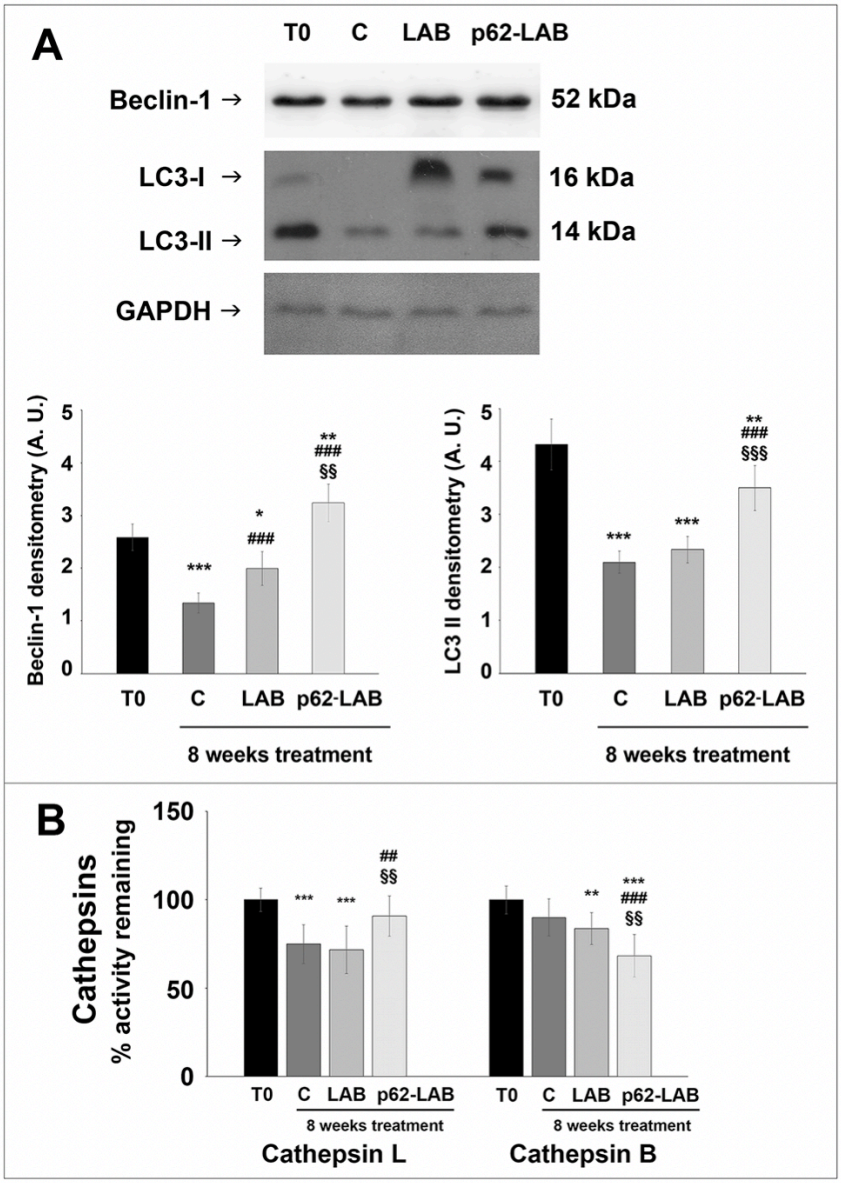

Figure 31: *Autophagic markers in the brain of 3xTg-AD mice. Beclin-1 and LC3 II expression in brain homogenates of 3xTg-AD mice (panel A). GAPDH was used as a control to check equal protein loading ($^{*}p<0.05$, $^{**}p<0.01$ and $^{***}p<0.001$ vs T0, $^{\#\#\#}p<0.001$ vs C, $^{\S\S}p<0.01$ and $^{\S\S\S}p<0.001$ vs LAB). Cathepsin L and B activity measured in brain homogenates of 3xTg-AD mice, T0, C, LAB and p62-LAB groups (panel B) ($^{**}p<0.01$ and $^{***}p<0.001$ vs T0, $^{\#\#}p<0.01$ and $^{\#\#\#}p<0.001$ vs C, $^{\S\S}p<0.01$ vs LAB).*

Cathepsin B (Cat B) was previously associated with amyloid plaques and related memory loss and its inhibition was suggested to reduce Aβ levels [190, 191]. Interestingly, a 25% inhibition of Cat B activity was observed in p62-LAB treated mice compared to 16-weeks-old untreated mice (group C). Conversely, cathepsin L (Cat L), whose activity was reduced in control and LAB-treated animals compared to T0 group (29% and 26% inhibition, respectively), was significantly restored by p62-LAB exposure (21% activation respect to C) (Figure 31, panel B). This finding is of extreme importance considering Cat L role in the production of numerous peptide neurotransmitters and its α-secretase activity that is known to suppress amyloid peptides levels [192].

3.2.6: Effects of p62-LAB treatment on macromolecules oxidation

Extensive oxidative damage to cellular macromolecules characterizes the AD brain and p62 protein plays a protective role in oxidative conditions [193, 194]. Homogenized brain tissues from T0, control, LAB and p62-LAB treated mice were analyzed for the detection of oxidative markers. Protein oxidation was evaluated measuring carbonyls and 3-nitrotyrosine (3-NT) levels and results are reported in figure 32, panel A. The treatment with the p62-transformed bacteria was successful in reducing the amount of both oxidation products with a 1.78- and a 1.37-fold decrease of 3-NT and carbonyls compared to control, respectively. Similar results were obtained for 4-hydroxy-2-nonenal (4-HNE), a product of lipid peroxidation, whose levels where strongly reduced upon mice treatment with engineered LAB (-65% compared to control, Figure 32, panel B). DNA oxidation was determined detecting 8-oxo-7,8-dihydro-2′-deoxyguanosine (8-oxodG), the most prevalent form among oxidative base

modifications, and the expression of 8-oxoguanine DNA glycosylase-1 (OGG1) responsible for the removal of oxidized guanine base lesions generated by free radicals [36]. Interestingly, lower levels of 8-oxodG were detected in p62-LAB treated mice (1.6-fold reduction compared to control animals) that also showed a parallel increased expression of the DNA repair enzyme (2.4-fold increase) (Figure 32, panel C).

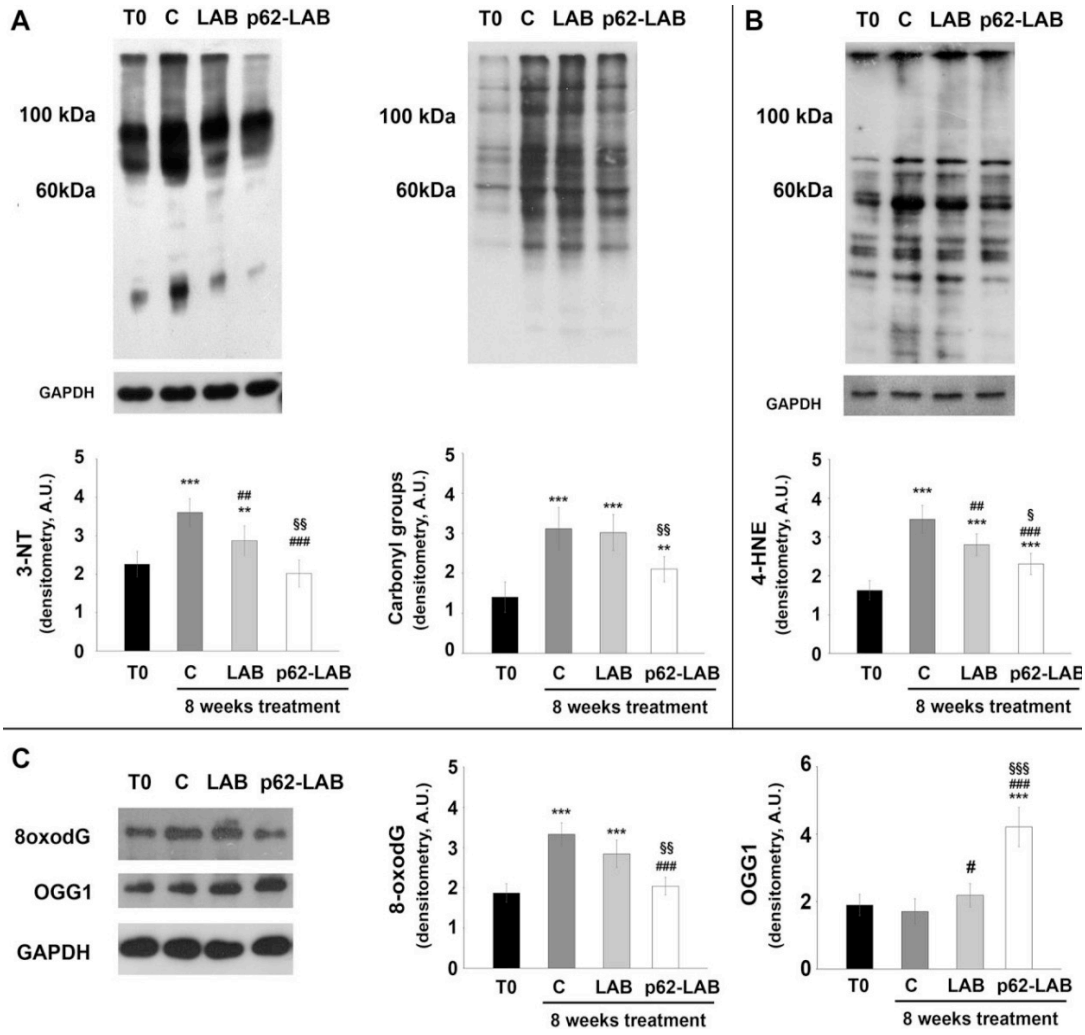

Figure 32: *Treatment effects on proteins, lipids and DNA oxidation. Determination of carbonyls and 3-NT (panel A), 4-HNE (panel B), 8-oxodG and OGG1 (panel C) in brain homogenates of 3xTg-AD mice (T0, C, LAB and p62-LAB groups). GAPDH was used as a control to check equal protein loading (*p<0.05, **p<0.01 and ***p<0.001 vs T0, ##p<0.01 and ###p<0.001 vs C, §p<0,05, §§p<0.01 and §§§p<0.001 vs LAB).*

3.2.7: Effects of p62-LAB treatment on inflammation

A panel of pro- and anti-inflammatory cytokines was monitored performing immunoassays to evaluate the modulatory effect of the treatment on brain inflammation (Figure 33). Our data definitely demonstrated that transformed LAB were able to significantly reduce the inflammatory status in AD mouse brain by stimulating the expression of anti-inflammatory molecules (Figure 33, panel A) and the simultaneous decrease of pro-inflammatory cytokines (Figure 33, panel B). In detail, the most consistent up-regulation for the anti-inflammatory cytokines was measured for IL-10 (3-fold increase compared to control). Conversely, all the pro-inflammatory molecules, that were heavily up-regulated with age (T0 vs C), resulted significantly reduced upon p62-LAB treatment (2.35-, 2.95-, 3.25- and 2.0-fold decrease for INF-γ, IL-1β, TNF-α and IL-2, respectively, compared to control). A weaker but still significant effect was also observed in mice administered with LAB.

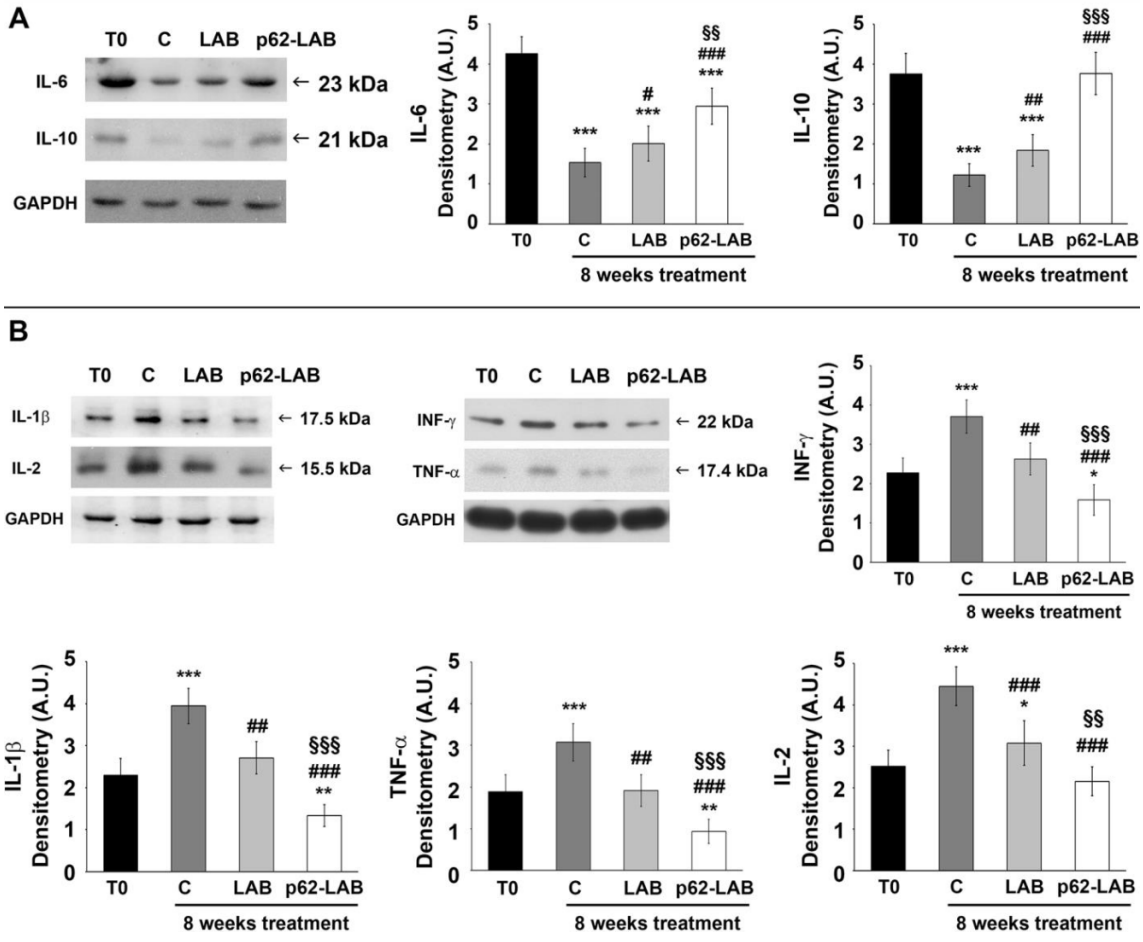

***Figure 33**: Treatment effects on brain anti- and pro-inflammatory cytokines. Detection of anti-inflammatory (panel A) and pro-inflammatory (panel B) cytokines by Western blot analysis in brain homogenates of 3xTg-AD mice (T0, C, LAB and p62-LAB groups). GAPDH was used as a control to check equal protein loading (*p<0.05 and ***p<0.001 vs T0, # p<0.05, ## p<0.01 and ###p<0.001 vs C, §§p<0.01 and §§§p<0.001 vs LAB).*

3.2.8: Effects of p62-LAB treatment on components of the gut-brain axis

Considering the ability of probiotics to exert neuroprotective effects through the modulation of components of the gut-brain axis [195], we measured the plasma concentration of gut peptide hormones and the microbiota composition in the four experimental groups. An age-dependent decrease of glucose-dependent insulinotropic polypeptide (GIP), glucagon like peptide-1 (GLP-1) and ghrelin concentration was detected in untreated AD mice (C) but no statistically significant changes were observed upon LAB or p62-LAB treatment (Figure 34).

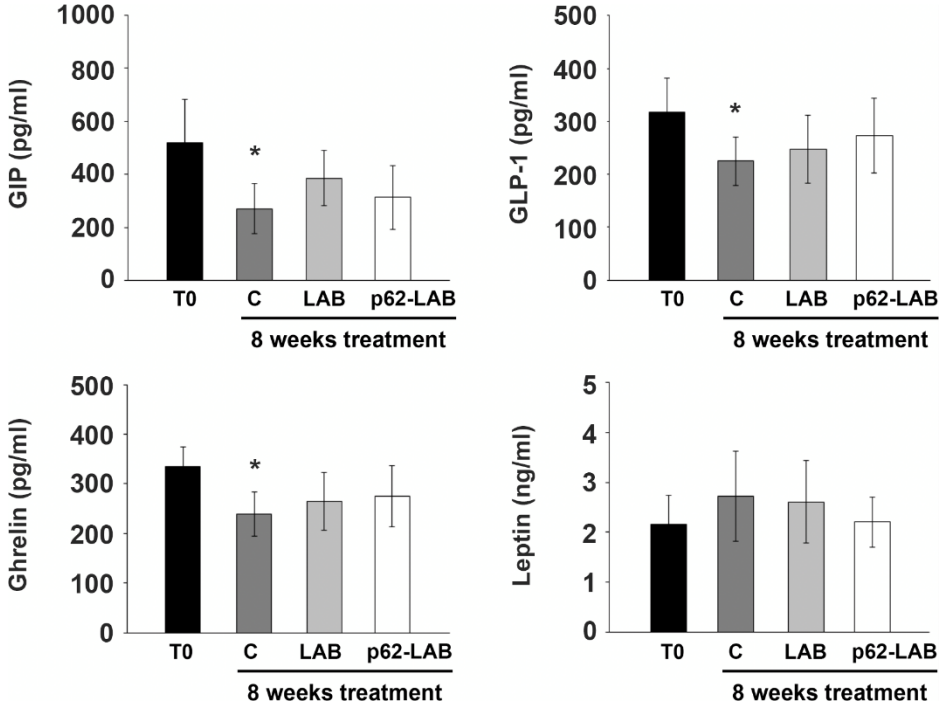

***Figure 34:** Plasma concentrations of gut hormones in 3xTg-AD mice. ELISA tests were performed following the instructions of the manufacturer (see Materials and Methods for further details). Data points marked with an asterisk are statistically significant compared to untreated 8-weeks-old mice (T0, *p<0.05).*

Microbiota composition was screened to check for changes in richness, the number of species present in a sample, and evenness, the related differences in abundance of species. Interestingly, the analysis of bacterial communities showed no significant difference in alpha diversity indices (Observed species, Chao1, and Shannon index), revealing no change in species richness and evenness (data not shown). Principal coordinate analysis (PCoA) based on unweighted Unifrac distance metric was used to assess beta-diversity, a parameter that compares bacterial communities among samples. The results obtained did not reveal significant clustering between groups (ANOSIMUnweighted: $R = 0.003$, $p = 0.475$, data not shown). Linear discriminate analysis effects size (LEfSe) detected few differentially abundant bacterial taxa on the phylogenetic levels (Figure 35). At the species level, the most evident change induced by the p62-LAB treatment was the increased abundance of unclassified species belonging to Rikenellaceae family (LDA score >4.0), whereas an increase in unclassified species belonging to Peptococcaceae family was associated to LAB administration (LDA score >2.9) (Figure 35, panel A). Univariate statistics revealed no significant differences between groups at phylum and class levels and only few differences at the other taxonomic levels including a decrease in Flexispira and in Erysipelotrichaceae in the p62-LAB group (C vs p62-LAB, $p<0.0093$ and $p<0.0409$, respectively) and an increase in family Ruminococcaceae in both LAB and p62-LAB group (C vs LAB 0.0455, C vs p62-LAB 0.0252). PICRUSt analysis to determine the predicted metabolic functions of the microbial communities detected changes in five pathways, with a LDA score between 2.0 and 2.4, in the gut microbiome of p62-LAB group (Figure 35, panel B). In addition, ten metabolic pathways differed with a $p<0.05$ between C and p62-LAB groups (Table 1).

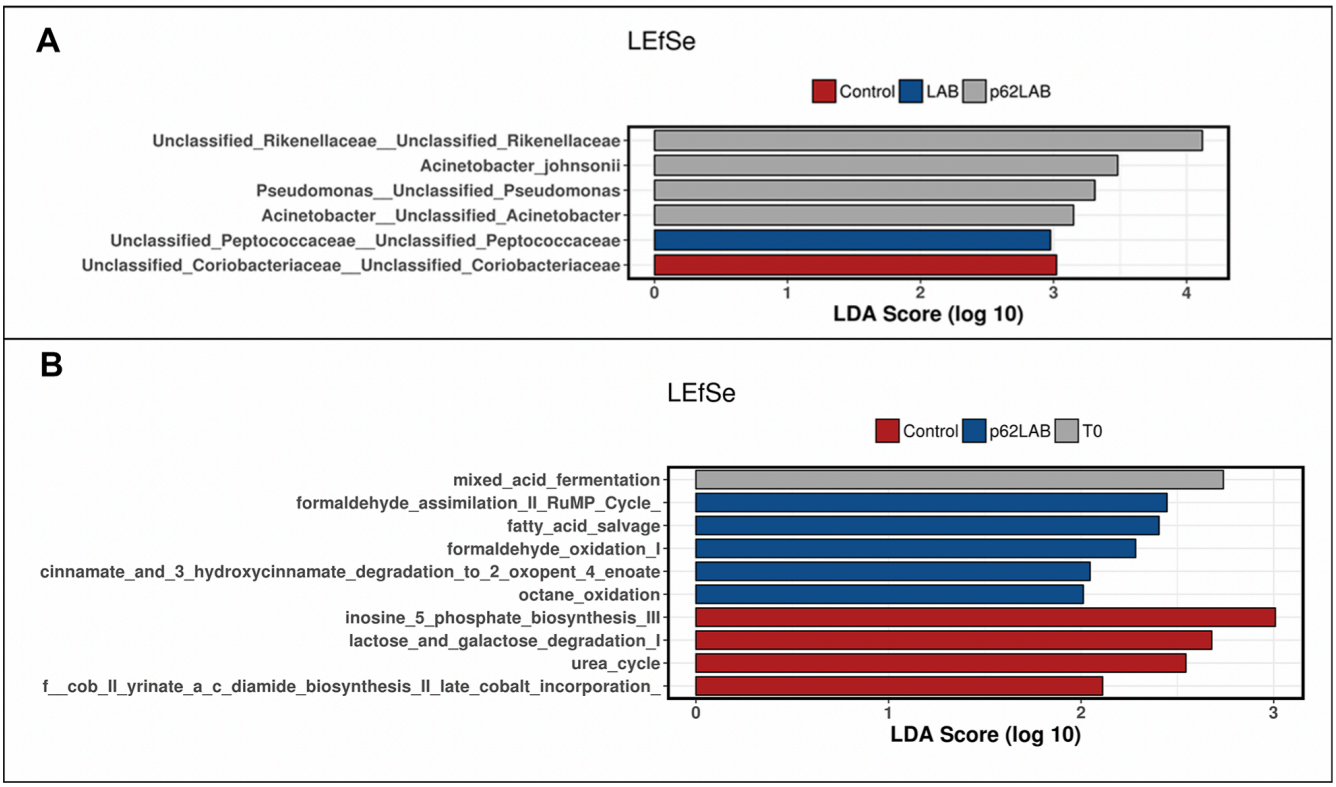

Figure 35: *Linear discriminant analysis effect size (LefSe) of bacterial taxa and KEEG pathways. LefSe of bacterial taxa and their association with C, LAB and p62-LAB groups. Only LefSe values >2 are shown (panel A). LEfSe of the differentially abundant KEGG pathways in T0, C and p62-LAB groups. Only LefSe values >2 are shown (panel B).*

Table 1: *KEGG pathways modified upon LAB and p62-LAB treatment. Only pathways with a p<0.05 are shown.*

KEGG pathways	***Groups***	***P-value***
catechol degradation to β-ketoadipate	Control vs. p62-LAB	0.0129
3-phenylpropanoate and 3-(3-hydroxyphenyl)propanoate degradation to 2-oxopent-4- enoate	Control vs. p62-LAB	0.0295
3-phenylpropanoate and 3-(3-hydroxyphenyl)propanoate degradation to 2-oxopent-4- enoate	LAB vs. p62-LAB	0.0097
3-phenylpropanoate degradation	Control vs. p62-LAB	0.0332
3-phenylpropanoate degradation	LAB vs. p62-LAB	0.0097
toluene degradation III (aerobic) (via p-cresol)	Control vs. p62-LAB	0.0078
catechol degradation III (ortho-cleavage pathway)	Control vs. p62-LAB	0.0129
aromatic compounds degradation via β-ketoadipate	Control vs. p62-LAB	0.0129
superpathway of salicylate degradation	Control vs. p62-LAB	0.0129
4-methylcatechol degradation (ortho cleavage)	Control vs. p62-LAB	0.0129
cinnamate and 3-hydroxycinnamate degradation to 2-oxopent-4-enoate	Control vs. p62-LAB	0.0218
cinnamate and 3-hydroxycinnamate degradation to 2-oxopent-4-enoate	LAB vs. p62-LAB	0.0295
3-phenylpropanoate and 3-(3-hydroxyphenyl)propanoate degradation	Control vs. p62-LAB	0.0218
3-phenylpropanoate and 3-(3-hydroxyphenyl)propanoate degradation	LAB vs. p62-LAB	0.0295

3.3: Discussion

AD is an age-associated disease characterized by numerous pathological hallmarks that slowly destroy memory and learning ability. Irrespective of considerable efforts made to develop new effective therapeutic agents, the drugs that are currently approved for the treatment of this disorder only provide symptomatic relief but cannot prevent the onset or block the progression of the pathology. Considering the multifactorial nature of AD, the design of novel drugs with a broad spectrum of activity could be a successful strategy for preventing its development. Recently, the use of recombinant bacteria, mainly Lactobacilli, has received great interest for their ability to act as delivery vectors of therapeutic molecules to mucosal surfaces [196]. These recombinant cells were tested in mouse models of colitis to reduce inflammation and re-establish intestinal homeostasis and of type 1 diabetes to restore antigen-specific tolerance [196]. In recent years, use of recombinant bacteria have also been extended to deliver optimized therapeutic molecules to multiple cancers [197], inflammatory bowel disease[198], nonalcoholic liver disease [199] etc.

In the light of these promising results, this work investigated the neuroprotective effects of a Lactobacillus lactis strain engineered with the pExu plasmid encoding the human p62 protein (pExu:p62 vector). This protein is widely recognized for its multiple roles in the cell and also emerged as a key factor in AD [200] In addition, previous data demonstrated that the administration of a p62-encoding plasmid exerted a powerful anti-osteoporotic, anti-inflammatory, and retinoprotective activity in animal models [201, 202].

Herein, we observed a marked increase in endogenous p62 levels in different tissues of p62-LAB treated mice, including the brain. Interestingly, a weak staining of the human p62 protein was detected in the three tested tissues analyzed with IHC, confirming previous findings on the ability of these bacteria to behave like vectors for local delivery of molecules to the gastrointestinal tract [178, 203]. However ,

no signal for the human p62 protein was detected in brain homogenates analyzed in WB, likely due to a low amount of cells expressing the protein or to a lower sensitivity of the antibody.

A possible mechanism induced by our treatment could be the activation of the p62-Keap1-Nrf2 axis, with a positive feedback loop activated by the exogenous p62. The increased amounts of this protein could activate Nrf2 by its dissociation from Keap1 and its translocation to the nucleus which then enables activation of various target genes, among them p62 and antioxidant response genes [260]. These processes are now under investigation in our laboratory. The analysis of the distribution of the p62 protein in p62-LAB treated animals performed by immunohistochemistry indicates the classical way of delivery of the protein from the gut mucosa to the brain, by lymphatic vessels and some neural terminations. In fact, a progressive decreased expression of the exogenous human-p62 peptide together with an increase of the endogenous mouse p62 protein were observed in the mesenteric lymph-nodes, in the spleen and in the brain. This dissemination route was also described in other disorders in which the infectious agents, such as viruses or bacteria, can gain access to the brain by using peripheral nerves (neural neuroinvasion) or the lymphatic/hematic way [204]. In our case, as shown by the results of IHC, the p62 protein follows both lymphatic and axonal pathways to finally reach the central nervous system (CNS). Comparatively, results from experimental sheep oral infections with the prion disease agent PrPsc showed that it reaches the brain through the early involvement of the enteric and abdominal ganglia. Data on the diffusion of the scrapie infectious agent described a three steps-based accumulation process upon oral ingestion of the prion protein: a first phase, with the accumulation in gut-associated lymphoid tissue (GALT), a second step involving the lymphatic dissemination of the protein to non-GALT lymphatic tissues and a final neuro-invasion phase until the CNS [205, 206].

Considering the numerous evidences associating decreased levels of p62 with AD pathology, it is reasonable to hypothesize that a re-establishment of its concentration could counteract AD signs [200,

207]. This assumption was confirmed by the NOR test that demonstrated a significant improvement in the recognition memory of treated mice. These encouraging outcomes positively correlated with lower brain deposition of APP and Aβ(1–40) and Aβ(1–42) peptides, the major agents responsible for plaques formation. Exploring neuronal proteolysis, p62-LAB treated animals showed proteasome inhibition and the simultaneous activation of autophagy, with increased LC3 and beclin-1 levels and selective modulation of cathepsin B and L activity. It is widely known that the two proteolytic pathways are closely related to each other and p62 is an important modulator of their cross-talk, and its presence contributes to the maintenance of protein homeostasis [122, 208-211]. Previous evidences described compensatory mechanisms between the two systems, with proteasome inhibition favoring autophagy stimulation [49, 51]. Increased autophagy and overexpression of beclin-1 and LC3 were previously demonstrated to exert neuroprotective effects favoring amyloid-beta protein clearance in AD mouse models [207, 212-214]. Autophagy is a highly dynamic multi-step process that can be modulated at different steps [215]. Thus, the expression of autophagy associated proteins is not always easy to interpret and several parameters must be considered. Our findings show that increasing p62 concentration upregulates autophagy-related proteins LC3II and beclin-1 and modulates cathepsins activity to finally promote autophagic removal of amyloid peptides. Lipidated form of LC3I to form LC3II is strongly bound to autophagosome and is widely used as autophagic marker [195]. Beclin-1 forms a highly regulated complex to regulate formation and maturation of autophagosome[216]. Cathepsins are key acid hydrolases present within the lysosome, and represent the principal effectors of protein catabolism and autophagy [217]. In particular, our results are in line with the findings of Caccamo et al., reporting that increasing brain expression of p62 favors the autophagy-mediated Aβ degradation [207]. However, differently from their gene therapy approach with direct injection of DNA into ventricles of newborn pups, we propose a non-toxic and non-invasive oral therapy.

Oxidative damage and inflammation are important components of AD brain pathology. Specifically, oxidation is observed in membranes, proteins and nucleic acids and associates with their loss of function whereas inflammatory alterations are accompanied by increased levels of pro-inflammatory cytokines [218-220].

DNA and RNA oxidation markedly increases the levels of nucleic acids oxidation markers 8OHdG and 8OHD; the markers are also reported to be present in NFT and Aβ plaques [221]. Oxidation of protein results in carbonylation of proteins; where carbonyl groups are being added to the protein by direct oxidation of lysine, arginine, proline and threonine residues, or from the cleavage of peptide bonds by the α-amidation pathway or by the oxidation of glutamyl residues [221] Measurement of protein carbonylation represents the extent of protein oxidation [221, 222] . The most toxic end products of Aβ induced membrane lipid peroxidation is reactive 4HNE [223]. 4HNE inhibits neuronal glucose and glutamate transporters, inhibition of Na-K ATPases, activation of kinases and dysregulation of intracellular calcium signaling; which evoke a cascade of mechanism leading to neuronal death [221, 224-226].

Here, we demonstrated that p62-LAB oral administration induces a clear reduction of oxidative and inflammatory markers, which is consistent with the previously identified anti-inflammatory and anti-oxidant properties of p62 [227-230]. In addition, since Aβ is a direct source of oxidative stress and that its deposition is linked to microglia activation and sustained pro-inflammatory signaling, reduction of its levels further contributes to counteract the two detrimental processes [218, 220, 231, 232]. A less evident but significant effect was observed upon treatment with control lactic acid bacteria that emerged as particularly successful in reducing inflammatory markers, thus confirming the health benefits associated to probiotic consumption [122, 233-235]. However, their use as delivery vectors for the p62-

pExu plasmid undoubtedly strengthens such effects and provides additional support to the therapeutic action of the proposed strategy in AD.

The analysis of microbiota composition revealed no side effects on gut microbiota nor major changes in composition in treated mice, with only a few taxa being shifted. Interestingly, in accordance with its anti-inflammatory properties, p62-LAB treatment decreased the relative abundance of the family Erysipelotrichaceae, previously demonstrated to be increased with age in AD mice and with a positive correlation with a pro-inflammatory gut micro-environment. In addition, an increase in the family *Ruminococcacea*, one of the major butyrate producing families and, remarkably, inversely correlated with intestinal permeability in AD, was observed [236-239]. The upregulated KEGG pathways were mainly related to the degradation of aromatic compounds that can be used as a source of carbon and energy, upon their conversion to substrates of the tricarboxylic acid cycle. Moreover, the absence of changes in gut hormones and the minor modifications in microbiota composition and related metabolic pathways suggest that the observed effects do not depend upon the modulation of gut-brain axis components.

Conclusively, our data demonstrate the therapeutic potential of p62-engineered Lactobacilli in an AD mouse model and propose a novel multi-target approach for AD treatment that takes advantage of the multifunctional activity of the p62 protein and of the beneficial properties and safety of these food grade bacteria. Nevertheless, additional pre-clinical studies are required to evaluate the long-term effects of the treatment and the persistence of the obtained results after the treatment is discontinued. Furthermore, once addressed the safety concerns on the use of engineered strains by humans and validated the strategies to optimize biocontainment and the translational potential of these modified microbes [240] clinical trials will be important steps to confirm the effective benefit of this approach for human AD patients. In fact, despite 3xTg-AD mice are a widely accepted model for human AD and

despite mouse and human share numerous similarities in physiology and anatomical structures, we should take into account that minor differences in the gastrointestinal tract (including microbiota composition), due to genetic background and environmental factors, could influence the final outcome of the study.

Chapter4: Effect of beer consumption on Alzheimer's disease: focus on microbiota modulation and inflammation

4.1: Materials and Method

4.1.1: Reagents and chemicals

Unfiltered unpasteurized beer with 9.2% alcohol content was provided by Kukà S.r.L. (Italy). SafAleTM T-58 yeast containing *Saccharomyces cerevisiae* and emulsifier E491was purchased from Fermentis (Italy). Protease inhibitors tosyl phenylalanyl chloromethyl ketone (TPCK) and 4-(2-Aminoethyl) benzenesulfonyl fluoride hydrochloride (AEBSF or Pefabloc) were from Sigma-Aldrich S.r.L. (Milano, Italy). Rat/Mouse Ghrelin (active) ELISA kit, Mouse Leptin ELISA, Rat/Mouse GIP (total) ELISA (Merk EZRMGIP-55K), and multi Species GLP-1 Total ELISA (Merk EZGLP1T-36K) were from Merk group.

4.1.2.: Animal model and experimental design:

Triple transgenic mice 3xTg-AD and their wild type (WT) counterpart were purchased from Jackson Laboratory (Bar Harbor, Maine, USA). This is a widely used animal model for AD due to its three distinguished mutations corresponding to familial AD (APP Swedish, tau P301L, and PSEN1 M146V). Translation of the overexpressed transgenes are confined to the central nervous system, including the hippocampus and cerebral cortex. Aβ deposition is continuous, with first signs surfacing within 3 to 4 months of age in the frontal cortex and becoming more extensive by 12 months [150, 179]. Eight-week-old AD and wt mice (n= 40), equal number of male and female, were divided in 4 groups and treated for a period of four months as follows: a group received water (n = 10), a group received 9.2% alcohol (n = 10, average of alcohol consumed per day by wt mice = 0.5g/day and AD mice = 0.4g/day), a group received unpasteurized beer (n = 10, average of beer consumed per day by wt mice = 0.19g/day and AD mice = 0.2g/day) and a group received unpasteurized beer enriched with yeast

(1,2*10^11 CFU) (n = 10, average of beer consumed per day by wt mice = 0.2g/day and AD mice = 0.2g/day).

Yeasts were daily dissolved in mice drinking beer and given to the animals. Cages were equipped with two bottles, one containing water and the other bottle containing alcohol or the unpasteurized beer, providing a free choice to the mice. The amount of ethanol, beer or water consumed was daily measured by comparing the volumes in the bottles before and after the access period. Liquid lost during handling by the experimenter or evaporation was estimated including same sets of bottles on empty cages. During the treatment the body weight was monitored every week to ensure food intake. After a four-month treatment, mice were sacrificed and fluids and organs collected and stored at -80°C. According to the guidelines of the European Communities Council (86/609/ECC) for the care and use of laboratory animals, mice were maintained in a temperature-controlled room (21±5 °C) under an inverted 12 h light/dark cycle (lights on at 8:00 pm) and provided with rodent standard food (Mucedula, Italy) and water *ad libitum*. All appropriate measures were taken to minimize pain and discomfort in these experimental animals. General observations regarding possible changes in skin and fur, mucous membranes, diarrhea, sleep, movements and posture were performed. Additionally, local injuries and mortality (if any) were recorded throughout the experimental period. The body weight was measured at the beginning of the treatment and then once a week to ensure adequate food intake.

4.1.3.: Novel object recognition

Behavioral tests were performed during the animals' dark phase starting from 8:00 to 15:00. Animals were handled for 3 days before testing in order to accustom them to the experimenter. The investigators were blinded to the groups' allocation during the tests. The novel-object recognition test (NOR, based on the spontaneous tendency of rodents to spend more time exploring a novel object than a familiar one) was used to evaluate recognition memory. The first step is the habituation, during which the animal is allowed to explore the empty arena for 5 min and then returns to the home cage. Following

a training period dedicated to the exploration of two identical objects, the animal is removed from the arena for a delay period of 3 h, and it is then placed back within the arena, where one of the two identical objects is replaced by a new, dissimilar novel object (test phase). The time the rodent spends exploring each object in 10 min provides a measurement of the extent of memory integrity and attention. Results were expressed as discrimination scores (the ratio between the time spent with novel object and total time spent with both objects). A lower score indicates memory impairment in this task. Objects were different in shape, color and texture and maintained throughout the study to obtain reproducible data. Preliminary experiments were done to select novel and familiar object pairs, so that each object in the pairs elicited the same amount of spontaneous investigation.

4.1.4.: Preparation of brain and plasma samples

Brain parts, respectively hippocampus (HIP) and prefrontal cortex (PFC), were homogenized (1:5 weight/volume of buffer) in 50 mM Tris buffer, 150 mM KCl, 2 mM EDTA, pH 7.5. Homogenates were immediately centrifuged at 13.000 x rpm for 20 min at 4°C and an aliquot of the supernatant was immediately supplemented with protease inhibitors (Pefabloc and TPCK) for ELISA determinations. The Bradford method was used to measure the protein concentration in homogenates, using bovine serum albumin (BSA) as a standard [151]. Blood samples were collected in tubes with 10% w/v (g/100ml) of K_2-EDTA, centrifuged at 13,000 rpm for 20 min at 4°C. Plasma was promptly supplemented with proteases.

4.1.5: ELISA for Aβ peptides levels

Brain homogenates supplemented with protease inhibitors (Pefabloc and TPCK) were used to measure Aβ(1–40) and Aβ(1–42) levels using enzyme-linked immunosorbent assay NOVEX® ELISA kits (Thermo Fisher Scientific Inc., Waltham, MA USA).

4.1.6: ELISA for gut hormones determination

Plasma supplemented with protease inhibitors (Pefabloc and TPCK) was used to measure the concentration of ghrelin, leptin, glucose-dependent insulinotropic polypeptide (GIP) and glucagon like peptide-1 (GLP-1). Sandwich ELISA kits were obtained from Merck KGaA, Darmstadt, Germany, and the assays were performed following manufacturer's indications.

4.1.7: ELISA for cytokines determination

Brain sections and plasma samples, from wt and AD mice, added with protease inhibitors were also used to measure pro- and anti-inflammatory cytokines using the following ELISA kits: the IL-10 Mouse ELISA Kit, the IL-1β Mouse ELISA Kit, the TNF-α Mouse ELISA Kit, High Sensitivity and the IL-4 Mouse ELISA Kit (Thermo Fisher Scientific Inc., Waltham, MA USA), following the manufacturer's instructions.

4.1.8: Western blotting

Brain homogenates (20 μg of proteins) were loaded on 12% SDS-PAGE and electroblotted onto polyvinylidene fluoride (PVDF) membranes. Membranes were activated with methanol and blocked with 5% BSA in freshly prepared TTBS (Tween 20 plus Tris-HCl and NaCl, pH 7.5). Antibodies were diluted in 2% BSA in TTBS. Proteins were detected with the enhanced chemiluminescence (ECL) system (Amersham Pharmacia Biotech, Milano, Italy). Primary antibodies used to detect pro- and anti-inflammatory cytokines were from Abcam plc (Cambridge, UK). Membranes for western blotting analyses were purchased from Millipore (Milano, Italy). Molecular weight markers (10 to 245 kDa, Abcam) were included in each gel. Glyceraldehydes-3-phosphate dehydrogenase (GAPDH) was used as equal protein loading control. Membranes were stripped using a stripping buffer containing 200 mM glycine, 0.1% SDS and 1% Tween 20 and re-probed with an anti-GAPDH antibody (Santa-Cruz Biotechnology, Heidelberg, Germany). Immunoblot images were quantified using ImageJ 1.52p software (NIH, USA).

4.1.9: Fungal and bacterial ribosomal DNA extraction.

Fecal samples from the sacrificed WT and AD mice were collected, kept in dry ice and immediately stored at -80°C until analysis. Microbial genomic DNA was extracted using the Maxwell® 16 LEV Blood DNA kit with the Maxwell® 16 instrument (Promega Italia S.r.l). In detail, each sample was lysed in 400 µl of lysis buffer and incubated at 95°C for 5 min and mixed at 800 rpm with a Eppendorf Thermomixer® R Thermal Mixer. After centrifugation at 13,000 rpm for 5 min, 30 µl of proteinase K was added before a second incubation step at 56°C in thermomixer for 20 min at 500 rpm. Then, the samples were loaded into the LEV cartridge to allow the extraction of DNA that was eluted in 100 µl of elution buffer. Genomic DNA concentration and quality was assessed by Nanodrop spectrophotometer (Thermo Fisher Scientific). Moreover, two blank samples have been also collected as control of this analytical step. Both bacterial and fungal communities were analyzed. For bacteria analysis, a multiplexed 16S rRNA amplicon-based approach coupled with the NGS system MiSeq (Illumina) was used. A 500 bp amplicon, spanning the V4-V6 hyper-variable regions of the 16S rRNA gene, has been obtained. Each sample was individually amplified and purified (AMPure XT beads, Beckman Coulter Genomics). Then, a second-round PCR has been performed to ligate at the end of each amplicon the adapters required for sequencing and a specific "index". Indexes are short, unique sequences used to univocally tag different samples allowing their multiplexing. Indeed, after a magnetic beads' purification, quality assessment (TapeStation, Agilent Technologies) and normalization, the barcoded amplification products from different DNA samples were pooled in equimolar ratios. In each PCR step, 2 negative controls were included to be further processed as contamination controls of the analytic procedure. The obtained multiple amplicon libraries were quality assessed (Agilent TapeStation) and quantified (Qubit, Life Technologies), before sequencing with the V3 300X2 PE MiSeq protocol (Illumina), according to the specifications of the manufacturer. For fungi analysis,

specific primers have been used for Internal transcribed spacer 1 (ITS1) amplification. After the first-round PCR to specifically amplify the target region, the amplicons were treated as specified above for the 16s rRNA. Also in this case, PCR controls have been processed together with the samples to provide analytic controls of any environmental contaminant. Sequencing reactions were carried out on the MiSeq System (V3 300X2 PE). FASTQ files were sent to CRG bioinformatic facility for primary data analysis. MOTHUR output package has been used for further analyses using microbiome analyst tool. Blank samples passed through the entire collection, extraction, and amplification process remained free of DNA amplification.

4.1.10.: Statistical analysis

Data are expressed as mean values ± S.D. Statistical analysis was performed with one-way ANOVA, followed by the Bonferroni test using Sigma-stat 3.1 software (SPSS, Chicago, IL, USA). p-Values $p<0.05$ were considered significant.

4.2 Results

4.2.1 Effect of beer consumption on cognitive performance

The effect of the treatments on the consolidation process of memories in mice was assessed through the novel object recognition (NOR) test, a widely used tool to investigate the neurobiology of memory. These studies involved the evaluation of different memory processes, such as acquisition, consolidation (and reconsolidation) and retrieval, as well as the brain mechanisms that underlie these processes [241]. After the treatment, NOR test was performed on both control and treated groups. No significant differences were observed in the discrimination scores of wt mice (figure 36). Interestingly, AD mice treated with beer and beer/yeast showed a better "discrimination index" ($p<0.05$) than control animals.

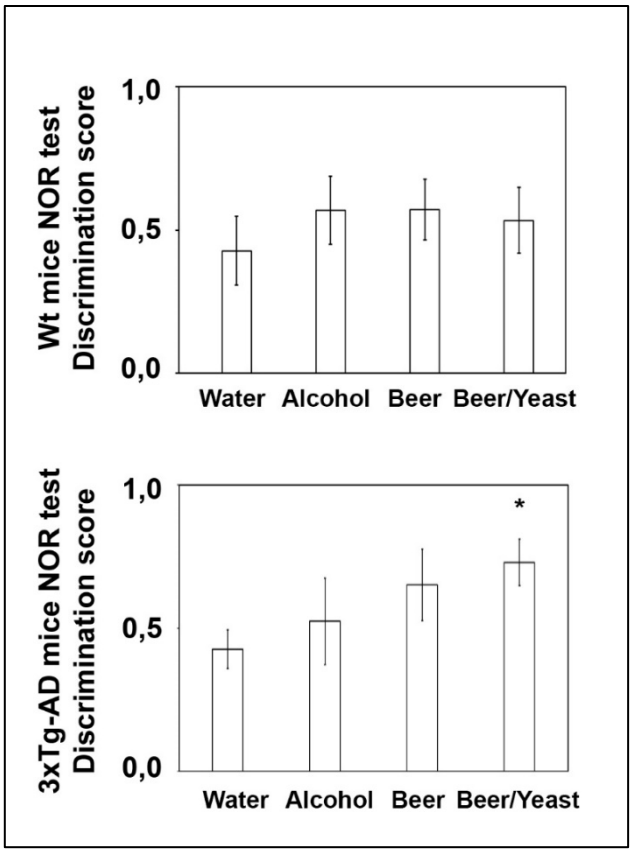

***Figure 36**: Novel Object Recognition (NOR) test. The discrimination scores obtained for the four groups of mice are reported. The asterisk (*p<0.05) indicates a significant statistical difference between the beer/yeast group and the water group*

In addition, the beer yeast group performed better on the NOR test than the alcohol treated group ($p<0.05$). These results suggest the beneficial effect of the treatment on hippocampus functions and recognition memory.

4.2.2 Effects of beer consumption on the amyloid load

Accumulation of amyloid beta peptides into plaques is a major hallmark of AD. To evaluate the effect of the treatment on the amount of these proteins, we measured the levels of amyloid (1-40) and (1-42) in hippocampus and frontal cortex of control and treated animals. The treatments were not effective in reducing the levels of the Aβ(1-40) peptide (Fig. 37).

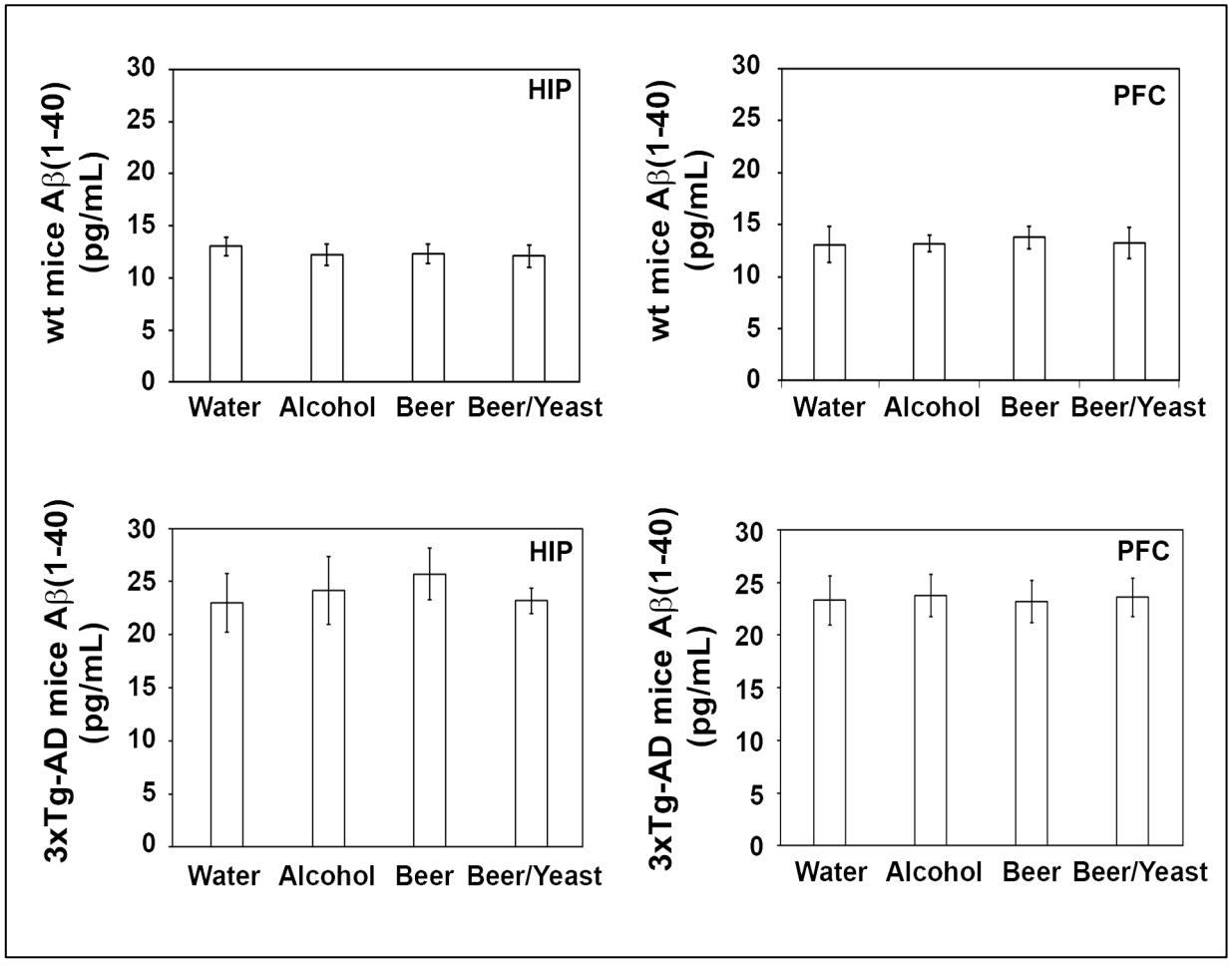

Figure 37: *Levels of Aβ(1-40) peptide measured by ELISA on brain homogenates of wt and 3xTg-AD mice in T0, Water, Alcohol, Beer and Beer/Yeast groups. Concentrations are expressed as pg/mL. HIP: hippocampus, PFC: prefrontal cortex.*

Conversely, the results showed a significant reduction of the Aβ(1-42) peptide, the most toxic and prone to aggregation, in the two brain regions of mice treated with beer/yeast compared to control animals and beer-treated mice (Fig. 38). In the hippocampus, a significant decrease of Aβ(1-42) levels with respect to control groups was also detected in mice treated with the beer.

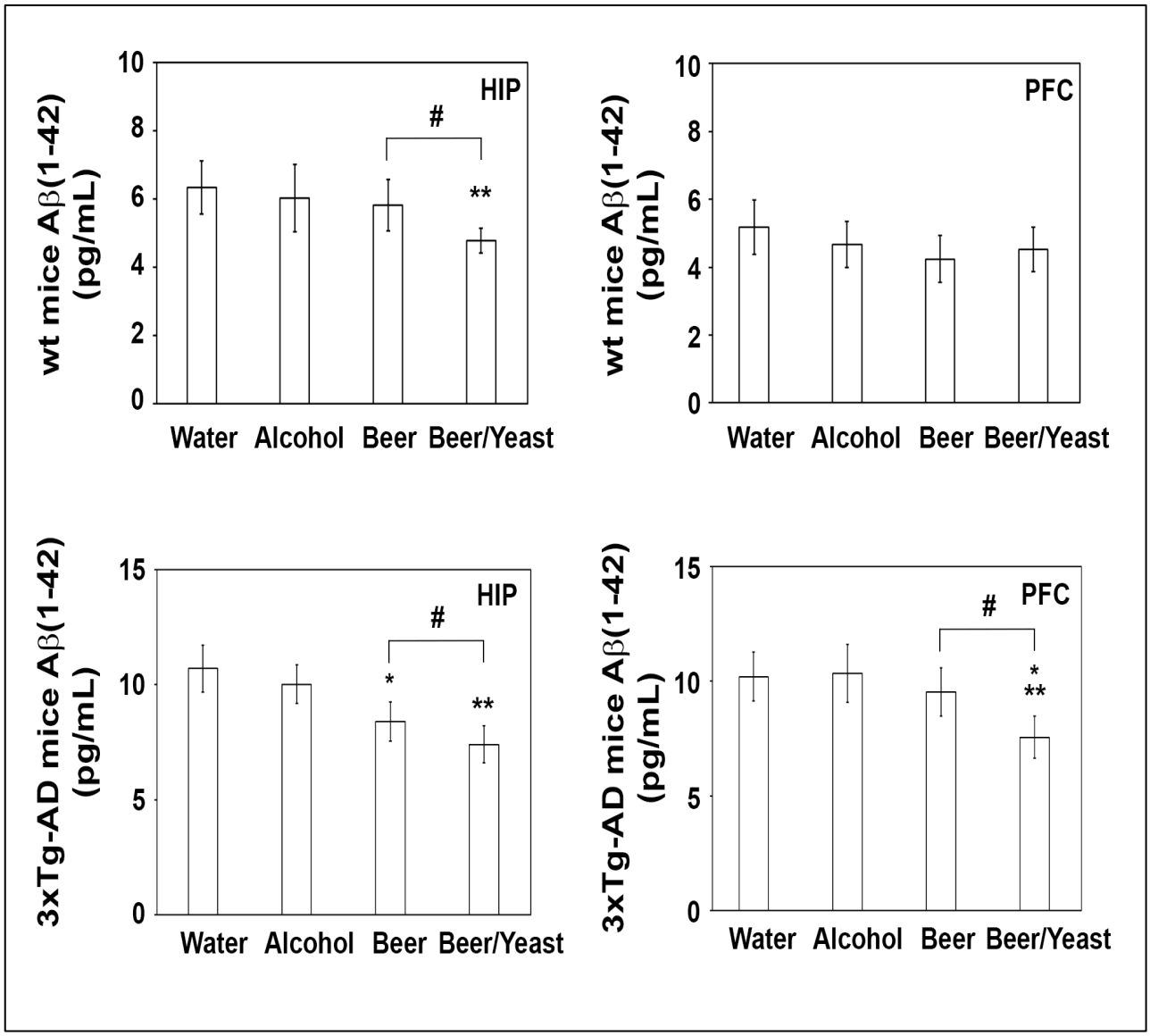

***Figure 38**: Levels of Aβ(1-42) peptide measured by ELISA on brain homogenates of wt and 3xTg-AD mice, T0, Water, Alcohol, Beer and Beer/Yeast groups. Concentrations are expressed as pg/mL. HIP: hippocampus, PFC: prefrontal cortex. (HIP: *p<0,05 B vs W and A, ** p<0,01 BY vs W and A, # p<0,05 BY vs B, PFC: ** p<0,01 BY vs W and A, # p<0,05 BY vs B).*

4.2.3 Effects of beer consumption on cytokines levels

Extensive inflammatory processes characterize the AD brain with increased amounts of pro-inflammatory molecules and decreased levels of anti-inflammatory cytokines. To evaluate possible effects of beer consumption on the inflammatory status of control and treated animals, we measured the amounts of pro- (IL-β and TNF-α) and anti-inflammatory (IL-4 and IL-10) cytokines in both the brain and plasma using ELISA kits. Samples from control and treated wt mice showed no difference in the levels of the cytokines IL-β and IL-4 (both measured in the brain) and TNF-α and IL-10 (both measured in the plasma) (Figures 39-40). Conversely, an evident modulation of the inflammatory condition was obtained in AD mice treated with the yeast-enriched treatment. In detail, a decrease of the pro-inflammatory molecules and a simultaneous increase of the anti-inflammatory cytokines was detected (Figures 39-40).

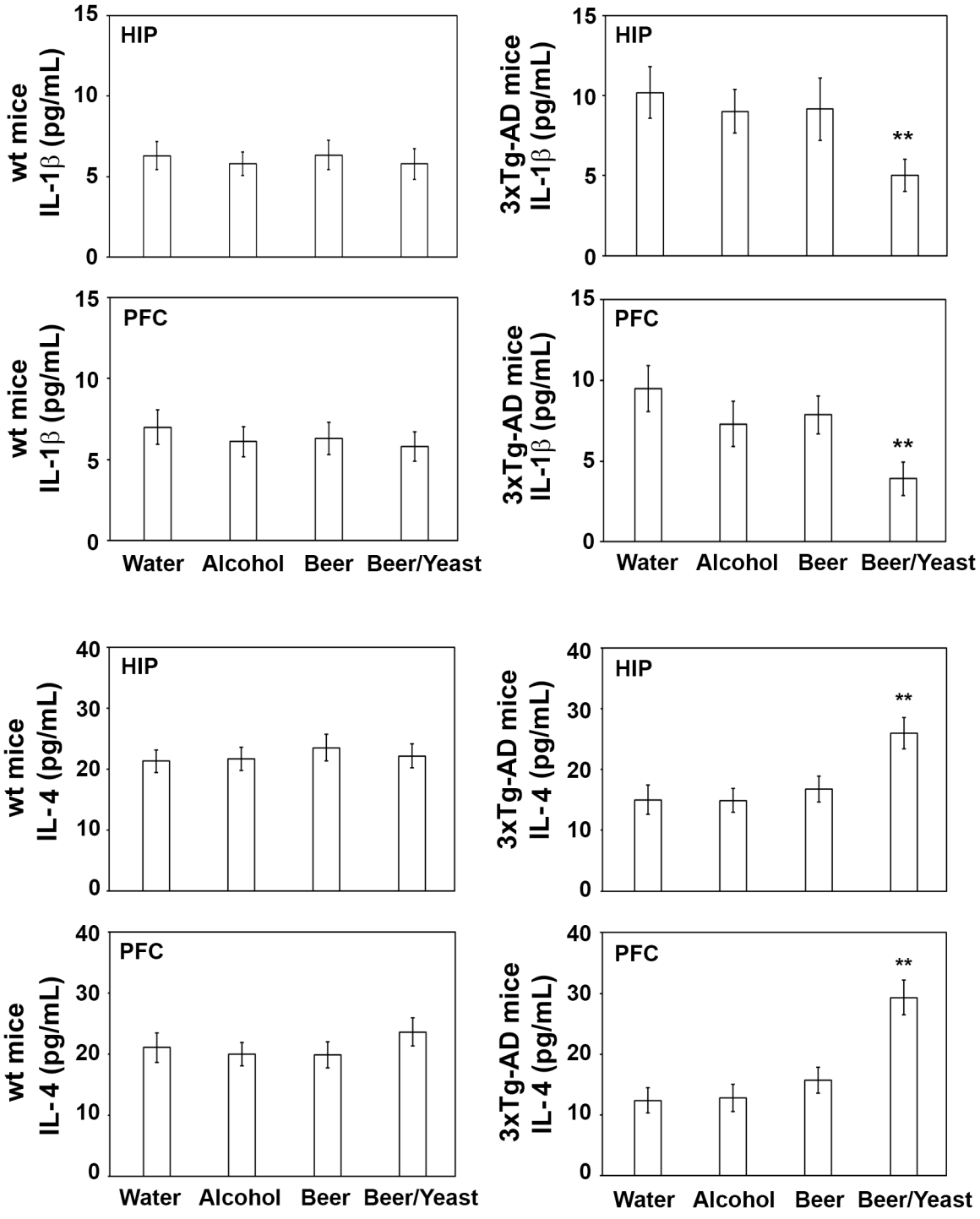

Figure 39:. *Levels of IL-1β and IL-4 measured by ELISA on brain homogenates of wt and 3xTg-AD mice, Water, Alcohol, Beer and Beer/Yeast groups. Concentrations are expressed as pg/mL. HIP: hippocampus, PFC: prefrontal cortex. (**p<0,01 BY vs W, A and B).*

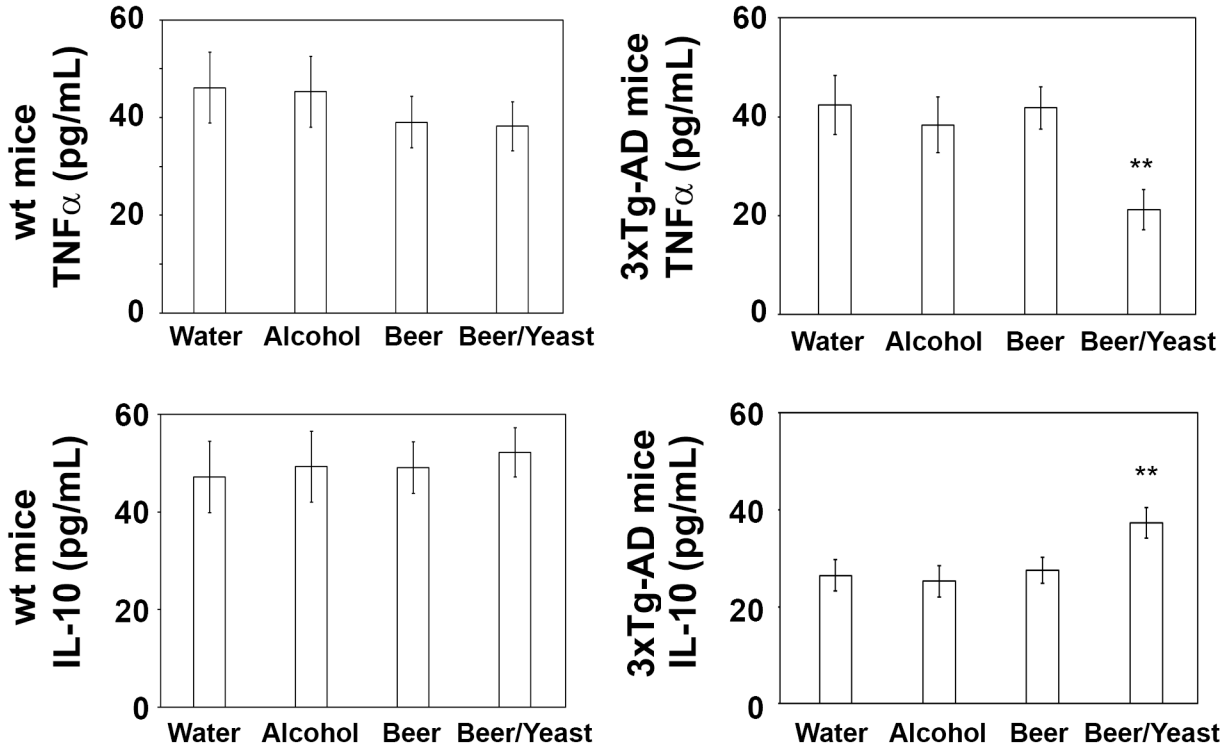

***Figure 40**: Levels of TNF-α and IL-10 measured by ELISA on plasma samples of wt and 3xTg-AD mice, Water, Alcohol, Beer and Beer/Yeast groups. Concentrations are expressed as pg/mL. HIP: hippocampus, PFC: prefrontal cortex. (**p<0,01 BY vs W, A and B)*

4.2.4 Effects of beer consumption on gut hormones levels

In order to assess an effect of the treatment on the gut-brain axis, the concentration of gut hormones, such as leptin, ghrelin, GIP and GLP-1, was determined in plasma samples using ELISA kits (Figure 41). The results show that treatment with beer and beer yeast did not significantly alter the levels of the four tested hormones.

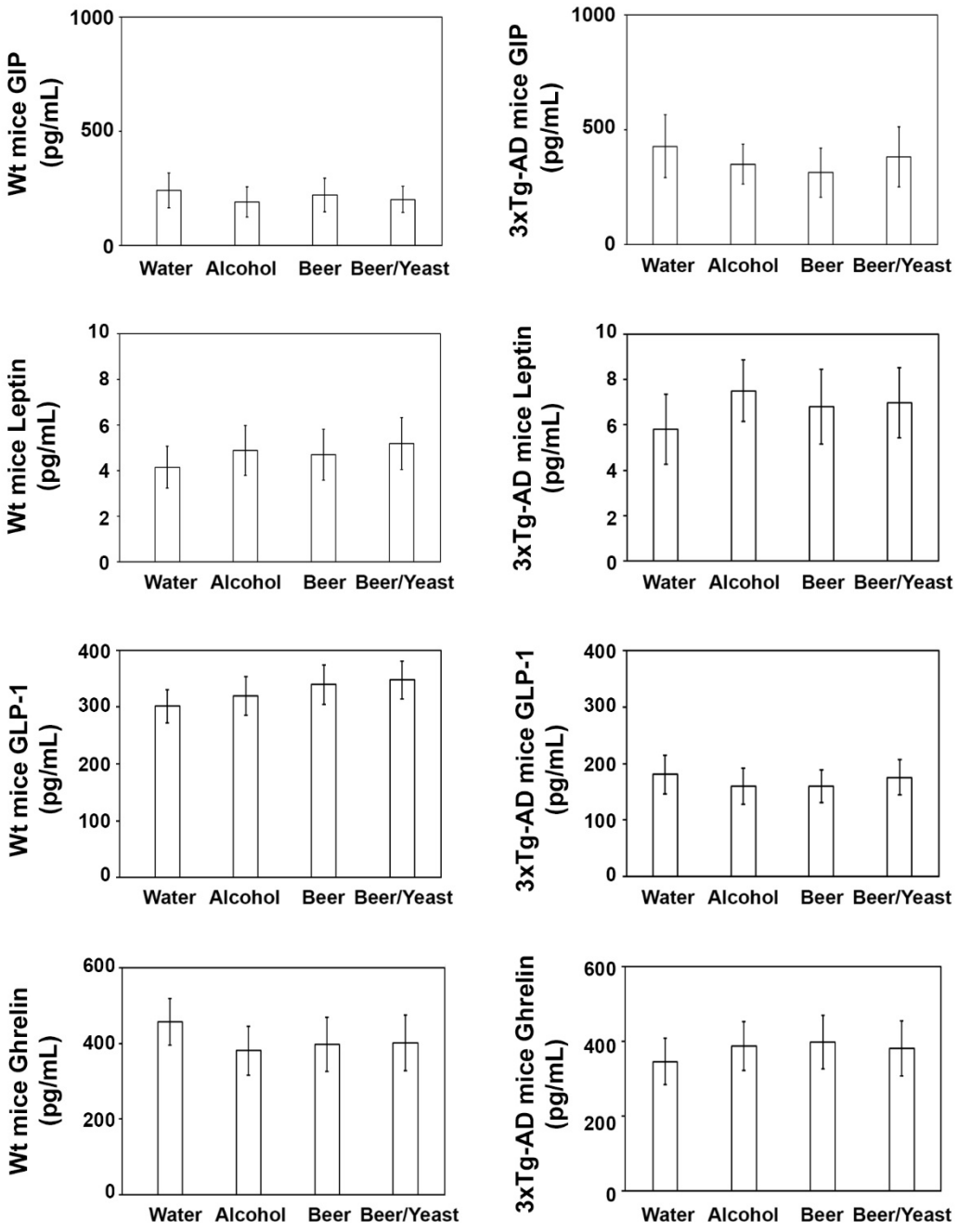

Figure 41: *ELISA tests were performed on plasma samples to determine the levels of GIP, Leptin, GLP-1 and Ghrelin in wt and 3xTg-AD mice. The assays were executed following the instructions of the manufacturer (see Materials and Methods for further details).*

4.2.5 Bacterial communities' evaluation through 16S rRNA analysis

Totally, an average of 29,030 reads/sample were obtained, allowing the identification of 126 operational taxonomic units (OTUs) for further analyses. Controls (blanks) unamplified DNA samples were removed for data analyses. Considering that the gut microbiota of AD patients and animal models displays reduced diversity and a typical taxonomic composition, with decreased Firmicutes and Bifodobacteria and increased Bacteroidetes compared to the microbiota of healthy controls [122, 242], the presence of bacterial dysbiosis in 3xTg-AD mice was verified and the ability of treatments to promote the establishment of beneficial taxa was studied. Alpha diversity was measured considering two key components: richness and evenness. Richness is the number of species (or OTUs) observed in the sample. Evenness describes relative differences in the abundance of various species in the community. Interestingly, AD mice treated with beer (B) or beer+yeast (BY) had a significantly higher richness (Fig 42) with respect to the other groups. These results indicate a higher heterogeneity of gut microbiota at all taxonomic levels upon beer consumption. Additionally, AD mice had a lower evenness with respect to wt animals, independently of the treatment (Fig. 43).

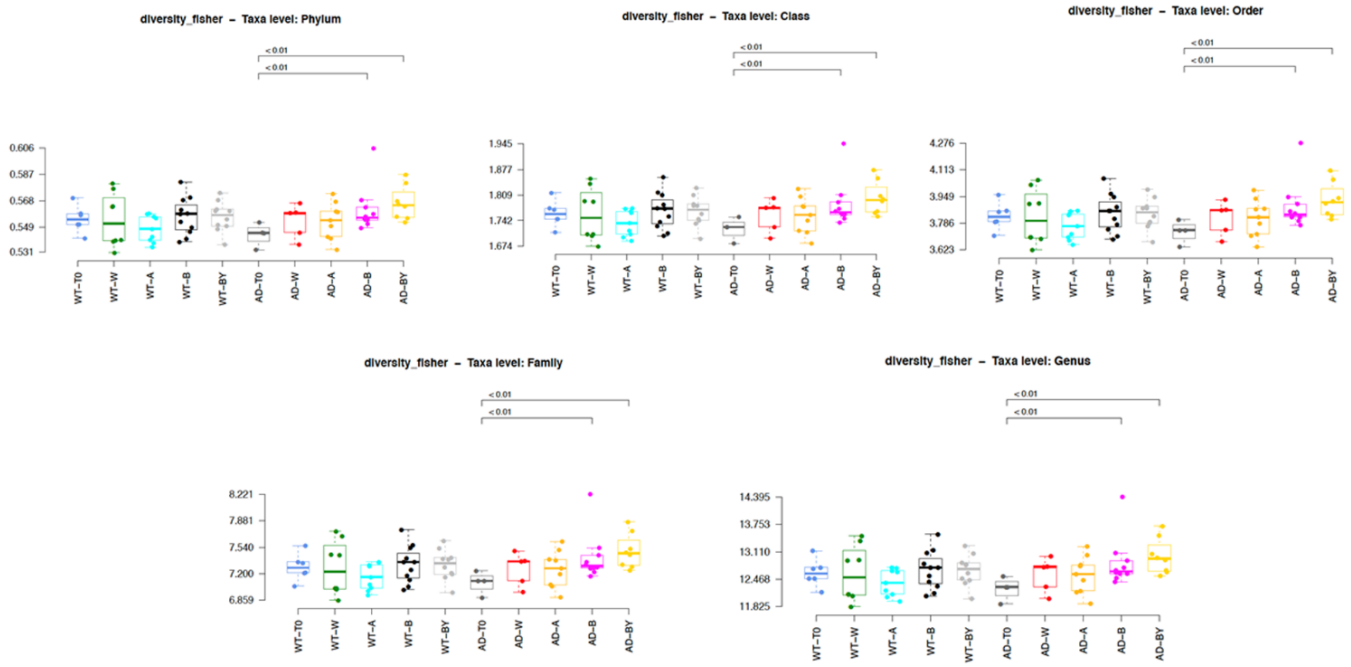

Figure 42: *Fisher diversity index to phylum, class, order, family, and genus level, for each treatment (T0, W, A, B and B+Y) in wt and AD mice. Significant differences with respect to 8 week-old mice (T0) by Tukey test are indicated (p≤ 0.01).*

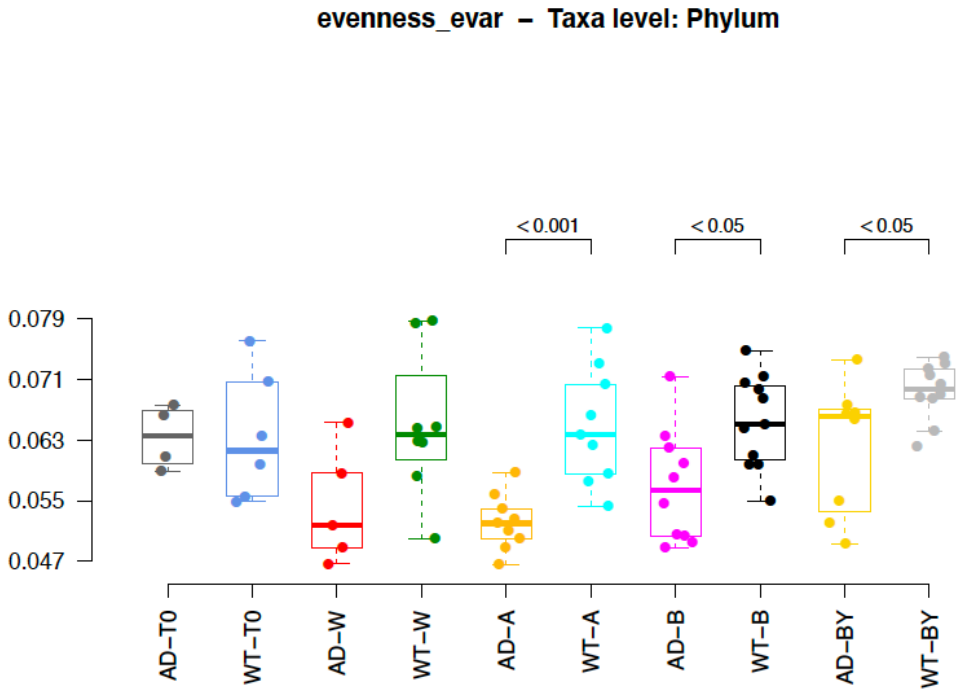

***Figure 43**: Fisher diversity index to phylum level, for each treatment (T0, W, A, B and B+Y) in wt and AD mice. Significant differences with respect to 8 week-old mice (T0) by Tukey test are indicated (p≤ 0.01).*

AD mice administered with water had a lower evenness and richness with respect to the other groups (Fig 44).

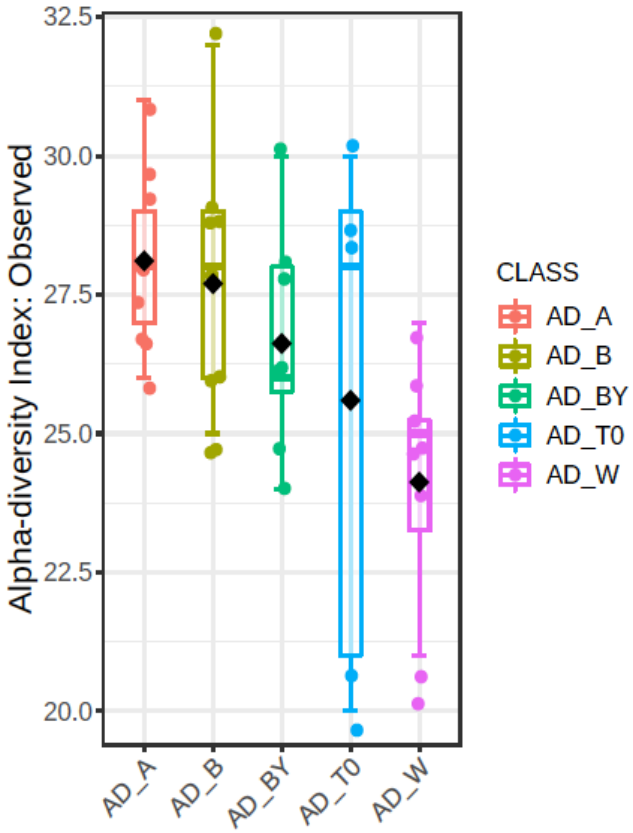

***Figure 44:** Alpha diversity between the tested conditions evaluated using observed species, Chao1 and Shannon metrics.*

Beta diversity was measured to verify samples clustering based on group status. PCoA was measured with both Unweighted and Weighted UniFrac Distance. The analysis of group similarities based on ANOSIM method showed an R value of 0.4 (P<0.003) and 0.06 (P<0.242) for the unweighted weighted methods, respectively (data not shown). No significant differences were observed in species richness between wt and AD mice.

Taxonomy assignment showed different bacterial profiles in the individual samples at phylum level. Merging samples/status, these differences are more evident: at phylum level, the AD mice

were featured by a lower abundance of Firmicutes and a higher abundance of Proteobacteria respect to the wt (Fig. 45). At genus level, the AD group was featured by an increase of Lactobacillus, Parasutterella and Clostridiales_unclassified and reduction of the Lachnospiraceae_unclassified, Ruminococcaceae_unclassified and Turibacter genera.

Univariate analysis (T-test/ANOVA) showed no significantly different taxa at phylum, class, order, family and genus level between the AD and wt groups. However, Deseq analysis, showing taxa that are differentially abundant in compared groups at p-value (adjusted for multiple testing) <0.05 and average relative abundance for either group above 1%, showed a significant difference just at phylum level highlighting the increase of Proteobacteria in the AD mice.

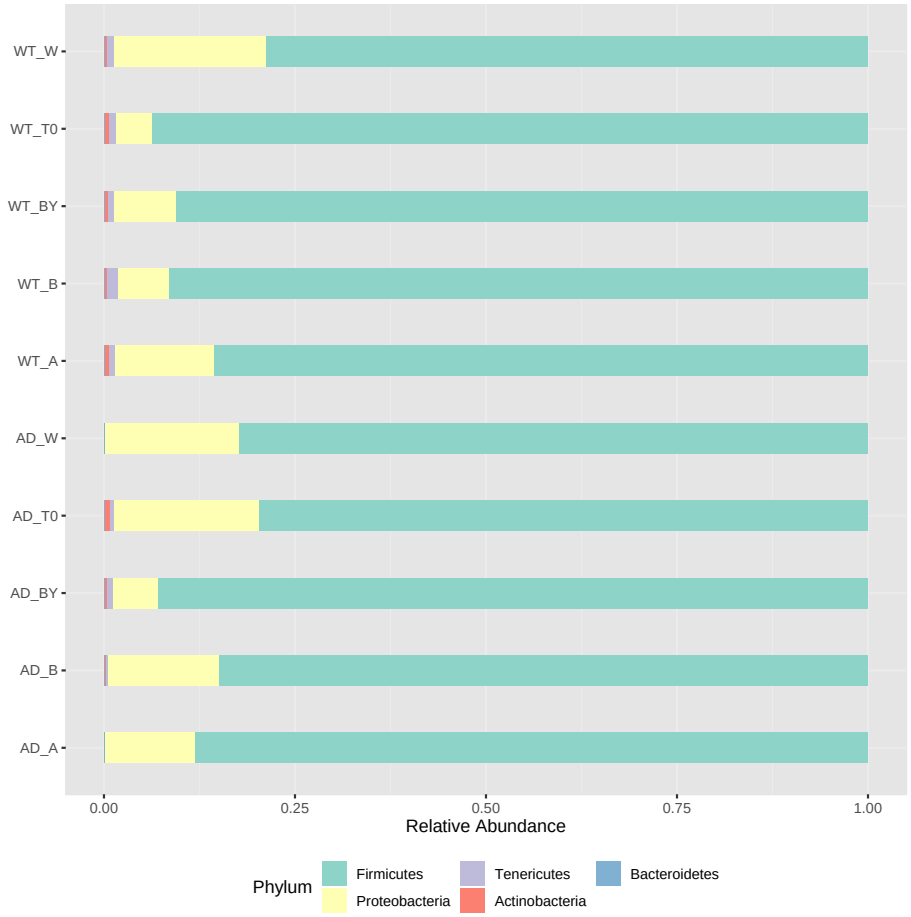

***Figure 45**:Bacterial profiles at phylum level obtained with the phylogeny-based taxonomy assignment approach.*

At phylum level, all treatments were able to increase the percentage of Protobacteria and reduce that of Firmicutes with respect to the WT_T0. Interestingly, AD mice treated with yeast-enriched beer showed a reduction of Protobacteria and an increase of Firmicutes that resemble the WT_T0 composition.

Interestingly, taxonomic assignment showed that the B+Y treatment is able to modify the microbiota and to promote changes that are more similar to the WT_T0 group. Abundances pie chart at phylum level shows that taxa of AD_BY group are more similar to WT with respect to both AD_T0 and AD_W groups. The treatment seems to be associated with an increase of Firmicutes and a decrease of Proteobacteria phyla (Fig. 46).

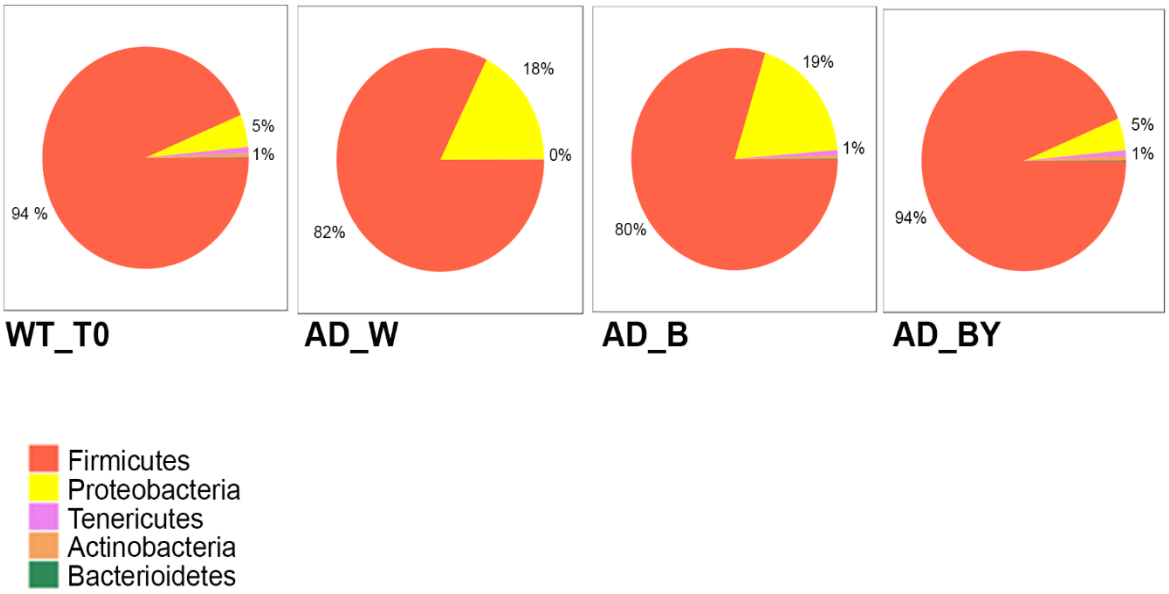

Figure 46: *Overall bacterial microbiota composition in mice untreated (W, water) or treated with beer (B) or beer and yeast (BY). Abundances pie chart at phylum level.*

4.2.6 Fungal communities' evaluation though ITS1 analysis

Fungal-specific internal transcribed spacer (ITS) amplicon sequencing was performed to investigate associations between the fungal gut microbiota and AD using the 16S rRNA high-throughput gene MiSeq platform and to evaluate a possible positive effect upon beer consumption. Totally, 469 OTUs were identified, and an average of 95,184 reads/sample were obtained. No differences were found in the alpha diversity between AD_T0 and WT_T0 using different methods. Similarly, beta diversity evaluated both as unweighted and weighted UniFrac Distance analyses, showed no clustering between the 2 tested groups at time 0 (data not shown). Although a large fraction falls within unclassified fungi, taxonomic assignment showed at phylum level a reduction of both Ascomycota and Basidiomycota in the AD mice with respect to the WT group (Fig. 47).

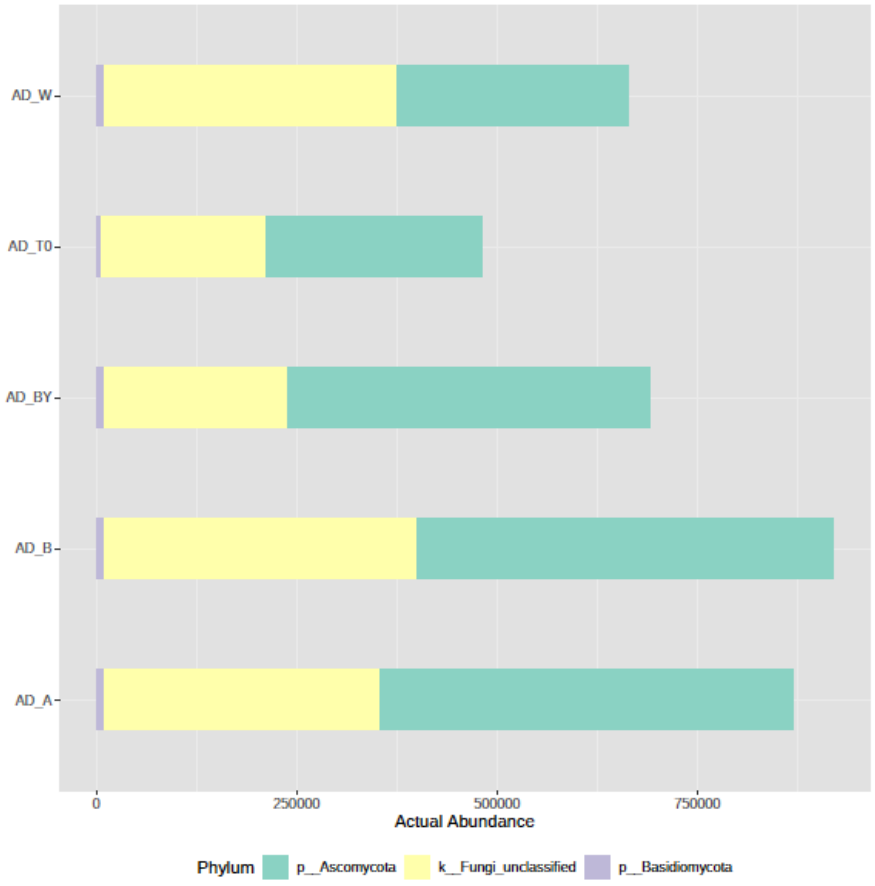

***Figure 47**: Fungal profiles at phylum level obtained with the phylogeny-based taxonomy assignment approach.*

At genus level, the AD group presents a reduced abundance of Blumeria, Pleosporales_unclassified, Malassezia and Aspergillus genera. Abundances pie chart at phylum level shows that taxa of AD_BY group are more similar to WT with respect to both AD_T0 and AD_W groups. The BY treatment is associated to an increase of the Ascomycota phylum (Fig. 48).

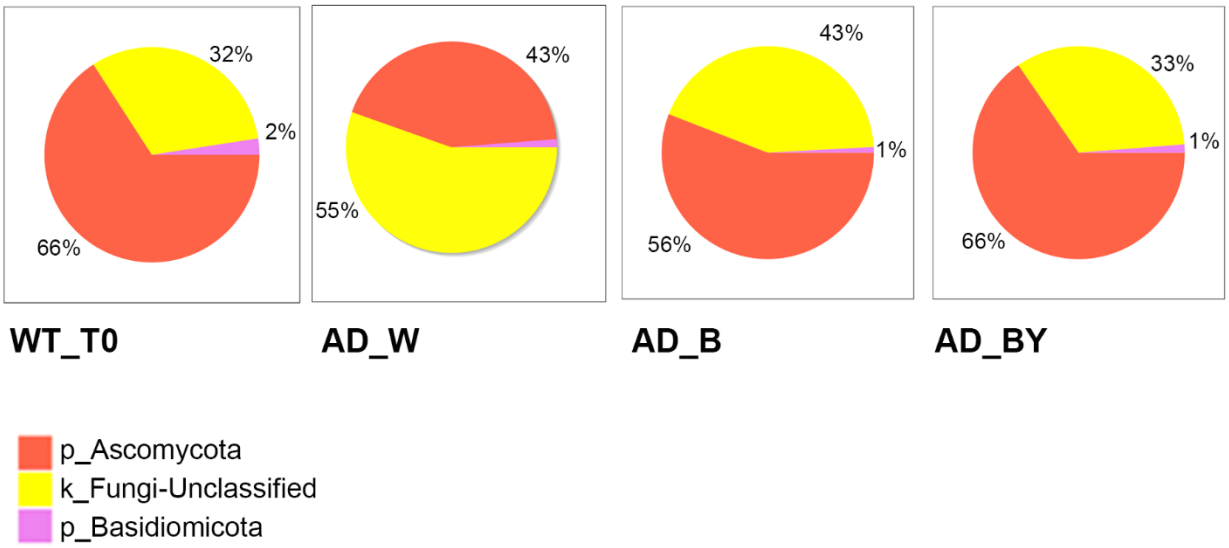

Figure 48: *Overall fungal microbiota composition in mice untreated (W, water) or treated with beer (B) or beer and yeast (BY). Abundances pie chart at phylum level.*

Fungal dysbiosis in AD is indicated by the decreased Basidiomycota/Ascomycota ratio with respect to age-matched WT animals. In fact, the Basidiomycota/Ascomycota ratio is considered to be an indicator of fungal dysbiosis [243] interestingly, this ratio increased upon treatments.

4.3 Discussion

Beer is the most widely consumed fermented beverage in the world [244], produced from water, malt (and its adjuncts), hops, and yeast, specifically *Saccharomyces cerevisiae.* Emerging studies are now highlighting that moderate consumption of beer may be beneficial and favor healthy aging [245]. Aging can come together with several medical conditions, including age-related disorders such as AD, characterized by massive deposition of Aβ peptides in senile plaques and other aggregates that lead to progressive cognitive dysfunctions. The use of probiotics to properly modulate microbiota composition and obtain positive effects on AD pathology is recently attracting researchers' interest. For this reason, considering the presence of yeasts and of other beneficial microbes or probiotics in fermented beverages, it is reasonable to hypothesize that beer could also protect against neurodegenerative conditions through microbiota modulation.

In the light of our previous studies that showed the neuroprotective effect of gut microbiota modulation through oral administration of probiotic formulation, the present work investigates the potential beneficial effects of a four-month treatment with unpasteurized beer in wild-type and 3xTg-AD mice. In addition, to better elucidate the role of the yeast used for beer brewing, a group of mice was administered with beer enriched with these microorganisms.

Our data demonstrate that the treatment with the yeast-enriched beer positively affected AD mice cognitive functions, as revealed by the discrimination scores obtained from the NOR test. No effects were observed in wt animals. Considering these data on ameliorated cognition, we then focused on two important AD molecular hallmarks, the amount of amyloid peptides and the inflammatory condition.

Interestingly, if compared to the other treatments, the yeast-enriched beer significantly reduced the levels of the Aβ(1–42) peptide, which is the most toxic form, in the PFC and hippocampus of AD mice. No effect of the same treatment was observed in wt animals. Beer treatment successfully diminished the levels of this peptide in the hippocampus of AD mice. Conversely, no effect of the

treatments on the Aβ(1–40) amyloid peptide was detected in both wt and AD mice. These results are in line with a post-mortem study performed by Kok *et al.* that investigated the association between consumption of different alcoholic beverages and Aβ aggregation in the brain, suggesting that beer consumption may protect against Aβ aggregation in brain [246].

AD is always accompanied by severe inflammation that slowly leads to neuronal death Moderate consumption of either wine or beer was previously associated with lower levels of systemic inflammatory markers in three different European areas [247]. In the light of these evidences, we analyzed plasma and brain levels of a panel of pro- (IL-1β and TNF-α) and anti-inflammatory (IL-4 and IL-10) cytokines obtaining that the yeast-enriched beer stimulated a significant anti-inflammatory response in both samples from AD mice. Treatment with beer did not significantly alter the amount of the considered cytokines. Again, no effect was detected in wt animals. These data therefore suggest that beer enrichment with the brewing yeast is effective in decreasing important toxic hallmarks of the pathology.

To better understand the mechanisms that promote these outcomes, we analyzed some of the components of the gut-brain axis, a complex communication system that integrates brain cognitive centers with intestinal functions through neuro-immuno-endocrine mediators [248]. First, we explored the levels of gut hormones in mice plasma and no significant changes were observed comparing the four experimental groups in both wt and AD mice.

Then, we screened microbiota composition for changes in the richness, that is the number of species present in a sample, and in the evenness, the related differences in abundance of species. Interestingly, treatments with beer and beer-yeast significantly increased the richness in AD mice bacterial population making the microbiota of these animals more similar to that of healthy subjects. Furthermore, an increase in Firmicutes and a simultaneous decrease in Proteobacteria was observed in AD mice treated with the yeast-enriched beer. Considering that previous studies demonstrated that,

compared to healthy subjects, AD individual showed a reduction of the phylum Firmicutes and an enrichment of Proteobacteria[249], our data suggest a positive impact of the treatment on bacterial population composition.

This study provides supportive evidences for a beneficial role of fermented beverages in neurodegenerative disorders associated with aging. Our results indicate that moderate beer intake, particularly through the action of its microbial content, can successfully counteract AD major hallmarks and associated clinical manifestations.

Chapter 5. Cog complex mutation enlightens mechanism of autophagy regulation

5.1. Materials and methods

5.1.1. Cell lines, culture media and treatment

Hek293T cells with stable Cog3 knockout generated using CRISPR cas9 technique were a gift from Lupashin lab [134]. In details, cells were grown in DMEM/F12 medium (Thermo Scientific) supplemented with 10% FBS (Atlas Biologicals). Cells were kept at 37°C and 5% CO_2 in a 90% humidified incubator. Cells were passaged via gentle resuspension. gRNA sequences were either provided by Horizon Discovery, Cog3 Guide ID: 113509 Target: GGCGCT GTTGCTGCTGCCTG. HEK293T cells were transfected with plasmid containing gRNA with Cas9-dasherGFP (Horizon Discovery) or Cas9 with mCherry (Genecopia).

Cells were grown to 80% confluence in 15 cm plates, organized as WT and Cog3 KO cells, and treated or not with Earle's balanced salt solution (EBSS) for 4 h after three times washing with PBS. After treatment, cells were washed with dPBS (Dulbecco's phosphate-buffered saline), harvested with trypsin and immediately centrifuged at 600 x g for 5 min. After snap freezing in liquid nitrogen, cells were stored at -80 ℃ until further use.

5.1.2. Sucrose density gradient subcellular fractionation

Pellets were resuspended in homogenization buffer (1:4 ratio, 10 mM Tris pH 7.4, 0.25 M sucrose and protease inhibitor cocktails) and homogenized on ice using Dounce homogenizer. Unbroken cells and nuclei were removed by low-speed centrifugation (700 × g, 5 min) and supernatant collected as post nuclear fractions (PNS). Equal protein amounts were adjusted to 2 M sucrose and loaded to the bottom of a SW41 tube (Beckman) which was followed by subsequent layering of 49%, 43%, 37%, 34% and 25% sucrose. The gradients were centrifuged on a SW41 rotor at 28,000 x rpm overnight at 4°C in

ultracentrifuge Beckman L-90K. Twelve fractions were collected carefully from top to bottom and their densities were calculated from refractive indices. 180 µl from each fraction were precipitated by 10% trichloroacetic acid (TCA) and the pellets were subjected to Western blot analysis. Each experiment was performed in triplicate.

5.1.3. Western blot analysis

Equal volumes of each sample were separated by 4-20% SDS PAGE (Mini-PROTEAN TGX Precast Protein Gels, Biorad) and immunoblotted on Trans-Blot Turbo Mini Nitrocellulose precut membranes using Trans-Blot Turbo transfer system (Biorad). Molecular weight markers (10-250 kDa) were included in each gel. Membranes were stained with Ponceau S (Sigma-Aldrich) and blocked 1 hour in 5% non-fat dry milk in PBS-T (1X Phosphate-buffered saline, 0.1% Tween® 20) followed by incubation with specific antibody. Primary antibodies were diluted in 1x dPBS plus sodium azide and secondary antibodies were diluted in 2.5% non-fat dry milk dissolved in PBS-T. Proteins were detected with the enhanced chemiluminescence (ECL) substrate (Biorad) in a Biorad ChemiDoc imaging system. Antibodies used for detection were Atg9 (Cell Signaling Technology), LC3 (Sigma-Aldrich), p62 (Abnova), ERGIC 53 (Abcam) and GM130 (Abcam). Immunoblot images were quantified using Image Studio Lite software.

5.2 Results

5.2.1 Deglycosylation of Atg9A

Immunoblotting of Atg9A in the cytoplasmic lysate revealed that Atg9A had a higher electrophoretic mobility in Cog3 KO cells compared to WT cells, as shown in Figure 49. In WT cells, Atg9A runs at 115kDa instead in Cog3 KO cells Atg9A was observed moving at 100kDa. This indicates that knock out of Cog3 results in incomplete glycosylation of Atg9A protein. Therefore, it was important to know the localization and sorting of Atg9A.

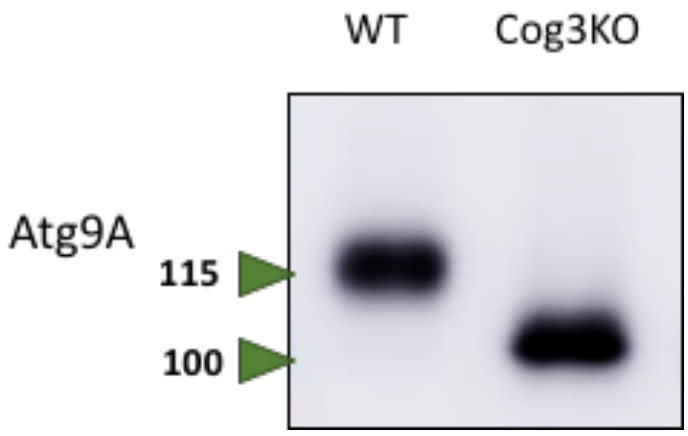

***Figure 49**: Atg9A has different electrophoretic mobility in Cog3 KO cells compared to WT cells. WT Atg9A runs at 115kDa and Cog3KO runs at 100kDa.*

5.2.2 Spatial translocation of Atg9A sorting from TGN to ERGIC

We observed two major peaks in Atg9A fractionation, points 1-4 represent autophagosomal fractions and points 8-12 represent cytosolic fractions. The peak observed in fractions 2, 3, and 4 represents Atg9A that co-fractioned with LC3B, as shown in figure 50 panel A and B . A high level of Atg9 in Cog3 KO cells, which also cofractionated with increased LC3B, was observed in fractions 2, 3 and 4.

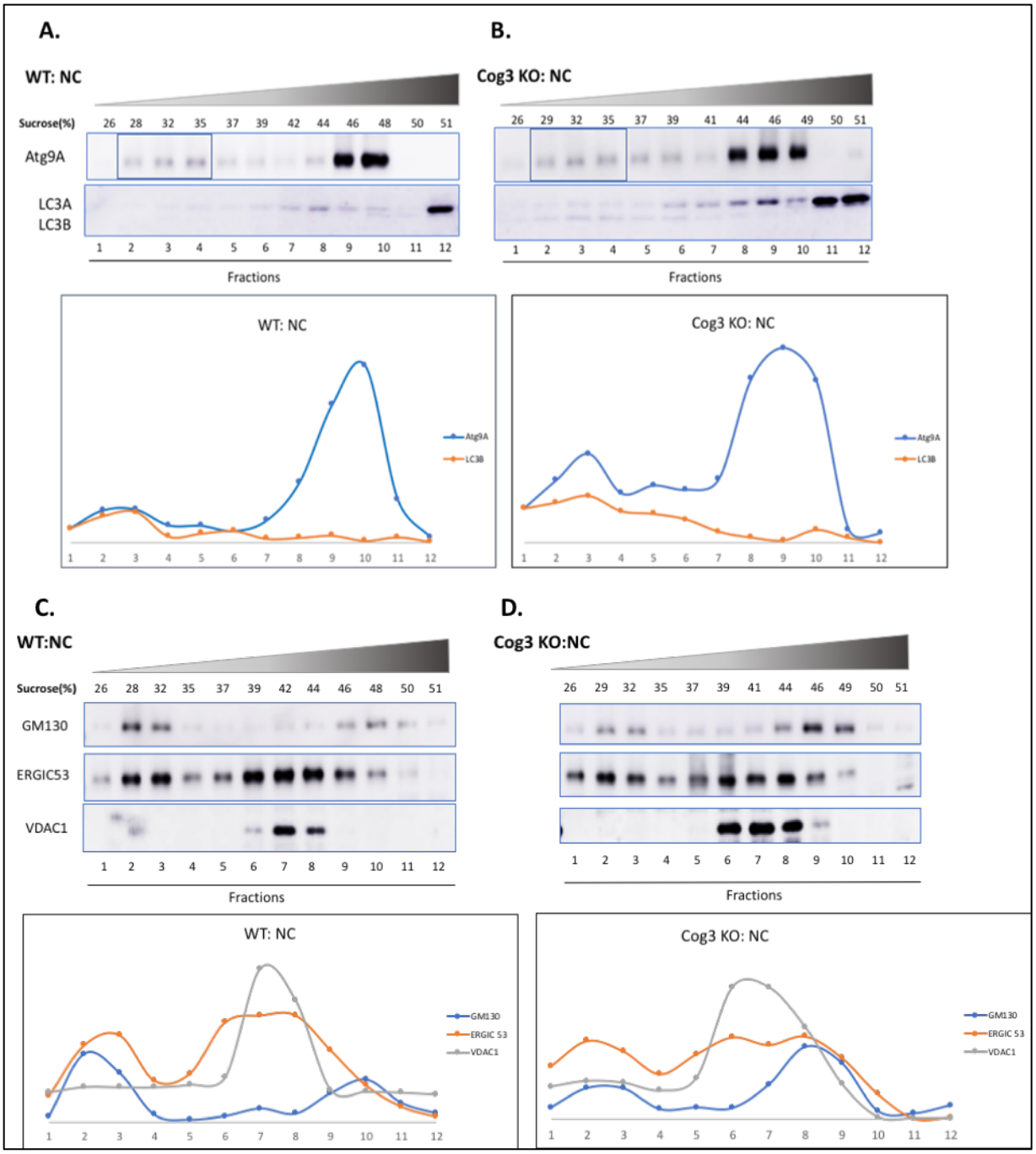
A.
WT: NC
Sucrose(%) 26 28 32 35 37 39 42 44 46 48 50 51
Atg9A
LC3A
LC3B
1 2 3 4 5 6 7 8 9 10 11 12
Fractions
B.
Cog3 KO: NC
26 29 32 35 37 39 41 44 46 49 50 51
1 2 3 4 5 6 7 8 9 10 11 12
Fractions
WT: NC
Atg9A
LC3B
Cog3 KO: NC
Atg9A
LC3B
C.
WT:NC
Sucrose(%) 26 28 32 35 37 39 42 44 46 48 50 51
GM130
ERGIC53
VDAC1
1 2 3 4 5 6 7 8 9 10 11 12
Fractions
D.
Cog3 KO:NC
26 29 32 35 37 39 41 44 46 49 50 51
1 2 3 4 5 6 7 8 9 10 11 12
Fractions
WT: NC
GM130
ERGIC 53
VDAC1
Cog3 KO: NC
GM130
ERGIC 53
VDAC1

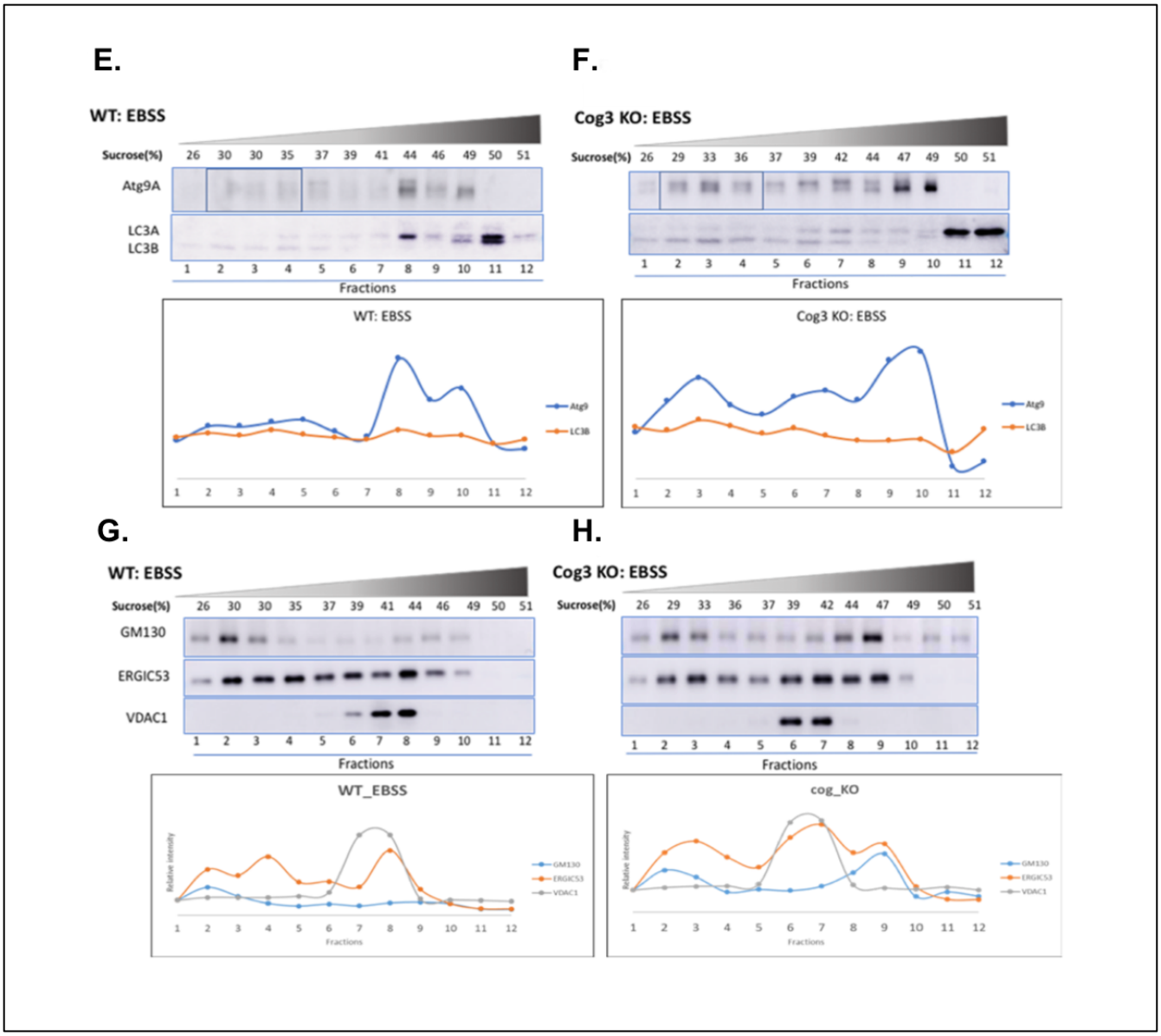

Figure 50: *Sucrose gradient subcellular fractionation of WT and Cog3 KO cells, with or without EBSS. A and B represents localization of Atg9A and LC3B in the autophagosomal fractions. C and D represent the markers of Golgi (GM130), ERGIC (ERGIC53) and Mitochondria (VDAC1). A, B, C and D are observations under nutrient control condition. E, F, G and H are observations under starvation conditions (with EBSS treatment for 4 h). E and F represent localization of Atg9A and LC3B to autophagosomal fractions. G and H represent the markers of Golgi (GM130), ERGIC (ERGIC53) and Mitochondria (VDAC1). Protein levels in the fractions were quantified using Image Studio Lite software.*

In WT cells, treatment with EBSS reduced localization of Atg9A to autophagosomes and a higher lipidated form of LC3 or LC3B was observed. EBSS-treated Cog3 KO cells exhibited higher autophagosomal puncta with Atg9A and higher lipidated LC3 (Figure 50 panel E and F). Panel C,D and

G, H represents the localization of the ER, Golgi and mitochondrial fractions in WT and Cog3 KO under nutrient rich and staved conditions respectively .

5.2.3 Localization of Atg9A and LC3B to the autophagosomal fraction

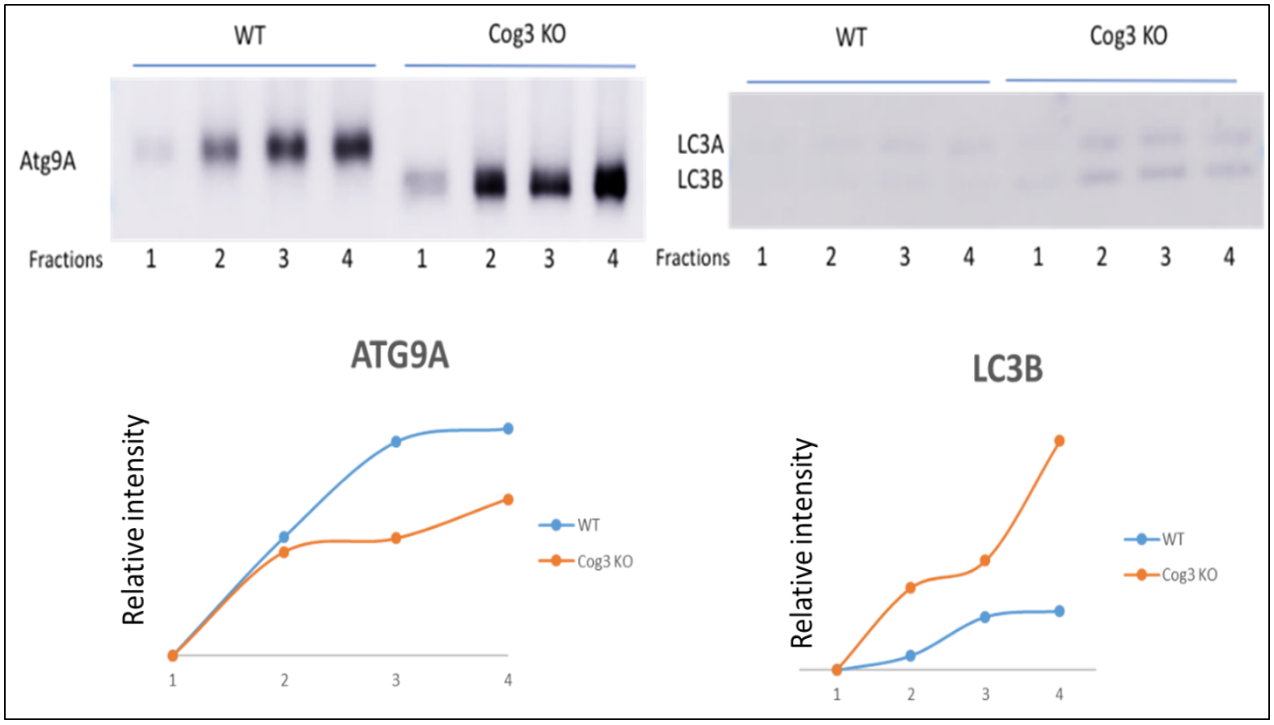

Figure 51: *Atg9A and LC3 in the autophagosomal fraction. Representative immunoblots and corresponding analyses derived from the same blots are shown. Protein levels in the fractions were quantified using Image Studio Lite software.*

The autophagosomal fractions-2,3 and 4 of WT were compared to the autophagosomal fractions of Cog3 KO (Figure 51). The fractions showed higher colocalization of Atg9A and LC3B in Cog3 KO as compared to WT.

5.2.4 Localization of p62 in WT and KO

p62 is the most predominant autophagic receptor and its characterization is a major concern in basal autophagic condition. Therefore, we studied the localization of p62 in WT and Cog3 KO cells under basal condition (Figure 52). We observed localization of p62 in fractions 1, 2 and 3, indicating its colocalization with autophagosome. p62 levels were increased in Cog3 KO compared to WT cells. The peak observed in fraction 6 in Cog3 KO cells corresponds to the mitophagy which thus opens up opportunity for further investigation.

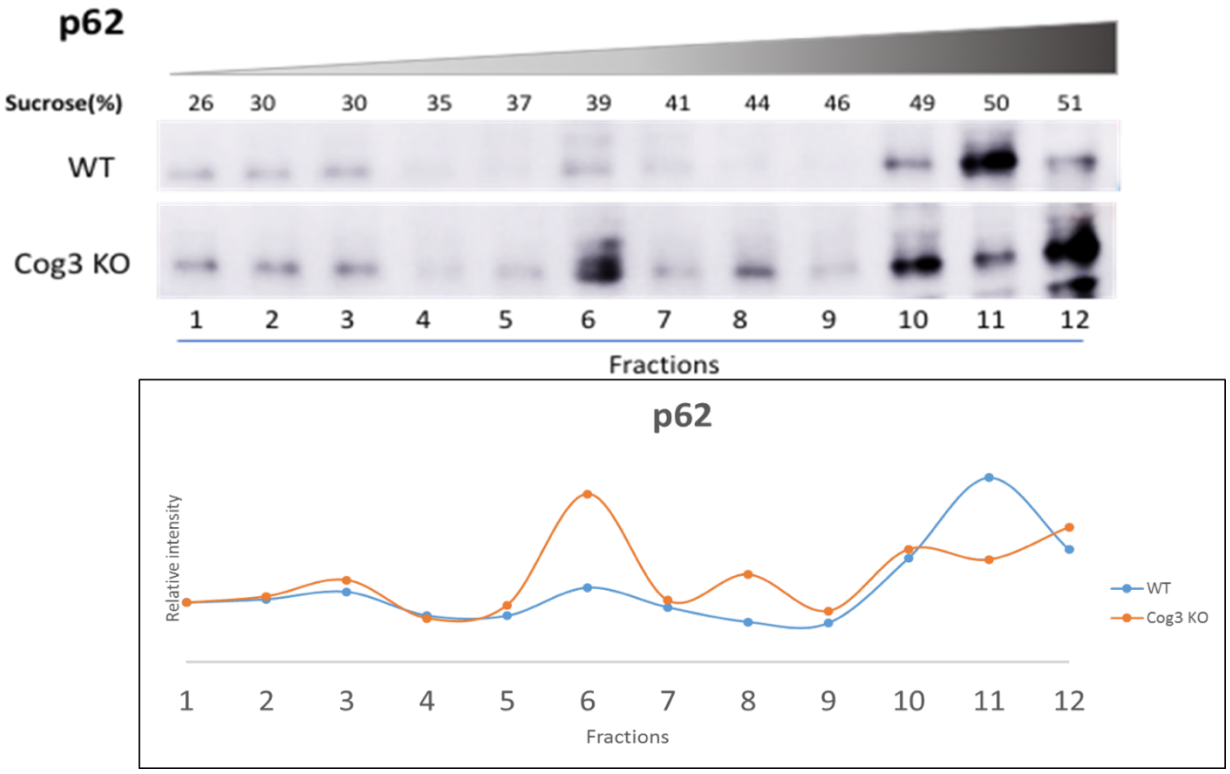

Figure 52: *p62 in the autophagosomal fraction under basal conditions in WT compared to Cog3 KO. Protein levels in the fractions were quantified using Image Studio Lite software.*

5.3 Discussion

Autophagy is a tightly regulated cellular degradation mechanism which is critical for cell survival. Autophagosome biogenesis is initiated by intricate protein signaling cascades to mobilize membranes from the endomembrane system [143]. The so-called core Atg proteins are essential for autophagosome formation, they are sequentially added to form the mature autophagosomes and the autophagic cargo is delivered to lysosomes [250]. An upstream autophagy protein Atg9A is the only known trans-membrane protein of autophagy machinery. Atg9A is synthesized in the ER and shuttles between the Golgi and endosomes [251]. Proteins are synthesized in the ER and post-translational modifications occur in the Golgi. In details, translated proteins from ER are released from ERES (ER exit site) and enter ER intermittent compartment (ERGIC) from which they are transported to the cis Golgi compartment. To maintain the proper function of the cellular machinery, efficient docking and fusion of intracellular transport carriers, also known as multi-subunit tethering complexes (MTC), are required and are evolutionarily conserved. This inter-compartmental transport of proteins from ERGIC to cis Golgi is mediated by Cog complexes. An impaired tethering complex can lead to Golgi fragmentation, an effect often observed in neurodegenerative disorders such as AD. Cog complex is an octamer and it is the major MTC operating in the intra-Golgi retrograde trafficking [134]. Cog3 subunit from lobe A is known to function between the ER and the Golgi.

We observed higher electrophoretic mobility of Atg9A in Cog3 KO cells as compared to WT. WT Atg9A runs at 115kDa while in Cog3 KO Atg9A runs at 100kDa. Higher electrophoretic mobility could be due to a faulty or mis-glycosylation process. This also corresponds to the inefficient sorting from ER to Golgi due to missing Cog3 subcomplex. Also disruption of the Cog subunits results into Golgi fragmentation, resulting into disruption of the core sorting machinery of the cell (data unpublished).

Thus we explored the role of Cog3 subcomplex in sorting of the autophagic protein Atg9A. Atg9A was found to be dispersed in the periphery between Golgi and ER (data not shown) in Cog3 KO cells, however its exact localization was not confirmed. Therefore, we explored the localization of Atg9A in the absence of Cog3. Under normal condition, Atg9A cofractionated with Golgi and ER whereas in Cog3 KO cells Atg9A cofractionated with ERGIC 53 (ERGIC marker) and the autophagosomal marker LC3B (Figure 2, A). Proteins are synthesized and modified in the ER and further post-translation modification and packaging into vesicles occurs in Golgi complex and then sorted to their destined location. Thus the observed phenotype corresponds to disrupted Golgi which is observed in a variety of neurodegenerative diseases. For example, in AD, sequential cleavage of APP by β- and γ-secretases instead of α- secretase requires APP and secretases to be in the same subcellular compartments and their distribution is solely controlled in Golgi compartments. Thus, the fragmentation of the Golgi complex can promote the biogenesis of AD progression.

Herein, WT and Cog3 KO cells, under basal and starvation conditions, were fractionated to understand their colocalization trafficking process. The colocalization of GM130 with autophagosomal Atg9A, as observed in fraction 2 and 3 of WT cells, indicates its trafficking from TGN, under basal condition. While in Cog3 KO cells, ERGIC53 was observed largely colocalizing with autophagosomal Atg9A in fraction 2 and 3, representing its trafficking from ERGIC instead of TGN, under basal condition. In order to understand how induction of autophagy may affect the localization of Atg proteins, cells were treated with EBSS to induce starvation. Results obtained from starvation condition indicate the boost in nonselective autophagy following the similar pattern as of the basal condition. A higher puncta of Atg9A along with LC3A and LC3B was seen. Atg9A was observed to be highly localized between cis Golgi and ER which may indicate that Atg9A is sorted to autophagosomes from intermittent compartment between ERES and cis Golgi, known as ERGIC.

Our data indicate that, due to disconnected tethering network, the newly formed Atg9A couldn't enter the Golgi compartment for further glycosylation modification. Instead, Atg9A gets bud-off from ERGIC and enters autophagic pathway where it serves as template for LC3 lipidation. ERGIC generates the small membrane precursors for LC3 lipidation in response to an activated PI3K/Beclin1 complex [143]. Atg9 colocalizes with Atg2 at the expanding edge of the isolation membrane where they receive phospholipids to drive the autophagosomal membrane expansion [73]. Atg9A forms the membrane contact sites between ER and phagophore to initiate the transfer of lipids for the growing phagophore membrane [252]. Thus, it is known that Atg9A is required at the early step of autophagosome formation during autophagy. The Beclin1 complex, also known as phosphatidylinositol-3 kinase (PI3K) complex, consists of Beclin1, VPS34 (the class III phosphatidylinositol-3 kinase), VPS15 (mammalian orthologue p150) and ATG14 (ATG14L) [253]. Damaged retrograde transport of autophagosome is also observed in Parkinson's Disease (PD). α-synuclein inclusions reduce omegasome formation by inducing the mis-localization of Atg9A [254].

Furthermore, fractions 1, 2, 3 and 4 of WT cells were compared to fractions 1, 2, 3 and 4 of Cog3 KO cells. This comparison reveals a higher autophagosomal puncta with Atg9A with membranes decorated with LC3B and gives a very interesting insight because even in the presence of mis-glycosylated Atg9A, LC3A was successfully lipidated to form LC3B, via phosphatidylethanolamine (PE) conjugation by Atg7. This again represents the bypass pathway of Cop II vesicles from ERGIC, as previously described by the study from Schekman's lab [143]. LC3B bound to the autophagosomal membrane also binds p62 through its LIR domain thus selectively recruits the ubiquitinated cargo bound for its degradation via autophagy. Thus, the basal autophagy is largely controlled by p62, where p62 undergoes oligomerization and delivers the cargo aggregates to the autophagosome via interacting with the autophagosomal membrane protein LC3B [255]. When the major organelle for trafficking, sorting and modification is disrupted, we observed that nonselective autophagy was highly influenced. While

on the other hand p62 kept functioning at the basal selective autophagy which is vital for cell survival. However, p62 recruitment to the site of autophagosome biogenesis is extremely complex and yet to be understood but this study would help us understand that p62 is critically important to determine the cell fate. p62 stands at the delicate balance between cell death and survival, which is fundamental for cell fate decision in the context of neurodegenerative diseases [256].Compared to WT cells, Cog3 KO cells had a predominant localization of p62 with the mitochondrial fraction 6 which may represent mitophagy, which would be further investigated in context of mitophagy in neurodegenerative diseases.

In conclusion, this study highlights the mechanism of autophagy regulation under severe conditions of Golgi fragmentation, prevalent in many neurodegenerative diseases. It stretches out the role of p62 in neurodegenerative diseases. It would be interesting to further investigate the mechanisms through which p62 regulates the crossroad between cell death and survival.

CONCLUSION

6: Conclusion

The present work of my PhD thesis has focused on the modulation of gut microbiota to induce beneficial effects on neuronal pathways consequently leading to delay the progression of AD. AD is the most common neurodegenerative disorder in elderly, with progressive decline of cognitive functions. With increase in population size and life expectancy AD has become a global challenge for the 21st century [257]. Modern life stress and lifestyle have strong clinical relevance to the rapid progression of cognitive disorders [258] AD is a complex multifactorial disease involving neuroinflammation, impaired metabolism and neurodegeneration. Neuroinflammation in AD is immune reaction activated in response to emerging Aβ plaque and NFT that in turn contributes more to the pathogenesis. Progression of AD is also accompanied by impaired glucose homeostasis largely contributed by inadequate glucose supply and impairment of major proteolytic system. The bidirectional communication between gut and brain plays a critical role in the onset and progression of different neurodegenerative disorders. With the emerging evidences on gut-microbiota-brain axis, it is undeniably a potent therapeutic approach that may redesign the future health care system.

In this study, we have used different strategies to illustrate the effect of gut microbiota modulation to delay the progression of AD. We demonstrated the role of the probiotic formulation SLAB51, p62-engineered *Lactobacilli* and of beer in the reduction of AD progression using 3xTg-AD mice as model. These strategies were explored to abate impaired cerebral glucose metabolism, neuronal proteolytic processes and neuroinflammation which are the major pathological conditions prevailing in AD brain.

Metabolic impairment and neuroinflammation are major events at the basis of AD onset and progression. SLAB51 oral administration successfully restored the major neuronal glucose transporters GLUT3 and GLUT1 and significantly decreased p-Tau levels in AD brain. The treatment was also able to repair the metabolic impairment and to reduce oxidative stress, as confirmed by the levels of key

metabolic regulators, AMPK and Akt, and AGEs. Further, the decreased levels of HbA1c in plasma of the treated group indicated its long-term glycemic history; representing the cognitive health of the treated mice group. Glycated hemoglobin is the non-enzymatic product of hemoglobin binding with glucose. Correlating with blood glucose levels and its elevated level is linked to cognitive impairment. Gut microbiota modulation through SLAB51 positively influences cellular proteolysis and metabolic homeostasis in the brain, contributing to a reduction in neuroinflammation. The data obtained in the present work reinforce the idea that gut microbiota modulation can strongly influence multiple signaling pathways in the host and contribute to ameliorate cognitive functions in AD mice.

Concerning cellular proteolysis, autophagy is the major system for aggregated cargo degradation that relies on the cargo receptors such as p62 [259]. p62 protein can critically drive the substrates to the UPS or to the autophagy for degradation. Under pathological and stressed condition, when UPS is overburdened, p62 sequesters the cellular Aβ aggregates towards autophagic degradation instead of UPS. The oral administration of p62-enginereed LAB improved neuronal proteolysis and reduced the load of Aβ deposition in AD brain. In addition, the treatment reduced oxidative stress and neuroinflammatory markers. The study evidences that the use of the pExu plasmid as a delivery vector for p62 can be considered as a beneficial strategy in AD. However, the produced effects did not have a pronounced effect upon the gut microbiota composition or gut-brain axis components. This indicates that the p62 plasmid incorporation didn't change the commensal behavior of LAB.

Although alcohol consumption is known to implement adverse effect on health, recently there are studies highlighting that moderate consumption of beer may be beneficial and favor healthy aging. Nevertheless, beer contains yeast, beneficial microbes or probiotics, thus we explored the effect of beer to ameliorate AD progression. And interestingly, we observed that beer enriched with brewing yeasts ameliorate the cognitive functions by reducing neuroinflammatory markers and the levels of the Aβ(1–42) peptide, in the PFC and hippocampus of AD mice. Treatments with beer and beer-yeast significantly

increased the richness in gut bacterial population of AD mice. Thus it shows that moderate drinking of beer may improve the gut microbiota composition and successfully counteract AD major hallmarks and associated clinical manifestations.

Furthermore, we explored the mechanical insight into regulation of autophagy. Autophagy is a tightly regulated system, which can be influenced by inefficient trafficking and signaling by Golgi. Neurodegenerative disorders such as AD have severe Golgi fragmentation that hampers the proper trafficking and sorting process in the cell. In addition, impaired tethering complex i.e. Cog complex can produce similar effect of Golgi fragmentation. In absence of Cog3 subunit, the disrupted tethering complex results into fragmentation of Golgi complex. Thus, the cellular trafficking, sorting and glycosylation is largely effected. Atg9A, an early component of autophagic process, was observed to have incomplete glycosylation and defective sorting from ERGIC instead of TGN. The cargo receptor p62 was observed to colocalize with the autophagosomal fraction without any glycosylation defect and observed functional under basal condition. Thus, this study is consistent with our previous findings demonstrating that p62 can rescue cell death even during the serious cellular insults such as fragmentation of Golgi complex, which is prevalent in progression of AD.

Thus, our study propose novel multi-target approach for AD treatment. Here we have shown that gut microbiota modulation can effectively reduce the molecular hallmarks of AD along with reduction of neuroinflammation and amelioration of proteolysis. Considering its noninvasive technique to reach and ameliorate CNS, it unfolds many opportunities that can be designed for development of precise therapy targeted at neurological disorders.

Further to understand the complete operating molecular mechanisms and to observe the chronic effect of the treatment, in vitro as well as in vivo studies would be required. It would be interesting to see how the probiotic formulations or the treatments communicate with the neuronal system to favor the observed effect; although the mechanism underlying the bidirectional communication of gut-microbiota

and brain axis is still very elusive. With further understanding and proper regulation, the proposed approach of treatments would be of great therapeutic value to address a variety of cellular deficit and pathological conditions.

7: List of publications during the PhD triennium

1. Valentina Cecarini, Laura Bonfili, Olee Gogoi, Solomon Lawrence, Franco M. Venanzi, Vasco Azevedo, Pamela Mancha-Agresti, Mariana Martins Drumond, Giacomo Rossi, Sara Berardi, Livio Galosi, Massimiliano Cuccioloni, Mauro Angeletti, Jan S. Suchodolski, Rachel Pilla, Jonathan A. Lidbury, Anna Maria Eleuteri., Neuroprotective effects of p62(SQSTM1)-engineered lactic acid bacteria in Alzheimer's disease: a pre-clinical study. Aging (2020) Vol. 12(16):15995-16020.
2. Laura Bonfili, Valentina Cecarini, Olee Gogoi, Chunmei Gong, Massimiliano Cuccioloni, Mauro Angeletti, Giacomo Rossi, Anna Maria Eleuteri Microbiota modulation as preventative and therapeutic approach in Alzheimer's disease. FEBS, (2021) vol. 288:2836–2855
3. Laura Bonfili, Valentina Cecarini, Olee Gogoi, Sara Berardi, Silvia Scarpona, Mauro Angeletti, Giacomo Rossi, Anna Maria Eleuteri., Gut microbiota manipulation through probiotics oral administration restores glucose homeostasis in a mouse model of Alzheimer's disease, Neurobiology of Aging 87 (2020) vol. 87 pp. 35-43.

REFERENCES

8: References:

1. Long, J.M. and D.M. Holtzman, *Alzheimer Disease: An Update on Pathobiology and Treatment Strategies.* Cell, 2019. **179**(2): p. 312-339.

2. Burns, A., et al., *Cause of death in Alzheimer's disease.* Age Ageing, 1990. **19**(5): p. 341-4.

3. McKhann, G.M., et al., *The diagnosis of dementia due to Alzheimer's disease: recommendations from the National Institute on Aging-Alzheimer's Association workgroups on diagnostic guidelines for Alzheimer's disease.* Alzheimers Dement, 2011. **7**(3): p. 263-9.

4. *2020 Alzheimer's disease facts and figures.* Alzheimers Dement, 2020.

5. Ives, D.G., et al., *Agreement between nosologist and cardiovascular health study review of deaths: implications of coding differences.* J Am Geriatr Soc, 2009. **57**(1): p. 133-9.

6. Bekris, L.M., et al., *Genetics of Alzheimer disease.* J Geriatr Psychiatry Neurol, 2010. **23**(4): p. 213-27.

7. Dorszewska, J., et al., *Molecular Basis of Familial and Sporadic Alzheimer's Disease.* Curr Alzheimer Res, 2016. **13**(9): p. 952-63.

8. Chen, X.Q. and W.C. Mobley, *Alzheimer Disease Pathogenesis: Insights From Molecular and Cellular Biology Studies of Oligomeric Abeta and Tau Species.* Front Neurosci, 2019. **13**: p. 659.

9. Michaelson, D.M., *APOE epsilon4: the most prevalent yet understudied risk factor for Alzheimer's disease.* Alzheimers Dement, 2014. **10**(6): p. 861-8.

10. Montagne, A., et al., *APOE4 leads to blood-brain barrier dysfunction predicting cognitive decline.* Nature, 2020. **581**(7806): p. 71-76.

11. Reitz, C. and R. Mayeux, *Alzheimer disease: epidemiology, diagnostic criteria, risk factors and biomarkers.* Biochem Pharmacol, 2014. **88**(4): p. 640-51.

12. van der Lee, S.J., et al., *The effect of APOE and other common genetic variants on the onset of Alzheimer's disease and dementia: a community-based cohort study.* Lancet Neurol, 2018. **17**(5): p. 434-444.

13. Karch, C.M. and A.M. Goate, *Alzheimer's disease risk genes and mechanisms of disease pathogenesis.* Biol Psychiatry, 2015. **77**(1): p. 43-51.

14. Koenigsknecht-Talboo, J. and G.E. Landreth, *Microglial phagocytosis induced by fibrillar beta-amyloid and IgGs are differentially regulated by proinflammatory cytokines.* J Neurosci, 2005. **25**(36): p. 8240-9.

15. Chow, V.W., et al., *An overview of APP processing enzymes and products.* Neuromolecular Med, 2010. **12**(1): p. 1-12.

16. Haass, C., et al., *Trafficking and proteolytic processing of APP.* Cold Spring Harb Perspect Med, 2012. **2**(5): p. a006270.

17. Kummer, M.P. and M.T. Heneka, *Truncated and modified amyloid-beta species.* Alzheimers Res Ther, 2014. **6**(3): p. 28.

18. Scheltens, P., et al., *Alzheimer's disease.* Lancet, 2016. **388**(10043): p. 505-17.

19. Chen, G.F., et al., *Amyloid beta: structure, biology and structure-based therapeutic development.* Acta Pharmacol Sin, 2017. **38**(9): p. 1205-1235.

20. Alonso, A.D., et al., *Hyperphosphorylation of Tau Associates With Changes in Its Function Beyond Microtubule Stability.* Front Cell Neurosci, 2018. **12**: p. 338.

21. Weingarten, M.D., et al., *A protein factor essential for microtubule assembly.* Proc Natl Acad Sci U S A, 1975. **72**(5): p. 1858-62.

22. Iqbal, K., et al., *Tau in Alzheimer disease and related tauopathies.* Curr Alzheimer Res, 2010. **7**(8): p. 656-64.

23. Alonso Adel, C., et al., *Polymerization of hyperphosphorylated tau into filaments eliminates its inhibitory activity.* Proc Natl Acad Sci U S A, 2006. **103**(23): p. 8864-9.

24. Simic, G., et al., *Tau Protein Hyperphosphorylation and Aggregation in Alzheimer's Disease and Other Tauopathies, and Possible Neuroprotective Strategies.* Biomolecules, 2016. **6**(1): p. 6.

25. Da Poian, A.T., El-Bacha, T. & Luz, M. R.M.P., *Nutrient Utilization in Humans: Metabolism Pathways.* Nature Education, 2010. **3**(9): p. 11.

26. Bloom, G.S., *Amyloid-beta and tau: the trigger and bullet in Alzheimer disease pathogenesis.* JAMA Neurol, 2014. **71**(4): p. 505-8.

27. Gandy, S., *The role of cerebral amyloid beta accumulation in common forms of Alzheimer disease.* J Clin Invest, 2005. **115**(5): p. 1121-9.

28. Vingtdeux, V., et al., *AMPK is abnormally activated in tangle- and pre-tangle-bearing neurons in Alzheimer's disease and other tauopathies.* Acta Neuropathol, 2011. **121**(3): p. 337-49.

29. Rickle, A., et al., *Akt activity in Alzheimer's disease and other neurodegenerative disorders.* Neuroreport, 2004. **15**(6): p. 955-9.

30. Sen, T., et al., *Sulfhydration of AKT triggers Tau-phosphorylation by activating glycogen synthase kinase 3beta in Alzheimer's disease.* Proc Natl Acad Sci U S A, 2020. **117**(8): p. 4418-4427.

31. Bhat, R.V. and S.L. Budd, *GSK3beta signalling: casting a wide net in Alzheimer's disease.* Neurosignals, 2002. **11**(5): p. 251-61.

32. Kim, B., et al., *The effects of insulin and insulin-like growth factor I on amyloid precursor protein phosphorylation in in vitro and in vivo models of Alzheimer's disease.* Neurobiol Dis, 2019. **132**: p. 104541.

33. Carro, E., et al., *Blockade of the insulin-like growth factor I receptor in the choroid plexus originates Alzheimer's-like neuropathology in rodents: new cues into the human disease?* Neurobiol Aging, 2006. **27**(11): p. 1618-31.

34. Lee, C.H., et al., *Decreased insulin-like growth factor-I and its receptor expression in the hippocampus and somatosensory cortex of the aged mouse.* Neurochem Res, 2014. **39**(4): p. 770-6.

35. Goldin, A., et al., *Advanced glycation end products: sparking the development of diabetic vascular injury.* Circulation, 2006. **114**(6): p. 597-605.

36. Goncalves, R.A., et al., *The Link Between Tau and Insulin Signaling: Implications for Alzheimer's Disease and Other Tauopathies.* Front Cell Neurosci, 2019. **13**: p. 17.

37. Vitek, M.P., et al., *Advanced glycation end products contribute to amyloidosis in Alzheimer disease.* Proc Natl Acad Sci U S A, 1994. **91**(11): p. 4766-70.

38. Bonfili, L., et al., *Gut microbiota manipulation through probiotics oral administration restores glucose homeostasis in a mouse model of Alzheimer's disease.* Neurobiol Aging, 2020. **87**: p. 35-43.

39. Heneka, M.T., et al., *Neuroinflammation in Alzheimer's disease.* Lancet Neurol, 2015. **14**(4): p. 388-405.

40. Dheen, S.T., C. Kaur, and E.A. Ling, *Microglial activation and its implications in the brain diseases.* Curr Med Chem, 2007. **14**(11): p. 1189-97.

41. Orre, M., et al., *Isolation of glia from Alzheimer's mice reveals inflammation and dysfunction.* Neurobiol Aging, 2014. **35**(12): p. 2746-2760.

42. Wyss-Coray, T. and J. Rogers, *Inflammation in Alzheimer disease-a brief review of the basic science and clinical literature.* Cold Spring Harb Perspect Med, 2012. **2**(1): p. a006346.

43. Dursun, E., et al., *The interleukin 1 alpha, interleukin 1 beta, interleukin 6 and alpha-2-macroglobulin serum levels in patients with early or late onset Alzheimer's disease, mild cognitive impairment or Parkinson's disease.* J Neuroimmunol, 2015. **283**: p. 50-7.

44. Sciacca, F.L., et al., *Interleukin-1B polymorphism is associated with age at onset of Alzheimer's disease.* Neurobiol Aging, 2003. **24**(7): p. 927-31.

45. Forlenza, O.V., et al., *Increased serum IL-1beta level in Alzheimer's disease and mild cognitive impairment.* Dement Geriatr Cogn Disord, 2009. **28**(6): p. 507-12.

46. Yin, Y., et al., *Interleukin-1beta Promoter Polymorphism Enhances the Risk of Sleep Disturbance in Alzheimer's Disease.* PLoS One, 2016. **11**(3): p. e0149945.

47. Trinchieri, G., S. Pflanz, and R.A. Kastelein, *The IL-12 family of heterodimeric cytokines: new players in the regulation of T cell responses.* Immunity, 2003. **19**(5): p. 641-4.

48. Vom Berg, J., et al., *Inhibition of IL-12/IL-23 signaling reduces Alzheimer's disease-like pathology and cognitive decline.* Nat Med, 2012. **18**(12): p. 1812-9.

49. Lee, C.Y. and G.E. Landreth, *The role of microglia in amyloid clearance from the AD brain.* J Neural Transm (Vienna), 2010. **117**(8): p. 949-60.

50. Guillot-Sestier, M.V., et al., *Il10 deficiency rebalances innate immunity to mitigate Alzheimer-like pathology.* Neuron, 2015. **85**(3): p. 534-48.

51. Chiroma, S.M., Baharuldin, M. T. H., Taib, C. N. M., Amom, Z., Jagadeesan, S., & Moklas, M. A. M., *Inflammation in Alzheimer's disease: A friend or foe?* Biomedical Research and Therapy, 2018. **5**(8): p. 2552-2564.

52. Scheepers, A., H.G. Joost, and A. Schurmann, *The glucose transporter families SGLT and GLUT: molecular basis of normal and aberrant function.* JPEN J Parenter Enteral Nutr, 2004. **28**(5): p. 364-71.

53. Cuello, A.C., *Early and Late CNS Inflammation in Alzheimer's Disease: Two Extremes of a Continuum?* Trends Pharmacol Sci, 2017. **38**(11): p. 956-966.

54. Hanzel, C.E., et al., *Neuronal driven pre-plaque inflammation in a transgenic rat model of Alzheimer's disease.* Neurobiol Aging, 2014. **35**(10): p. 2249-62.

55. Yorimitsu, T. and D.J. Klionsky, *Autophagy: molecular machinery for self-eating.* Cell Death Differ, 2005. **12 Suppl 2**: p. 1542-52.

56. Gozuacik, D. and A. Kimchi, *Autophagy as a cell death and tumor suppressor mechanism.* Oncogene, 2004. **23**(16): p. 2891-906.

57. Frake, R.A., et al., *Autophagy and neurodegeneration.* J Clin Invest, 2015. **125**(1): p. 65-74.

58. Rubinsztein, D.C., G. Marino, and G. Kroemer, *Autophagy and aging.* Cell, 2011. **146**(5): p. 682-95.

59. Netea-Maier, R.T., et al., *Modulation of inflammation by autophagy: Consequences for human disease.* Autophagy, 2016. **12**(2): p. 245-60.

60. Gomes, L.C. and I. Dikic, *Autophagy in antimicrobial immunity.* Mol Cell, 2014. **54**(2): p. 224-33.

61. Farre, J.C. and S. Subramani, *Mechanistic insights into selective autophagy pathways: lessons from yeast.* Nat Rev Mol Cell Biol, 2016. **17**(9): p. 537-52.

62. Nowikovsky, K., et al., *Determination of yeast mitochondrial KHE activity, osmotic swelling and mitophagy.* Methods Enzymol, 2009. **457**: p. 305-17.

63. Walter, K.M., et al., *Hif-2alpha promotes degradation of mammalian peroxisomes by selective autophagy.* Cell Metab, 2014. **20**(5): p. 882-897.

64. Wang, X., et al., *Redox regulated peroxisome homeostasis.* Redox Biol, 2015. **4**: p. 104-8.

65. Zaffagnini, G. and S. Martens, *Mechanisms of Selective Autophagy.* J Mol Biol, 2016. **428**(9 Pt A): p. 1714-24.

66. Lim, J., et al., *Proteotoxic stress induces phosphorylation of p62/SQSTM1 by ULK1 to regulate selective autophagic clearance of protein aggregates.* PLoS Genet, 2015. **11**(2): p. e1004987.

67. Stolz, A., A. Ernst, and I. Dikic, *Cargo recognition and trafficking in selective autophagy.* Nat Cell Biol, 2014. **16**(6): p. 495-501.

68. Feng, Y., et al., *The machinery of macroautophagy.* Cell Res, 2014. **24**(1): p. 24-41.

69. Mizushima, N., *Autophagy: process and function.* Genes Dev, 2007. **21**(22): p. 2861-73.

70. Mizushima, N., T. Yoshimori, and Y. Ohsumi, *The role of Atg proteins in autophagosome formation.* Annu Rev Cell Dev Biol, 2011. **27**: p. 107-32.

71. Suzuki, K., et al., *Hierarchy of Atg proteins in pre-autophagosomal structure organization.* Genes Cells, 2007. **12**(2): p. 209-18.

72. Xie, Z. and D.J. Klionsky, *Autophagosome formation: core machinery and adaptations.* Nat Cell Biol, 2007. **9**(10): p. 1102-9.

73. Matoba, K., et al., *Atg9 is a lipid scramblase that mediates autophagosomal membrane expansion.* Nat Struct Mol Biol, 2020. **27**(12): p. 1185-1193.

74. Schwartz, A.L. and A. Ciechanover, *Targeting proteins for destruction by the ubiquitin system: implications for human pathobiology.* Annu Rev Pharmacol Toxicol, 2009. **49**: p. 73-96.

75. Groll, M., et al., *A gated channel into the proteasome core particle.* Nat Struct Biol, 2000. **7**(11): p. 1062-7.

76. Borissenko, L. and M. Groll, *20S proteasome and its inhibitors: crystallographic knowledge for drug development.* Chem Rev, 2007. **107**(3): p. 687-717.

77. Miller, Z., et al., *Inhibitors of the immunoproteasome: current status and future directions.* Curr Pharm Des, 2013. **19**(22): p. 4140-51.

78. Heinemeyer, W., et al., *The active sites of the eukaryotic 20 S proteasome and their involvement in subunit precursor processing.* J Biol Chem, 1997. **272**(40): p. 25200-9.

79. Kocaturk, N.M. and D. Gozuacik, *Crosstalk Between Mammalian Autophagy and the Ubiquitin-Proteasome System.* Front Cell Dev Biol, 2018. **6**: p. 128.

80. Gong, B., et al., *The Ubiquitin-Proteasome System: Potential Therapeutic Targets for Alzheimer's Disease and Spinal Cord Injury.* Front Mol Neurosci, 2016. **9**: p. 4.

81. Ronai, Z.A., *Monoubiquitination in proteasomal degradation.* Proc Natl Acad Sci U S A, 2016. **113**(32): p. 8894-6.

82. Du, Y., M.C. Wooten, and M.W. Wooten, *Oxidative damage to the promoter region of SQSTM1/p62 is common to neurodegenerative disease.* Neurobiol Dis, 2009. **35**(2): p. 302-10.

83. Zaffagnini, G., et al., *p62 filaments capture and present ubiquitinated cargos for autophagy.* EMBO J, 2018. **37**(5).

84. Shaid, S., et al., *Ubiquitination and selective autophagy.* Cell Death Differ, 2013. **20**(1): p. 21-30.

85. Cecarini, V., et al., *Neuroprotective effects of p62(SQSTM1)-engineered lactic acid bacteria in Alzheimer's disease: a pre-clinical study.* Aging (Albany NY), 2020. **12**(16): p. 15995-16020.

86. Qin, J., et al., *A human gut microbial gene catalogue established by metagenomic sequencing.* Nature, 2010. **464**(7285): p. 59-65.

87. Seo, D.O. and D.M. Holtzman, *Gut Microbiota: From the Forgotten Organ to a Potential Key Player in the Pathology of Alzheimer's Disease.* J Gerontol A Biol Sci Med Sci, 2020. **75**(7): p. 1232-1241.

88. Fouhy, F., et al., *Composition of the early intestinal microbiota: knowledge, knowledge gaps and the use of high-throughput sequencing to address these gaps.* Gut Microbes, 2012. **3**(3): p. 203-20.

89. Marques, T.M., et al., *Programming infant gut microbiota: influence of dietary and environmental factors.* Curr Opin Biotechnol, 2010. **21**(2): p. 149-56.

90. Sarkar, A., et al., *Psychobiotics and the Manipulation of Bacteria-Gut-Brain Signals.* Trends Neurosci, 2016. **39**(11): p. 763-781.

91. Roy Sarkar, S. and S. Banerjee, *Gut microbiota in neurodegenerative disorders.* J Neuroimmunol, 2019. **328**: p. 98-104.

92. Jarbrink-Sehgal, E. and A. Andreasson, *The gut microbiota and mental health in adults.* Curr Opin Neurobiol, 2020. **62**: p. 102-114.

93. Montacute, R., et al., *Enhanced susceptibility of triple transgenic Alzheimer's disease (3xTg-AD) mice to acute infection.* J Neuroinflammation, 2017. **14**(1): p. 50.

94. Wang, X., et al., *Sodium oligomannate therapeutically remodels gut microbiota and suppresses gut bacterial amino acids-shaped neuroinflammation to inhibit Alzheimer's disease progression.* Cell Res, 2019. **29**(10): p. 787-803.

95. Stojanov, S., A. Berlec, and B. Strukelj, *The Influence of Probiotics on the Firmicutes/Bacteroidetes Ratio in the Treatment of Obesity and Inflammatory Bowel disease.* Microorganisms, 2020. **8**(11).

96. Vaiserman, A., et al., *Differences in the gut Firmicutes to Bacteroidetes ratio across age groups in healthy Ukrainian population.* BMC Microbiol, 2020. **20**(1): p. 221.

97. Brestoff, J.R. and D. Artis, *Commensal bacteria at the interface of host metabolism and the immune system.* Nat Immunol, 2013. **14**(7): p. 676-84.

98. Sender, R., S. Fuchs, and R. Milo, *Revised Estimates for the Number of Human and Bacteria Cells in the Body.* PLoS Biol, 2016. **14**(8): p. e1002533.

99. Richard, M.L. and H. Sokol, *The gut mycobiota: insights into analysis, environmental interactions and role in gastrointestinal diseases.* Nat Rev Gastroenterol Hepatol, 2019. **16**(6): p. 331-345.

100. Donaldson, G.P., S.M. Lee, and S.K. Mazmanian, *Gut biogeography of the bacterial microbiota.* Nat Rev Microbiol, 2016. **14**(1): p. 20-32.

101. Jiang, T.T., et al., *Commensal Fungi Recapitulate the Protective Benefits of Intestinal Bacteria.* Cell Host Microbe, 2017. **22**(6): p. 809-816 e4.

102. Nash, A.K., et al., *The gut mycobiome of the Human Microbiome Project healthy cohort.* Microbiome, 2017. **5**(1): p. 153.

103. Zhang, Z., et al., *Peripheral Lymphoid Volume Expansion and Maintenance Are Controlled by Gut Microbiota via RALDH+ Dendritic Cells.* Immunity, 2016. **44**(2): p. 330-42.

104. Distrutti, E., et al., *Modulation of intestinal microbiota by the probiotic VSL#3 resets brain gene expression and ameliorates the age-related deficit in LTP.* PLoS One, 2014. **9**(9): p. e106503.

105. Utzschneider, K.M., et al., *Mechanisms Linking the Gut Microbiome and Glucose Metabolism.* J Clin Endocrinol Metab, 2016. **101**(4): p. 1445-54.

106. Gerard, C. and H. Vidal, *Impact of Gut Microbiota on Host Glycemic Control.* Front Endocrinol (Lausanne), 2019. **10**: p. 29.

107. Sandhu, K.V., et al., *Feeding the microbiota-gut-brain axis: diet, microbiome, and neuropsychiatry.* Transl Res, 2017. **179**: p. 223-244.

108. Silva, Y.P., A. Bernardi, and R.L. Frozza, *The Role of Short-Chain Fatty Acids From Gut Microbiota in Gut-Brain Communication.* Front Endocrinol (Lausanne), 2020. **11**: p. 25.

109. Kimura, H., *Metabolic turnover of hydrogen sulfide.* Front Physiol, 2012. **3**: p. 101.

110. Vinolo, M.A., et al., *Regulation of inflammation by short chain fatty acids.* Nutrients, 2011. **3**(10): p. 858-76.

111. Larraufie, P., et al., *SCFAs strongly stimulate PYY production in human enteroendocrine cells.* Sci Rep, 2018. **8**(1): p. 74.

112. Zhou, X., et al., *Physiological and Pathological Regulation of Peripheral Metabolism by Gut-Peptide Hormones in Drosophila.* Front Physiol, 2020. **11**: p. 577717.

113. Moon, M., et al., *Ghrelin ameliorates cognitive dysfunction and neurodegeneration in intrahippocampal amyloid-beta1-42 oligomer-injected mice.* J Alzheimers Dis, 2011. **23**(1): p. 147-59.

114. Stoyanova, II, *Ghrelin: a link between ageing, metabolism and neurodegenerative disorders.* Neurobiol Dis, 2014. **72 Pt A**: p. 72-83.

115. Niedowicz, D.M., et al., *Leptin regulates amyloid beta production via the gamma-secretase complex.* Biochim Biophys Acta, 2013. **1832**(3): p. 439-44.

116. Fewlass, D.C., et al., *Obesity-related leptin regulates Alzheimer's Abeta.* FASEB J, 2004. **18**(15): p. 1870-8.

117. Greco, S.J., et al., *Leptin reduces pathology and improves memory in a transgenic mouse model of Alzheimer's disease.* J Alzheimers Dis, 2010. **19**(4): p. 1155-67.

118. Crowe, E., et al., *Activation of proteasome by insulin-like growth factor-I may enhance clearance of oxidized proteins in the brain.* Mech Ageing Dev, 2009. **130**(11-12): p. 793-800.

119. Hullar, M.A. and J.W. Lampe, *The gut microbiome and obesity.* Nestle Nutr Inst Workshop Ser, 2012. **73**: p. 67-79.

120. Folch, J., et al., *The role of leptin in the sporadic form of Alzheimer's disease. Interactions with the adipokines amylin, ghrelin and the pituitary hormone prolactin.* Life Sci, 2015. **140**: p. 19-28.

121. Theodoropoulou, A., et al., *Ghrelin and leptin secretion in patients with moderate Alzheimer's disease.* J Nutr Health Aging, 2012. **16**(5): p. 472-7.

122. Bonfili, L., et al., *Microbiota modulation counteracts Alzheimer's disease progression influencing neuronal proteolysis and gut hormones plasma levels.* Sci Rep, 2017. **7**(1): p. 2426.

123. Holscher, C., *The incretin hormones glucagonlike peptide 1 and glucose-dependent insulinotropic polypeptide are neuroprotective in mouse models of Alzheimer's disease.* Alzheimers Dement, 2014. **10**(1 Suppl): p. S47-54.

124. Simon, M.C., et al., *Intake of Lactobacillus reuteri improves incretin and insulin secretion in glucose-tolerant humans: a proof of concept.* Diabetes Care, 2015. **38**(10): p. 1827-34.

125. Cerovic, M., G. Forloni, and C. Balducci, *Neuroinflammation and the Gut Microbiota: Possible Alternative Therapeutic Targets to Counteract Alzheimer's Disease?* Front Aging Neurosci, 2019. **11**: p. 284.

126. Clarke, G., et al., *Minireview: Gut microbiota: the neglected endocrine organ.* Mol Endocrinol, 2014. **28**(8): p. 1221-38.

127. Cuadrado-Tejedor, M., et al., *Phenylbutyrate is a multifaceted drug that exerts neuroprotective effects and reverses the Alzheimer s disease-like phenotype of a commonly used mouse model.* Curr Pharm Des, 2013. **19**(28): p. 5076-84.

128. Cattaneo, A., et al., *Association of brain amyloidosis with pro-inflammatory gut bacterial taxa and peripheral inflammation markers in cognitively impaired elderly.* Neurobiol Aging, 2017. **49**: p. 60-68.

129. Bonfili, L., et al., *SLAB51 Probiotic Formulation Activates SIRT1 Pathway Promoting Antioxidant and Neuroprotective Effects in an AD Mouse Model.* Mol Neurobiol, 2018. **55**(10): p. 7987-8000.

130. Yang, X., et al., *Probiotics modulate the microbiota-gut-brain axis and improve memory deficits in aged SAMP8 mice.* Acta Pharm Sin B, 2020. **10**(3): p. 475-487.

131. Kobayashi, Y., et al., *Therapeutic potential of Bifidobacterium breve strain A1 for preventing cognitive impairment in Alzheimer's disease.* Sci Rep, 2017. **7**(1): p. 13510.

132. Lupashin, V. and E. Sztul, *Golgi tethering factors.* Biochim Biophys Acta, 2005. **1744**(3): p. 325-39.

133. Yu, I.M. and F.M. Hughson, *Tethering factors as organizers of intracellular vesicular traffic.* Annu Rev Cell Dev Biol, 2010. **26**: p. 137-56.

134. Bailey Blackburn, J., et al., *COG Complex Complexities: Detailed Characterization of a Complete Set of HEK293T Cells Lacking Individual COG Subunits.* Front Cell Dev Biol, 2016. **4**: p. 23.

135. Ungar, D., et al., *Characterization of a mammalian Golgi-localized protein complex, COG, that is required for normal Golgi morphology and function.* J Cell Biol, 2002. **157**(3): p. 405-15.

136. Ungar, D., et al., *Subunit architecture of the conserved oligomeric Golgi complex.* J Biol Chem, 2005. **280**(38): p. 32729-35.

137. Willett, R., D. Ungar, and V. Lupashin, *The Golgi puppet master: COG complex at center stage of membrane trafficking interactions.* Histochem Cell Biol, 2013. **140**(3): p. 271-83.

138. Climer, L.K., M. Dobretsov, and V. Lupashin, *Defects in the COG complex and COG-related trafficking regulators affect neuronal Golgi function.* Front Neurosci, 2015. **9**: p. 405.

139. Yen, W.L., et al., *The conserved oligomeric Golgi complex is involved in double-membrane vesicle formation during autophagy.* J Cell Biol, 2010. **188**(1): p. 101-14.

140. Deng, S., et al., *Golgi Apparatus: A Potential Therapeutic Target for Autophagy-Associated Neurological Diseases.* Front Cell Dev Biol, 2020. **8**: p. 564975.

141. Yamamoto, H., et al., *Atg9 vesicles are an important membrane source during early steps of autophagosome formation.* J Cell Biol, 2012. **198**(2): p. 219-33.

142. Ge, L., L. Wilz, and R. Schekman, *Biogenesis of autophagosomal precursors for LC3 lipidation from the ER-Golgi intermediate compartment.* Autophagy, 2015. **11**(12): p. 2372-4.

143. Ge, L., M. Zhang, and R. Schekman, *Phosphatidylinositol 3-kinase and COPII generate LC3 lipidation vesicles from the ER-Golgi intermediate compartment.* Elife, 2014. **3**: p. e04135.

144. Freeze, H.H., et al., *Solving glycosylation disorders: fundamental approaches reveal complicated pathways.* Am J Hum Genet, 2014. **94**(2): p. 161-75.

145. Bonifacino, J.S. and B.S. Glick, *The mechanisms of vesicle budding and fusion.* Cell, 2004. **116**(2): p. 153-66.

146. Guardia, C.M., et al., *Structure of Human ATG9A, the Only Transmembrane Protein of the Core Autophagy Machinery.* Cell Rep, 2020. **31**(13): p. 107837.

147. Maeda, S., et al., *Structure, lipid scrambling activity and role in autophagosome formation of ATG9A.* Nat Struct Mol Biol, 2020. **27**(12): p. 1194-1201.

148. Misra, M. and I. Dikic, *RNA binding to p62 impacts selective autophagy.* Cell Res, 2019. **29**(7): p. 512-513.

149. Relic, B., et al., *Serum starvation raises turnover of phosphorylated p62/SQSTM1 (Serine 349), reveals expression of proteasome and N-glycanase1 interactive protein RAD23B and sensitizes human synovial fibroblasts to BAY 11-7085-induced cell death.* Oncotarget, 2018. **9**(88): p. 35830-35843.

150. Oddo, S., et al., *Triple-transgenic model of Alzheimer's disease with plaques and tangles: intracellular Abeta and synaptic dysfunction.* Neuron, 2003. **39**(3): p. 409-21.

151. Bradford, M.M., *A rapid and sensitive method for the quantitation of microgram quantities of protein utilizing the principle of protein-dye binding.* Anal Biochem, 1976. **72**: p. 248-54.

152. Rossi, G., et al., *Comparison of microbiological, histological, and immunomodulatory parameters in response to treatment with either combination therapy with prednisone and*

metronidazole or probiotic VSL#3 strains in dogs with idiopathic inflammatory bowel disease. PLoS One, 2014. **9**(4): p. e94699.

153. Lee, K.Y., et al., *Decrease in glucose transporter 1 levels and translocation of glucose transporter 3 in the dentate gyrus of C57BL/6 mice and gerbils with aging.* Lab Anim Res, 2018. **34**(2): p. 58-64.

154. Harr, S.D., N.A. Simonian, and B.T. Hyman, *Functional alterations in Alzheimer's disease: decreased glucose transporter 3 immunoreactivity in the perforant pathway terminal zone.* J Neuropathol Exp Neurol, 1995. **54**(1): p. 38-41.

155. Sherwani, S.I., et al., *Significance of HbA1c Test in Diagnosis and Prognosis of Diabetic Patients.* Biomark Insights, 2016. **11**: p. 95-104.

156. Lin, K.H., et al., *The preventive effects of edible folic acid on cardiomyocyte apoptosis and survival in early onset triple-transgenic Alzheimer's disease model mice.* Environ Toxicol, 2018. **33**(1): p. 83-92.

157. Bhattacharjee, S. and W.J. Lukiw, *Alzheimer's disease and the microbiome.* Front Cell Neurosci, 2013. **7**: p. 153.

158. Wang, Y. and L.H. Kasper, *The role of microbiome in central nervous system disorders.* Brain Behav Immun, 2014. **38**: p. 1-12.

159. Douglas-Escobar, M., E. Elliott, and J. Neu, *Effect of intestinal microbial ecology on the developing brain.* JAMA Pediatr, 2013. **167**(4): p. 374-9.

160. Duncan, S.H. and H.J. Flint, *Probiotics and prebiotics and health in ageing populations.* Maturitas, 2013. **75**(1): p. 44-50.

161. Hsiao, E.Y., et al., *Microbiota modulate behavioral and physiological abnormalities associated with neurodevelopmental disorders.* Cell, 2013. **155**(7): p. 1451-63.

162. Saulnier, D.M., et al., *The intestinal microbiome, probiotics and prebiotics in neurogastroenterology.* Gut Microbes, 2013. **4**(1): p. 17-27.

163. Weisova, P., et al., *Regulation of glucose transporter 3 surface expression by the AMP-activated protein kinase mediates tolerance to glutamate excitation in neurons.* J Neurosci, 2009. **29**(9): p. 2997-3008.

164. Domise, M., et al., *AMP-activated protein kinase modulates tau phosphorylation and tau pathology in vivo.* Sci Rep, 2016. **6**: p. 26758.

165. Shah, K., S. Desilva, and T. Abbruscato, *The role of glucose transporters in brain disease: diabetes and Alzheimer's Disease.* Int J Mol Sci, 2012. **13**(10): p. 12629-55.

166. Liu, F., et al., *Reduced O-GlcNAcylation links lower brain glucose metabolism and tau pathology in Alzheimer's disease.* Brain, 2009. **132**(Pt 7): p. 1820-32.

167. Lauretti, E., et al., *Glucose deficit triggers tau pathology and synaptic dysfunction in a tauopathy mouse model.* Transl Psychiatry, 2017. **7**(1): p. e1020.

168. O'Connor, T., et al., *Phosphorylation of the translation initiation factor eIF2alpha increases BACE1 levels and promotes amyloidogenesis.* Neuron, 2008. **60**(6): p. 988-1009.

169. Cai, Z., et al., *Roles of AMP-activated protein kinase in Alzheimer's disease.* Neuromolecular Med, 2012. **14**(1): p. 1-14.

170. Liu, Y., et al., *Deficient brain insulin signalling pathway in Alzheimer's disease and diabetes.* J Pathol, 2011. **225**(1): p. 54-62.

171. Velazquez, R., et al., *Corrigendum to "Central insulin dysregulation and energy dyshomeostasis in two mouse models of Alzheimer's disease" [Neurobiol. Aging 58 (2017) 1-13].* Neurobiol Aging, 2017. **58**: p. 241.

172. Zhang, X., et al., *Increased resting state functional irregularity of T2DM brains with high HbA1c: sign for impaired verbal memory function?* Brain Imaging Behav, 2021. **15**(2): p. 772-781.

173. Tolhurst, G., et al., *Short-chain fatty acids stimulate glucagon-like peptide-1 secretion via the G-protein-coupled receptor FFAR2.* Diabetes, 2012. **61**(2): p. 364-71.

174. Gasparini, L. and H. Xu, *Potential roles of insulin and IGF-1 in Alzheimer's disease.* Trends Neurosci, 2003. **26**(8): p. 404-6.

175. Frazier, H.N., et al., *Elevating Insulin Signaling Using a Constitutively Active Insulin Receptor Increases Glucose Metabolism and Expression of GLUT3 in Hippocampal Neurons.* Front Neurosci, 2020. **14**: p. 668.

176. Ko, S.Y., et al., *The Possible Mechanism of Advanced Glycation End Products (AGEs) for Alzheimer's Disease.* PLoS One, 2015. **10**(11): p. e0143345.

177. Rungratanawanich, W., et al., *Advanced glycation end products (AGEs) and other adducts in aging-related diseases and alcohol-mediated tissue injury.* Exp Mol Med, 2021. **53**(2): p. 168-188.

178. Mancha-Agresti, P., et al., *A New Broad Range Plasmid for DNA Delivery in Eukaryotic Cells Using Lactic Acid Bacteria: In Vitro and In Vivo Assays.* Mol Ther Methods Clin Dev, 2017. **4**: p. 83-91.

179. Billings, L.M., et al., *Intraneuronal Abeta causes the onset of early Alzheimer's disease-related cognitive deficits in transgenic mice.* Neuron, 2005. **45**(5): p. 675-88.

180. Hong, S.L., R. Polsky-Cynkin, and L. Levine, *Stimulation of prostaglandin biosynthesis by vasoactive substances in methylcholanthrene-transformed mouse BALB/3T3.* J Biol Chem, 1976. **251**(3): p. 776-80.

181. Steele, R.J., et al., *The p53 tumour suppressor gene.* Br J Surg, 1998. **85**(11): p. 1460-7.

182. Thorpe, G.H., et al., *Phenols as enhancers of the chemiluminescent horseradish peroxidase-luminol-hydrogen peroxide reaction: application in luminescence-monitored enzyme immunoassays.* Clin Chem, 1985. **31**(8): p. 1335-41.

183. Garcia-Mazcorro, J.F., et al., *Abundance and short-term temporal variability of fecal microbiota in healthy dogs.* Microbiologyopen, 2012. **1**(3): p. 340-7.

184. Pilla, R. and J.S. Suchodolski, *The Role of the Canine Gut Microbiome and Metabolome in Health and Gastrointestinal Disease.* Front Vet Sci, 2019. **6**: p. 498.

185. Callahan, B.J., et al., *DADA2: High-resolution sample inference from Illumina amplicon data.* Nat Methods, 2016. **13**(7): p. 581-3.

186. DeSantis, T.Z., et al., *Greengenes, a chimera-checked 16S rRNA gene database and workbench compatible with ARB.* Appl Environ Microbiol, 2006. **72**(7): p. 5069-72.

187. Langille, M.G., et al., *Predictive functional profiling of microbial communities using 16S rRNA marker gene sequences.* Nat Biotechnol, 2013. **31**(9): p. 814-21.

188. Zakrzewski, M., et al., *Calypso: a user-friendly web-server for mining and visualizing microbiome-environment interactions.* Bioinformatics, 2017. **33**(5): p. 782-783.

189. Stoka, V., V. Turk, and B. Turk, *Lysosomal cathepsins and their regulation in aging and neurodegeneration.* Ageing Res Rev, 2016. **32**: p. 22-37.

190. Dorninger, F., et al., *Ether lipid deficiency does not cause neutropenia or leukopenia in mice and men.* Cell Metab, 2015. **21**(5): p. 650-1.

191. Hook, V., et al., *Inhibition of cathepsin B reduces beta-amyloid production in regulated secretory vesicles of neuronal chromaffin cells: evidence for cathepsin B as a candidate beta-secretase of Alzheimer's disease.* Biol Chem, 2005. **386**(9): p. 931-40.

192. Hook, V., et al., *Cysteine Cathepsins in the secretory vesicle produce active peptides: Cathepsin L generates peptide neurotransmitters and cathepsin B produces beta-amyloid of Alzheimer's disease.* Biochim Biophys Acta, 2012. **1824**(1): p. 89-104.

193. Tonnies, E. and E. Trushina, *Oxidative Stress, Synaptic Dysfunction, and Alzheimer's Disease.* J Alzheimers Dis, 2017. **57**(4): p. 1105-1121.

194. Ichimura, Y. and M. Komatsu, *Activation of p62/SQSTM1-Keap1-Nuclear Factor Erythroid 2-Related Factor 2 Pathway in Cancer.* Front Oncol, 2018. **8**: p. 210.

195. Hansen, T.E. and T. Johansen, *Following autophagy step by step.* BMC Biol, 2011. **9**: p. 39.

196. Bermudez-Humaran, L.G., et al., *Engineering lactococci and lactobacilli for human health.* Curr Opin Microbiol, 2013. **16**(3): p. 278-83.

197. Liang, K., et al., *Genetically engineered Salmonella Typhimurium: Recent advances in cancer therapy.* Cancer Lett, 2019. **448**: p. 168-181.

198. Chiabai, M.J., et al., *Mucosal delivery of Lactococcus lactis carrying an anti-TNF scFv expression vector ameliorates experimental colitis in mice.* BMC Biotechnol, 2019. **19**(1): p. 38.

199. Oh, J.H., et al., *Secretion of Recombinant Interleukin-22 by Engineered Lactobacillus reuteri Reduces Fatty Liver Disease in a Mouse Model of Diet-Induced Obesity.* mSphere, 2020. **5**(3).

200. Salminen, A., et al., *Emerging role of p62/sequestosome-1 in the pathogenesis of Alzheimer's disease.* Prog Neurobiol, 2012. **96**(1): p. 87-95.

201. Sabbieti, M.G., et al., *Plasmid DNA-coding p62 as a bone effective anti-inflammatory/anabolic agent.* Oncotarget, 2015. **6**(6): p. 3590-9.

202. Kolosova, N.G., et al., *p62 /SQSTM1 coding plasmid prevents age related macular degeneration in a rat model.* Aging (Albany NY), 2018. **10**(8): p. 2136-2147.

203. Chatel, J.M., et al., *In vivo transfer of plasmid from food-grade transiting lactococci to murine epithelial cells.* Gene Ther, 2008. **15**(16): p. 1184-90.

204. Siso, S., L. Gonzalez, and M. Jeffrey, *Neuroinvasion in prion diseases: the roles of ascending neural infection and blood dissemination.* Interdiscip Perspect Infect Dis, 2010. **2010**: p. 747892.

205. Jeffrey, M., et al., *Onset and distribution of tissue prp accumulation in scrapie-affected suffolk sheep as demonstrated by sequential necropsies and tonsillar biopsies.* J Comp Pathol, 2001. **125**(1): p. 48-57.

206. Looper, K.J. and J. Paris, *What dimensions underlie cluster B personality disorders?* Compr Psychiatry, 2000. **41**(6): p. 432-7.

207. Caccamo, A., et al., *p62 improves AD-like pathology by increasing autophagy.* Mol Psychiatry, 2017. **22**(6): p. 865-873.

208. Cecarini, V., et al., *The fine-tuning of proteolytic pathways in Alzheimer's disease.* Cell Mol Life Sci, 2016. **73**(18): p. 3433-51.

209. Bonfili, L., et al., *Ghrelin induces apoptosis in colon adenocarcinoma cells via proteasome inhibition and autophagy induction.* Apoptosis, 2013. **18**(10): p. 1188-200.

210. Cecarini, V., et al., *Crosstalk between the ubiquitin-proteasome system and autophagy in a human cellular model of Alzheimer's disease.* Biochim Biophys Acta, 2012. **1822**(11): p. 1741-51.

211. Cecarini, V., et al., *Wild type and mutant amyloid precursor proteins influence downstream effects of proteasome and autophagy inhibition.* Biochim Biophys Acta, 2014. **1842**(2): p. 127-34.

212. Hung, S.Y., et al., *LC3 overexpression reduces Abeta neurotoxicity through increasing alpha7nAchR expression and autophagic activity in neurons and mice.* Neuropharmacology, 2015. **93**: p. 243-51.

213. Pickford, F., et al., *The autophagy-related protein beclin 1 shows reduced expression in early Alzheimer disease and regulates amyloid beta accumulation in mice.* J Clin Invest, 2008. **118**(6): p. 2190-9.

214. Zhou, F., et al., *APP and APLP1 are degraded through autophagy in response to proteasome inhibition in neuronal cells.* Protein Cell, 2011. **2**(5): p. 377-83.

215. Klionsky, D.J., et al., *Guidelines for the use and interpretation of assays for monitoring autophagy (3rd edition).* Autophagy, 2016. **12**(1): p. 1-222.

216. Menon, M.B. and S. Dhamija, *Beclin 1 Phosphorylation - at the Center of Autophagy Regulation.* Front Cell Dev Biol, 2018. **6**: p. 137.

217. Olson, O.C. and J.A. Joyce, *Cysteine cathepsin proteases: regulators of cancer progression and therapeutic response.* Nat Rev Cancer, 2015. **15**(12): p. 712-29.

218. Butterfield, D.A., *Amyloid beta-peptide (1-42)-induced oxidative stress and neurotoxicity: implications for neurodegeneration in Alzheimer's disease brain. A review.* Free Radic Res, 2002. **36**(12): p. 1307-13.

219. Butterfield, D.A. and C.M. Lauderback, *Lipid peroxidation and protein oxidation in Alzheimer's disease brain: potential causes and consequences involving amyloid beta-peptide-associated free radical oxidative stress.* Free Radic Biol Med, 2002. **32**(11): p. 1050-60.

220. Kinney, J.W., et al., *Inflammation as a central mechanism in Alzheimer's disease.* Alzheimers Dement (N Y), 2018. **4**: p. 575-590.

221. Gella, A. and N. Durany, *Oxidative stress in Alzheimer disease.* Cell Adh Migr, 2009. **3**(1): p. 88-93.

222. Korolainen, M.A., et al., *Multiplexed proteomic analysis of oxidation and concentrations of cerebrospinal fluid proteins in Alzheimer disease.* Clin Chem, 2007. **53**(4): p. 657-65.

223. Mustafa, A.G., M.A. Alfaqih, and O. Al-Shboul, *The 4-hydroxynonenal mediated oxidative damage of blood proteins and lipids involves secondary lipid peroxidation reactions.* Exp Ther Med, 2018. **16**(3): p. 2132-2137.

224. Keller, J.N., et al., *Impairment of glucose and glutamate transport and induction of mitochondrial oxidative stress and dysfunction in synaptosomes by amyloid beta-peptide: role of the lipid peroxidation product 4-hydroxynonenal.* J Neurochem, 1997. **69**(1): p. 273-84.

225. Mattson, M.P. and S.L. Chan, *Neuronal and glial calcium signaling in Alzheimer's disease.* Cell Calcium, 2003. **34**(4-5): p. 385-97.

226. Tamagno, E., et al., *H2O2 and 4-hydroxynonenal mediate amyloid beta-induced neuronal apoptosis by activating JNKs and p38MAPK.* Exp Neurol, 2003. **180**(2): p. 144-55.

227. Kim, J.Y. and K. Ozato, *The sequestosome 1/p62 attenuates cytokine gene expression in activated macrophages by inhibiting IFN regulatory factor 8 and TNF receptor-associated factor 6/NF-kappaB activity.* J Immunol, 2009. **182**(4): p. 2131-40.

228. Tilija Pun, N. and P.H. Park, *Role of p62 in the suppression of inflammatory cytokine production by adiponectin in macrophages: Involvement of autophagy and p21/Nrf2 axis.* Sci Rep, 2017. **7**(1): p. 393.

229. Wang, L., et al., *Biology of p62/sequestosome-1 in Age-Related Macular Degeneration (AMD).* Adv Exp Med Biol, 2016. **854**: p. 17-22.

230. Zou, X., et al., *Stimulation of GSH synthesis to prevent oxidative stress-induced apoptosis by hydroxytyrosol in human retinal pigment epithelial cells: activation of Nrf2 and JNK-p62/SQSTM1 pathways.* J Nutr Biochem, 2012. **23**(8): p. 994-1006.

231. Butterfield, D.A. and D. Boyd-Kimball, *Oxidative Stress, Amyloid-beta Peptide, and Altered Key Molecular Pathways in the Pathogenesis and Progression of Alzheimer's Disease.* J Alzheimers Dis, 2018. **62**(3): p. 1345-1367.

232. Hickman, S.E., E.K. Allison, and J. El Khoury, *Microglial dysfunction and defective beta-amyloid clearance pathways in aging Alzheimer's disease mice.* J Neurosci, 2008. **28**(33): p. 8354-60.

233. Athari Nik Azm, S., et al., *Lactobacilli and bifidobacteria ameliorate memory and learning deficits and oxidative stress in beta-amyloid (1-42) injected rats.* Appl Physiol Nutr Metab, 2018. **43**(7): p. 718-726.

234. Luerce, T.D., et al., *Anti-inflammatory effects of Lactococcus lactis NCDO 2118 during the remission period of chemically induced colitis.* Gut Pathog, 2014. **6**: p. 33.

235. Ramalho, J.B., et al., *In Vitro Probiotic and Antioxidant Potential of Lactococcus lactis subsp. cremoris LL95 and Its Effect in Mice Behaviour.* Nutrients, 2019. **11**(4).

236. Bauerl, C., et al., *Shifts in gut microbiota composition in an APP/PSS1 transgenic mouse model of Alzheimer's disease during lifespan.* Lett Appl Microbiol, 2018. **66**(6): p. 464-471.

237. Kaakoush, N.O., *Insights into the Role of Erysipelotrichaceae in the Human Host.* Front Cell Infect Microbiol, 2015. **5**: p. 84.

238. Leclercq, S., et al., *Intestinal permeability, gut-bacterial dysbiosis, and behavioral markers of alcohol-dependence severity.* Proc Natl Acad Sci U S A, 2014. **111**(42): p. E4485-93.

239. Parkar, S.G., A. Kalsbeek, and J.F. Cheeseman, *Potential Role for the Gut Microbiota in Modulating Host Circadian Rhythms and Metabolic Health.* Microorganisms, 2019. **7**(2).

240. Charbonneau, M.R., et al., *Developing a new class of engineered live bacterial therapeutics to treat human diseases.* Nat Commun, 2020. **11**(1): p. 1738.

241. Springer, M.S. and J. Gatesy, *The gene tree delusion.* Mol Phylogenet Evol, 2016. **94**(Pt A): p. 1-33.

242. Vogt, N.M., et al., *Gut microbiome alterations in Alzheimer's disease.* Sci Rep, 2017. **7**(1): p. 13537.

243. Coker, O.O., et al., *Enteric fungal microbiota dysbiosis and ecological alterations in colorectal cancer.* Gut, 2019. **68**(4): p. 654-662.

244. Renaud, S. and M. de Lorgeril, *Wine, alcohol, platelets, and the French paradox for coronary heart disease.* Lancet, 1992. **339**(8808): p. 1523-6.

245. de Gaetano, G., et al., *Effects of moderate beer consumption on health and disease: A consensus document.* Nutr Metab Cardiovasc Dis, 2016. **26**(6): p. 443-67.

246. Sanchez-Muniz, F.J., et al., *The Nutritional Components of Beer and Its Relationship with Neurodegeneration and Alzheimer's Disease.* Nutrients, 2019. **11**(7).

247. Imhof, A., et al., *Overall alcohol intake, beer, wine, and systemic markers of inflammation in western Europe: results from three MONICA samples (Augsburg, Glasgow, Lille).* Eur Heart J, 2004. **25**(23): p. 2092-100.

248. Carabotti, M., et al., *The gut-brain axis: interactions between enteric microbiota, central and enteric nervous systems.* Ann Gastroenterol, 2015. **28**(2): p. 203-209.

249. Liu, P., et al., *Altered microbiomes distinguish Alzheimer's disease from amnestic mild cognitive impairment and health in a Chinese cohort.* Brain Behav Immun, 2019. **80**: p. 633-643.

250. Dikic, I. and Z. Elazar, *Mechanism and medical implications of mammalian autophagy.* Nat Rev Mol Cell Biol, 2018. **19**(6): p. 349-364.

251. Orsi, A., et al., *Dynamic and transient interactions of Atg9 with autophagosomes, but not membrane integration, are required for autophagy.* Mol Biol Cell, 2012. **23**(10): p. 1860-73.

252. Sawa-Makarska, J., et al., *Reconstitution of autophagosome nucleation defines Atg9 vesicles as seeds for membrane formation.* Science, 2020. **369**(6508).

253. Russell, R.C., et al., *ULK1 induces autophagy by phosphorylating Beclin-1 and activating VPS34 lipid kinase.* Nat Cell Biol, 2013. **15**(7): p. 741-50.

254. Park, H., J.H. Kang, and S. Lee, *Autophagy in Neurodegenerative Diseases: A Hunter for Aggregates.* Int J Mol Sci, 2020. **21**(9).

255. Zhang, Y., et al., *ZZ-dependent regulation of p62/SQSTM1 in autophagy.* Nat Commun, 2018. **9**(1): p. 4373.

256. Emanuele, S., et al., *p62: Friend or Foe? Evidences for OncoJanus and NeuroJanus Roles.* Int J Mol Sci, 2020. **21**(14).

257. Dartigues, J.F., *Alzheimer's disease: a global challenge for the 21st century.* Lancet Neurol, 2009. **8**(12): p. 1082-3.

258. Marcello, E., F. Gardoni, and M. Di Luca, *Alzheimer's disease and modern lifestyle: what is the role of stress?* J Neurochem, 2015. **134**(5): p. 795-8.

259. Johansen, T. and T. Lamark, *Selective Autophagy: ATG8 Family Proteins, LIR Motifs and Cargo Receptors.* J Mol Biol, 2020. **432**(1): p. 80-103.

260. Jain A, Lamark T, Sjøttem E, Larsen KB, Awuh JA, Øvervatn A, McMahon M, Hayes JD, Johansen T. *p62/SQSTM1 is a target gene for transcription factor NRF2 and creates a positive feedback loop by inducing antioxidant response element-driven gene transcription*. J Biol Chem, 2010. **285**(29): p. 22576-91.